42157

NASA CR-132448

File with
N74-27413

DESIGN AND FABRICATION OF A BORON REINFORCED INTERTANK SKIRT

By Jim Henshaw
Paul A. Roy
Paul Pylypetz

Prepared by Avco Systems Division
Lowell, Mass. 01851

for

LANGLEY RESEARCH CENTER
NATIONAL AERONAUTICS AND SPACE ADMINISTRATION

FOREWORD

This report was prepared by Avco System Division under NASA Contract NAS 1-9938 and covers the work involved in the design and fabrication of a boron reinforced test shell. The contract was administered by the NASA Langley Research Center.

CONTENTS

TABLES

FIGURES

FIGURES - Concluded

SYMBOLS

Physical quantities defined in this paper are given in both the U.S. customary units and in the international system of units (SI) (Reference 7). Conversion factors pertinent to the present investigation are presented in Appendix B.

A	area
AB	area of boron epoxy
d	spacing
DB	diameter of boron epoxy
E	Young's modulus of elasticity
h	stringer height
I	moment of inertia
L	length
M	number of 1/2 axial waves
N	number of circumferential waves
N	end load/unit width
P	end load
S	stringer
t	shell or stringer web thickness
$\bar{t}$	average thickness of shell
$\bar{x}$	ring height

Subscripts		
	x	axial direction
	y	circumferential direction
	R	ring
	S	stringer
	eg	equivalent to aluminum

SUMMARY

Analytical and experimental studies were performed to evaluate the structural efficiency of a boron reinforced shell, where the medium of reinforcement consists of hollow aluminum extrusions infiltrated with boron epoxy. This unique process of "infiltration" was previously evaluated in phase one of this program (Reference 1), where the efficiency in terms of weight savings was demonstrated by the analysis and test of large and small compression panels. The process of "infiltration" consists of first extruding the required cross-section in aluminum in which is situated one or more continuous hollow voids. These voids are subsequently filled with unidirectional boron epoxy by the relatively inexpensive process of drawing the fibers through the voids by hand, then pumping resin through the section to form the composite and to bond the composite to the aluminum. The voids are situated at selected positions such that when the unidirectional boron epoxy is assembled in the voids the resultant section demonstrates maximum stability and strength for least weight.

Studies were completed for the design of a one-half scale minimum weight shell using boron reinforced stringers and boron reinforced rings. Parametric and iterative studies were completed for the design of minimum weight stringers, rings, shells without rings and shells with rings. Boron reinforced shells exhibit a weight savings of 40% as compared to a longitudinal stiffened all metal shells, using a surprisingly small volume of boron epoxy in each stringer. The efficiency of the boron reinforced stringers was proven to be dependent upon the volume and spacing of the boron epoxy elements, with the maximum use of boron not necessarily providing a minimum weight design. Computer studies were completed for the final evaluation of a minimum weight shell using highly buckled minimum gage skin.

The program concluded with the detail design of a practical minimum weight test shell which demonstrates a weight savings of 30% as compared to an all aluminum longitudinal stiffened shell. Sub-element tests were successfully conducted on representative segments of the compression surface at maximum stress and also on segments of the load transfer joint. Various sub-element specimens were delivered to NASA Langley for test. A 10 foot long, 77 inch diameter (3.65 meter long, 1.95 meter diameter) shell was fabricated and delivered to the NASA Langley Research Center for test.

INTRODUCTION

Selective reinforcement of aluminum structure with a high strength/high modulus composite is a probable means by which the next generation of commercial aircraft will utilize these relatively new materials. Various NASA promoted industry studies are in the process of evaluation and from these it appears that selective reinforcement offers the potential for significant weight savings, yet avoids either the high new technology risk factor, or the necessity of a complete change of production tooling--both of which are generally associated with the use of all composite structure.

A method conceived for the efficient fabrication of a selectively reinforced aluminum structure is that called "infiltration". In this process boron epoxy is infiltrated into preformed hollow extrusions--requiring only the minimum of tooling (no requirement for molds) and conveniently allows for metal to metal riveting and conventional load transfer technology. The composite is completely shielded from the environment by an aluminum sheath and accidental damage is repaired by metal splicing requiring no field repair using composite materials. A desirable feature of this concept is that, having developed a procedure for infiltration, it is applicable without modification to any extruded shape conceived--be it flat or curved.

The investigation of infiltrated extrusions as a method for reinforcement of metal structures was conducted in the first phase of the program by the design and test of various sub-elements and compression panels (Reference 1). As a result it was concluded that the next desirable step in the development of the concept was the fabrication and test of large structure. In this task it was intended that the infiltrated elements would be fully evaluated, in terms of weight savings, in a structure that was representative of a flight vehicle and tested in a manner that included all failure modes. The test vehicle selected to accomplish this objective was a shell structure, for there existed with all metal shells (both at NASA and throughout the industry) a significant volume of test experience, test data and analytical data. All of which would serve as a base for comparison and also assist in qualifying the proposed analyses. Another reason for selecting a shell structure was the upcoming development of structural concepts for the space shuttle orbiter. The test of a representative section of the shuttle would provide useful data for that program. The section of the orbiter selected for evaluation, was the section that joins together the cryogenic tanks in the Integral Tank and Reference designs. The design loads are well defined, the attachment mechanism was similar to previous experience with shell design and the predominantly axial load was amenable to the efficient use of the unidirectional reinforcement (infiltrated boron epoxy stringers). The program plan envisaged was the optimization of a shell for minimum weight, the confirmation of the design by test of sub-element specimens and finally the fabrication of a complete shell for test by the NASA Langley Research Center.

SELECTION AND CONCEPTUAL DESIGN OF THE TEST STRUCTURE

At the time of a program conception there were many shuttle orbiter design concepts available for evaluation, one of which was the Integral Tank concept wherein the major fuselage bending loads were transmitted by axial loads in the tank skins. As the previous evaluation phase (Reference 1) has shown, infiltrated structure is most efficient in designs where a high degree of load orthotropocity occurs, requiring a high percentage of reinforcement (boron reinforced extrusions) in one direction and minimal material for transverse loads. Two sections of the tank assembly appeared particularly suitable for the use of infiltrated extrusions. These were; the section that joined the two cryogenic tanks together and a similar section that joined the tanks to the thrust structure (See Figure 1). Both of these sections are required to transmit heavy axial thrust and bending loads with minimal requirement for transverse shear or tension; hence a design concept was formulated for a shell structure with maximum potential for resistance of axial and bending loads with minimum weight expended for transverse (circumferential) support.

As shown on Figure 1 the concept formulated for investigation and optimization was a conventional ring/stringer stiffened shell design, with boron reinforced extrusions used for both the rings and stringers. The skin would be minimum gage, as selected by a minimum weight design, with consideration for early buckling of the skin between stringers. A buckled skin design was proposed so as to allow the use of heavy stringer sections with the maximum use of composites. With respect to the detail design of the elements of the shell it was decided to use "hat" shaped stringers and "tee" shaped rings. The selection of the particular stringer geometry was based upon previous compression panel studies (Reference 1), where the hat stiffener (with a rod of boron placed at each corner), was proven to be a superior design and comparable to the very efficient NACA Y section. Symmetrical placement of boron epoxy would reduce thermal distortions, and with two of these lobes placed adjacent to the skin, precipitation of the skin buckle into the body of the stringer will be minimized. The tee section design for the ring was selected as being suitable for roll forming to the shell radius.

The general geometry of the reference design and the boron reinforced shell is as shown in Figure 1. The cross-section is circular (so as to be readily compared to existing test data), with an optimum spacing of rings and stringers. As an economy measure, only the compression surface uses boron reinforced stringers. The lower two-thirds uses all aluminum stringer of the same stiffness. From available reports a running load of 533.75 kN/m (3,000 lbf/in) (compression) is established as the maximum line load resulting from axial thrust and lateral bending. However, as the capacity of the NASA test fixture precluded the test of a full scale

section (at that load), it was decided to design, fabricate and test a 1/2 scale section and then extrapolate those results for the design of a full scale, 4.2 m (14 ft) diameter section. The test proposed was that of pure bending, which is a typical mode of testing large cylinders and can be related to failure in axial compression. The maximum line load of 533.75 kN/m (3,000 lbf/in) was by definition determined to be the Design Failure Load which converted to a Design Bending Moment of 1.57×10^6 N-cm (13.96×10^6 lbf-in).

ANALYSIS FOR MINIMUM WEIGHT SHELLS

In advance of the discussions of shell analysis and design, an outline of the basic approach is presented, where instead of developing a totally integrated computer design program to derive minimum weight, it was decided to proceed on an iterative basis, whereby each parameter that influenced the design could be examined in detail before proceeding to the next. One reason that prompted this approach is of course the cost of implementing a complex shell design program, however, the more basic reason was the need to fully understand the effects of the hybrid design, using a mix of composite and metal. The hybrid stringers and rings, being a mixture of two materials with different strength, and moduli; present a particular problem, for the minimum weight stiffener is not necessarily that which is fully stressed, nor that which contains the maximum amount of boron epoxy composite. To fully understand the effect of volume of boron and effective stress levels, it was considered necessary to first produce a family of efficient stringer designs which would satisfy various loads, and then integrate those stringers into shell designs. The effect of ring spacing when combined with buckled skins was also of interest, for it was thought that the minimum weight design would be more influenced by the stiffness of the stringers and spacing of the stringers--hence shells without rings were first investigated prior to evaluation of the full length shell with rings.

The iterative design procedure adopted would, as discussed above, examine each factor of the design. This procedure is outlined in the graphic format presented in Figure 2 where four steps are involved.

Step 1 - This is the design of a family of stiffeners where for various lengths (lengths between intended ring positions), minimum weight designs were established for various axial loads that bound the maximum and minimum stringer loads that are expected to be present when attached to the shell skin. The minimum weight stringer section is defined by that required to sustain the axial load without exceeding allowable stress levels, incurring a local or general instability failure, and not trespassing on minimum gage or other practical constraints.

Step 2 - Integrates the stiffeners into the shell analysis (without rings) using the family of stiffeners as defined by their failure load and length. Shell failure load curves are plotted for various skin thicknesses, stringer spacings and shell lengths. From the family of shell design curves generated, various minimum weight shell designs are formulated (without rings) that satisfy the design load.

Step 3 - Integrates the minimum weight stringer stiffened shells of stipulated length into ring/stiffened shells of multiples of the above stipulated length, using ring section properties that will enforce a buckled wave pattern with a nodal point at each ring position.

Step 4 - Scale up of design parameters to derive a minimum weight full size shell.

Generation of a Family of Minimum Weight Stringers

As described previously, the first step in the design procedure was the generation of a family of minimum weight stringers that would withstand a range of axial compressive loads that were expected to be present in the stringer when they are attached to the shell at various spacings around the circumference. Utilizing the stringer design computer program described in the appendix, a number of cases were evaluated for loads of 53,000 N (12,000 lbf), 107,000 N (24,000 lbf), and 160,000 N (36,000 lbf). For each load, data was generated for stringer lengths of 91.4 cm (36 in), 61 cm (24 in), and 46 cm (18 in) being the range of lengths between rings that were considered practical for the final shell design.

Figures 3, 4, and 5 illustrate the results of the analysis where, for various areas of boron epoxy, the weight of the stringer is defined for each load/length combination. As illustrated in these figures, all the curves indicate that there is an optimum amount of boron epoxy reinforcement for minimum weight. For no reinforcement (or minimum reinforcement) the section design is controlled by the aluminum, meaning a relatively deep section with thick webs; as the amount of reinforcement is increased the section depth is diminished, requiring less aluminum. Beyond a given amount of reinforcement however, the section depth becomes so small that larger quantities of boron epoxy reinforcement are needed to achieve the proper bending stiffness and these increases in reinforcement can no longer be offset by corresponding reductions in aluminum; hence the weight tends to increase. From figures 3, 4, and 5 there exists a minimum weight design for each load and length, and from the data generated the basic geometry for these designs is tabulated as shown in Table 1. Of the nine stringer length/load combination investigated, three of the minimum weight designs have stress levels in the aluminum of 34,472 N/cm^2 (50,000 lbf/in^2) and over. This is approaching the yield strain for the 7075-T6 stringer. In addition to the high stresses predicted for the aluminum, the three minimum weight designs for the 46 cm (18 in) long stringers exhibit undesirable geometric profiles in terms of minimum gage for the webs and/or a shallow height. These values are marked by an asterisk in Table 1, where the concern for practicality of

extruding geometrically undesirable designs coincides with two of the higher stressed designs, (18 in at 24,000 lbf, and 18 in at 36,000 lbf). As it was highly probable that the 46 cm (18 in) sections would prove to be heavier in the final evaluation, it was decided to remove from further considerations all 46 cm (18 in) designs. The remaining design which exhibited 34,472 N/cm^2 (50,000 lbf/in^2) in the aluminum (36,000 lbf at 24 in) was accepted with reservation and the expectation of some modification in future iterations.

As a result of the deliberations discussed above, minimum weight designs were established as a base for a family of stringer designs that are described in Figures 6 through 12. In these figures the complete data for the family of minimum weight stringers is presented as a function of the load they will sustain, i.e., $P_{(crit\text{-}strg)}$ for lengths of 61 cm (24 in) and 91 cm (36 in). Factors such as weight, web thickness, height of section, moment of inertia, diameter of boron, area of boron, total area, etc., are all presented; such that given a common parameter (i.e., load that the stringer will sustain, $P_{(crit\text{-}strg)}$ all of the stiffnesses, areas, geometry, etc., that are required for input to shell analysis can be determined. Note that as shown, stringer loads other than 53,376 N (12,000 lbf), 106,752 N (24,000 lbf), and 160,128 N (36,000 lbf) were finally evaluated so as to ensure a smooth curve.

The next section shows how the family of stringer designs were integrated into the analysis for minimum weight shells.

Stringer Stiffened Shell Design - Between Rings

Following the generation of a family of minimum weight stringers, the next step in the design procedure was to incorporate these designs into the parametric evaluation of stringer stiffened shells varying stringer spacing, skin thickness and shell length. Shell lengths chosen were 91.4 cm (36 in) and 61 cm (24 in), corresponding to the range of ring spacings anticipated for the full length shell. Stringer spacings of 10.2 cm (4.03 in) and 20.5 cm (8.03 in) were selected so as to divide the circumference of the shell into sixty (60) and thirty (30) equal increments respectively. Standard sheet gages ranging from .025 cm (.010 in) to .152 cm (.063 in) were evaluated for the skin.

Given shell length, stringer spacing, and skin gage, shell buckling loads (as a function of stringer size) were determined using the shell local instability code (see Appendix A). These results were plotted in the form of shell buckling load versus stringer size parameter for fixed shell geometries. For convenience, the stringer size parameter selected for these plots was $P_{(crit\text{-}strg)}$, since this facilitated the identification of the stringer geometry

from Figure 6 through 12. The intercept of each of these curves with the shell design load of 6566 N/cm (3750 lbf/in) (i.e., shell ultimate line load of 3000 lb/in plus the 25% knockdown factor) determined the $P_{(crit-strg)}$ of the stringer which satisfied the design load and hence from Figures 6 through 12 the geometry of the stringer is established.

The results of the analysis discussed above are presented in Figures 13 through 17. Figures 13 through 16 are the interpolation curves for selection of the required stringer parameter $P_{(crit-strg)}$ and Figure 17 is the weights of the shells presented as a function of the shell thickness. The interpolation procedure is self-evident where for 61 cm (24 in) and 91.4 cm (36 in) long shells with stringers spaced at 10.2 cm (4.03 in) and 20.5 cm (8.06 in) and various skin thickness; the associated $P_{(crit's)}$ for shells that satisfy the desired load are defined. As shown in Figure 17 the weight of the shell for various combinations of length and spacing are plotted as a function of shell thickness, with the curve illustrating the absolute minimum weight being the 61 cm (24 in) - 10.2 cm (4.03 in) design. All but one curve approached its particular minimum weight at or near zero skin thickness (no analyses were conducted for skins thicknesses of less than .01 inch). The explanation for this is that in these designs the geometry was such that the shell restraint (circumferential membrane effect) was ineffectual in stabilizing the stringer. The exception is the 91.4 cm (36 in) - 10.2 cm (4.03 in) design, where the closer spacing combined with the longer shell length means that there is a longer and less stiff stringer that can be more easily restrained by the skin, even though it is buckled. In this case a minimum weight occurred at a skin thickness of approximately .052 cm (.02 in).

Considering only standard gages for the skin, Figure 17 contains twenty potential candidates for the final ring stiffened shell design as indicated by the points on the curve. Although all twenty concepts were considered further as presented in the following section, two designs were selected at this stage to determine the feasibility of the designs and for detailed stress analysis. The two designs selected are noted in Figure 17 and correspond to the two minimum weight designs allowing for the fact that an .020 inch was taken as a practical lower limit on skin thickness. A detailed summary of the two designs is presented in Table 2. For the most part these results indicated that both designs were feasible. The stress levels in the aluminum stringers were acceptable . The diameter of boron epoxy is within practical limitations and is geometrically acceptable when associated with the height of the stringer. The thickness requirements for the web of the stringer is below that possible by the extrusion process, but could be attained by subsequent chemical milling.

Ring and Stringer Stiffened Shell Design

Ring Design. - The final stage in the design iteration cycle involved the sizing of rings such that the optimized intermediate length shells could be integrated into a full length shell. It had been a design premise that the final test article would fail in interbay buckling, consequently the rings would have to be sufficiently stiff to enforce a node at their respective attachment points.

A study of the literature has revealed two particular studies for the derivation of rings geometry that will enforce panel instability between rings. Namely, Shanley (Reference 2) and Van der Neut (Reference 3). As reported by Shanley there exists a relationship between the required flexural stiffness (EI) of the ring and the shell failure load as follows:

$$I_{(Ring)} = \frac{C_F N_X 4 R^4}{L_R 10^7} \qquad (1)$$

Where C_F is a constant, N_X is the axial load per inch, R is the shell radius and L_R is the length between rings. Equation (1) is the result of a semi-imperical approach whereby a coefficient of 6.25×10^{-5} is established. Van der Neut is his analysis considers the required area (A) of the ring and expresses this term as a function of the shell geometry as follows:

$$A_{(Ring)} = \frac{4 \pi^2 R^2 I_s}{L_R^3 d_s} \qquad (2)$$

where R is the shell radius, I_s is the area moment of the stiffener, L_R is the length between rings, and d_s is the spacing of the stringers.

These two expressions (Equation (1) and (2) cannot be integrated to provide a single expression for ring properties, and as the literary search provided no additional guidance, it was decided to solve each equation independently so as to establish the required ring stiffness for selected shell designs. In Table 3 is the result of the analysis for the required area and area moment of the ring, as expressed by Van der Neut and Shanley. As the table shows the ring section properties for the 91.4 cm (36 in) and 61 cm (24 in) long shell (bay lengths) are calculated, with the required section properties increasing as the ring spacing decreases and the stringer spacing increases. Logically more ring material is required to enforce a nodal point in the stringers as their support length is decreased and/or their section properties increased as a result of larger stringer spacing.

Upon examination of the data presented in Table 3, it is determined that the area required for the ring, as determined by the Van der Neut equation, is extremely small and although the analysis reported in the next section indicated a lack of sensitivity to the area of the ring, it was considered advisable to reconsider the Van der Neut results. The questionable factor that resulted from the reconsideration was the relationship between the circumferential wave length and the ring spacing. Van der Neut indicates that the hinge line (circumferential wave node point) occurs at the centerline of each stringer--however with a 61 cm (24 in) and 91.4 cm (36 in) ring spacing it is plausible to assume a general wave length in the circumferential direction that is larger than the 10.2 cm (4.03 in) and 20.5 cm (8.06 in) stringer spacing. This is supported by the shell local instability analysis reported earlier where wave lengths of between 75 cm (30 in) and 152 cm (60 in) occur. Accordingly the Van der Neut equation was modified by removing the stringer spacing value, which had the approximately same effect as increasing the wave length of the buckled in the circumferential direction to that indicated by shell stability analysis. The modified results are as shown in Table 3.

In order to select a minimum weight representative ring design, five ring stiffener sections were parametrically evaluated using equations (1) and (2); generating the area, moment of inertia and the weight for each ring geometry. The sections and the data are presented in Figure 18 and as seen the five sections ranged from a non-reinforced hat stiffener, through a single bulb reinforced stiffener, to a double bulbed section. Each section was considered in three heights, such that a wide range of geometries were available for consideration. Figure 18 displays the 25 designs as a series of curves. Each curve is a particular ring shape with selected positions on the curve being a particular height of each section. From Figure 18, minimum weight ring stiffener designs were selected that satisfied as nearly as possible the area and inertia. The geometry and weight of the selected rings are presented in Table 3 for each of the designs that were evaluated in the final shell analysis. As the reader will observe from Figure 18, a .57 cm^4 (.014 in^4) and .81 cm^4 (.02 in^4) moment of inertia is required for the 91.4 cm (36 in) and all 61 cm (24 in) long shells respectively, and is satisfied by the minimum weight design Number 5. In contrast the area requirement ranging from .25 cm^2 (.038 in^2) to 3.1 cm^2 (.48 in^2) generally dictates the use of boron reinforced sections with the exception in only two cases.

Full Length Shell Design. - Using the ring properties given in Table 3, all twenty intermediate length shells cited in Figure 17, were integrated into full length [183 cm (72 in)] ring and stringer stiffened shells and analyzed using the local instability analysis computer program. Table 4 summarizes the results obtained giving the predicted failure load and the corresponding wave number for each shell. As the reader will observe, the results of the analyses failed to substantiate the original design premise, for in each shell (various ring spacing/stringer spacing/skin thickness combinations),

the failure loads ranged from below to above the design value of 3750 lb/in. Also the value for M, being the number axial half waves for the shell was such as to produce an $M < 1$ for each bay, suggesting a general instability failure in each case.

To investigate this unexpected anomaly several analyses were conducted using a constant shell geometry while the ring and stringer stiffnesses were varied independently of each other. The results are presented in Figure 19 with the predicted failure load plotted as a function of "area" and "moment of inertia" of the rings. As shown the inertia of the ring is the more dependent factor; indicating a significant increase in failure load as the I_R is increased as compared to a minimal increase in failure load as the area of the ring (A_R) is increased. A more important result was that for all cases the code predicted a general instability failure, indicating a failure of the rings to enforce a nodal point even though the ring size was increased by an order of magnitude greater than that predicted by Shanley and Van der Neut. It was therefore concluded that the program presently being used would not predict the correct failure load or skin buckling pattern for the length of shell being considered. The local instability code utilizes smeared ring theory which, as the stiffnesses of the ring are increased do not enforce nodal points but in fact simply stiffen the whole length of the shell with resultant higher failure loads. As reported by Block (Reference 4), the rings must be closely spaced, and additionally the number of rings must approach four or more, before smeared ring theory results approach those predicted by discrete ring theory.

As a result of the inability of the smeared ring code to correctly determine the buckling load and hence the failure to prove the adequacy of the ring stringer stiffened shell design, it was necessary to conduct further analyses using a finite difference code and discrete ring theory. The code selected was the BAMSOC program which being operational at the Langley Research Center was first implemented at Langley to assess its usefulness, and subsequently acquired for use by AVCO.

Using the stringer geometry, stringer pitch ring spacing and shell thickness given in Table 7 for a reference design (selected from Table 4), seven BAMSOC analyses were conducted, varying the "moment of inertia" and the "area" of the rings above and below the baseline values. As this program does not include analysis for buckled skin, such as utilized in local instability code, a reduced modulus of $1.28\ N/cm^2 \times 10^6$ ($1.86\ lbf/in^2 \times 10^6$) and $5.46\ N/cm^2 \times 10^6$ ($7.92\ lbf/in^2 \times 10^6$) was used for E_x and E_y respectively. These were determined by extracting from the local instability code the "beta x" and "beta y" factors which are the reduction factors applied to the skin moduli in the determination of general instability failure load with buckled skins. Table 5 is the input data and resultant failure loads for the seven designs considered, and Figures 20 through 25 are the buckling deformations as constructed from the computed radial deflections.

Cases 1 through 3 are shell designs, where the inertia and area of the ring stiffener is varied so as to encompass the baseline design (Case 2). The results indicate a negligible increase in critical failure load for an increase in inertia by a factor of two (Case 3); and an 11% decrease in critical failure load for a decrease by one half and one third for inertia and area respectively (Case 1). As shown in Figures 20 through 22 the radial buckling deformation indicate buckling of the rings into four circumferential waves.

For Cases 4 through 6, the inertia and area of the rings are increased significantly over the base design and the resultant predicted critical failure loads are substantially higher. However, the deformation patterns, as shown in Figures 23, 24, and 25 indicate ring failure. Case 4 is a four fold increase in moment of inertia with an accompanying one and one half times increase in area; here the critical load has increased from 9543 N/cm (5450 lbf/in) (Case 2) to 10,944 N/cm (6250 lbf/in) with an unsymmetrical radial deformation for N = 3. For N = 4 the axial wave pattern is symmetrical, however, as with all designs the pattern of radial deformation indicates ring buckling. Case 5 is an order of magnitude increase in inertia with an approximately doubling of the area. The critical load has increased to 11,645 N/cm (6650 lbf/in) with a dramatic failure of the rings. Finally, Case 6 is an input of an infinite value for inertia and area; resulting in a critical failure load at 15,322 N/cm (8750 lbf/in) and a dramatic skin buckling failure between rings. The minimum N_x in this case occurred at an N of 1 with of course no buckling of the rings.

The immediate observation from the above analyses is that the results for the baseline Case 2 are not comparable to the results as predicted by the local instability code. The BAMSOC failure load is 9543 N/cm (5450 lbf/in), compared to 7332 N/cm (4187 lbf/in) (see Table 4) from the local instability code. Further analyses, using linear theory with a skin effective moduli as suggested by Peterson (Reference 6), indicated an error in the use of a reduced moduli for only E_x and E_y. Experience by Peterson indicates that it is also necessary to reduce the G_{xy} for the skin also. Table 6 is the repeat of Case 2 including a reduced G_{xy} of .996 $N/cm^2 \times 10^6$ (1.44 $lbf/in^2 \times 10^6$) in lieu of 2.66 $N/cm^2 \times 10^6$ (3.86 $lbf/in^2 \times 10^6$), with the result that the failure load is reduced from 9543 N/cm (5450 lbf/in) to 7442 N/cm (4250 lbf/in). This is very close to the 7332 N/cm (4187 lb/in) failure load predicted by Dickson and Brolliar with buckled skins. However, as before the buckled pattern was indicative of a general instability failure.

The results of the BAMSOC analyses were disappointing, having not proven the premise that a number of sections of shells may be joined together with rings of predicted stiffnesses that will enforce an instability failure in the panels between the rings. The Shanley and Van der Neut equations, if the above analysis is believed, predict ring stiffnesses far below that which are required to enforce panel instability. An insufficient number of cases were run to establish a point at which the rings enforced

a node point, however, the point is academic for the failure load is far in excess of the design load with the probability of an early stress failure occurring. The analysis conducted by AVCO may not have: (a) have paid sufficient attention to the effect of radial restraint in the design of the short length of shells and/or (b) the BAMSOC analysis should perhaps have considered a longer length of shells with more bay lengths so as to reduce the effect of the radial support imposed at the end of the shell.

An alternative explanation to the apparent inconsistency may very well be the incompatibility of the two computer programs used for predicting the shell buckling loads. On the one hand the shell segments were designed using the local instability program which through an approximate manner accounts for skin buckling but uses smeared ring properties. For the complete shell analysis on the other hand a discrete ring program (BAMSOC) without skin buckling effects included was employed. Granted reduced skin properties were used in BAMSOC, but, in truth the effective skin properties are load dependent not to mention the possibility of being mode depend also. Consequently, it is virtually impossible to obtain a one for one correlation between the two approaches if prebuckled skins are employed. Furthermore, the results seem to suggest that a long shell with rings will have a higher buckling load than that predicted for an equivalent shell of only one bay length simply supported at both ends. Granted under special conditions this could occur, but, for this to consistently occur appears slightly unusual. This behavior is readily explained for the analyses conducted using the local instability code, since it utilized smeared ring theory. It is reasonable to assume therefore that above a specific ring stiffness the averaged properties for the rings tend to overshadow the shell properties and hence the apparent increase in buckling load.

For the BAMSOC analyses, employing discrete ring theory, on the other hand no such effect should occur. In fact, an a priori judgment would be that as the ring stiffness increased the shell buckling load would increase, approaching as an asymptote the single bay buckling load, assuming, of course that column failure did not preempt shell failure. Upon a reexamination of the limited BAMSOC results where the ring properties are varied (Table 5) the results tend to favor this conclusion. Note that as the ring stiffnesses are increased the buckling loads progressively increase reaching a limit for infinite rings. One vital piece of data is lacking to support this hypothesis and that is BAMSOC's predicted failure load for the equivalent shell but only one bay in length. If this short shell had a predicted buckling load of 8750 lb/in or greater, then the hypothesis would be substantiated.

Additionally, if this were the case it would allow for the possibility of combining optimized discrete shell segments into a full scale ring stiffened shell.

DESIGN OF PRACTICAL BORON REINFORCED TEST SHELL

As a result of the analyses previously discussed, a shell reference design was selected so that the procurement of the extrusions may be initiated and sub-element tests conducted. The reference shell design is outlined in Table 7, where details of shell geometry and section properties are fully delineated together with the material specifications. The reason for the selection of this particular shell geometry is explained in part by reference to Table 4. Here it is shown that the reference design is that which exhibits a shell failure load above the required failure load of 6566 N/cm (3750 lbf/in), (3000 lb/in plus 25% knockdown factor) and as shown in Figure 17 is of a low weight. This in effect provides an added margin of safety to the design for there is perhaps a lighter weight shell, for example, preliminary design Number 1, which although not supported by the analysis adopted in this program should withstand the required load. Also shown in Figure 17 is a series of designs with even lower weights, however these designs require a stringer spacing of 20.5 cm (8.03 in) which raises the question of the large buckled skin panels possibly affecting the stability of the stringers. Further justification for selection of the baseline design is presented in Figure 26. This is a load index versus weight index plot presented by Peterson (Reference 5) (initially for various all metal shell configurations) on which is positioned the load and weight data for the shell designs discussed previously. Here it is shown that all of the boron reinforced designs are of significantly less weight than the most superior all metal design--hence there is no significant penalty in proposing a conservative design. As shown in Table 7 the baseline design includes a theoretical and selected ring stiffener geometry. The unreinforced design is of less weight, however as one intent of this program was to demonstrate the use of circular boron infiltrated sections and as the theory for ring design was not proven, it was decided to use the section shown, being a double lobed section infiltrated with boron epoxy.

Based upon the reference design shown in Table 7, ALCOA attempted to fabricate the hat stringer, only to find that (at the state of development achieved) it was impossible to obtain the requirement without design changes. The design change was due to the inability of ALCOA to extrude (at the particular time period) a minimum weight stringer, where instead of the seamless extrusion only a thicker section with slits running the full length of each void was possible. Physical details of the resultant stringer and qualification tests are described later in this report, the reason for the discussion here is to describe the effect upon the design and shell weight. The extruded stringer section as received was weighed and two stringer designs formulated, based upon chemical milling to a web thickness of either .063 cm (.025 in) or .101 cm (.040 in). Using the baseline design geometry with revised section properties for the stringer for input to the local instability code, shell failure loads and weights were predicted at various stringer spacings between 10.2 cm (4.03 in) and 20.5 cm (8.06 in).

Table 8 is the calculated weight of the various shell designs and a presentation of the failure loads as computed by the local instability code. The results show that if the aluminum section is chemically milled to a thickness of .101 cm (.040 in) in the webs and flanges, the spacing can be increased to 17.06 cm (6.72 in) before the predicted failure load reduces to below 6566 N/cm (3750 lbf/in). Likewise, for designs where additional chemical milling is utilized to reduce the thickness to .063 cm (.025 in), the stringer spacing may be increased to 15.4 cm (6.07 in). Although this increase in stringer spacing reduces the weight (dt/R) the individual stringer loads and associated stress levels are increased. The problem of load introduction will also be more dramatic, and also the possibility of premature stress rupture prior to instability failure is evident. Also, the wider spacing of stringers with heavily buckled skins may prove a problem for there is very little shell experience with skin buckling at 5% of final design load.

The above variation in design, using two levels of chemical milling and various stringer spacings are presented also in Figure 26 so as to fully assess the impact of the now possible design. As shown by the shaded area the overweight stringer has forced the weight index up to a level with the all metal sandwich design and there is little benefit in changing the stringer spacing, for the analysis shows a reduction in load index with a reduction in weight index. As increased stringer spacing also increases the stress levels (see Table 8) it was decided to establish a final design for fabrication and test based upon least weight for least level of stress in the stringer. Design Number 8, (Table 8) was selected. This is shown in Figure 26, exhibiting less weight than the all sandwich construction and approximately 30% weight savings as compared to the longitudinally stiffened shell. As to the expected failure load of the test shell, the 8934 N/cm 5101 lbf/in) shell instability load derived by the analysis is considered optimistic. It is expected that the highly buckled skin will cause premature local failure of the stringer prior to achieving the stress of 32,894 N/cm^2 (47,696 lbf/in^2) (see Table 8).

The following Table presents the pertinent details of the "as fabricated test shell". The reader is referred to the section on sub-element testing where the selection of this design is confirmed.

AS FABRICATED SHELL DESIGN DETAILS

Shell Thickness	.081 cm	.032 in
Stringer Spacing	10.2 cm	4.03 in
Ring Spacing	61 cm	24.00 in
Shell Weight	6.3 kg/m^2	1.3 lbm/ft^2

Stringer Details

Diameter of Boron Epoxy	.286 cm	.1125 in
Height of Stringer	2.10 cm	.83 in
Thickness of Web	.063 cm	.025 in
EI	14.34 $N\text{-}cm^2$	.50 $lbf\text{-}in^2$
EA	15.61 N x 10^6	3.51 lbf x 10^6

Ring Details

EI	16.29 x 10^6 $N\text{-}cm^2$	.568 x 10^6 lbf-in
EA	15.27 x 10^6 N	3.42 x 10^6 lbf
Diameter of Boron	.381 cm	.15 in

Detail Design of Test Shell

The detail design of the test shell consists of the integration of the theoretically deduced data into the "nut and bolts" of practical hardware. The test shell (as shown in Figure 27) consists of four 24 inch bay lengths. The middle three rings are boron reinforced and the end two rings are solid aluminum hat sections of a design previously used at NASA Langley for other test shells. The top one third of the shell circumference consists of boron reinforced stringers (being the area subjected to compression), while the lower two thirds uses solid hat sections stringers of identical stiffness as the reinforced sections. The skin is divided into five circumferential sections, each being the full length of the test shell with a longitudinal splice at 42°, 126°, 180°, 234°, and 318° from the top centerline. (A clean splice free surface was required in the maximum compression area--0°.) The rings were designed to be roll formed to shape with a splice joint positioned at 90° and 270°, again keeping the top compression surface free from splices and doublers. At each end of the shell a load transfer plate is bolted and riveted to the shell, which is in turn bolted to the attachment ring of the test fixture.

Skin - The skin of the test shell is .081 cm (.032 in) thick 2024-T3. Clad material was selected for superior spot welding to the "bare" 7075 stringers.

Rings - Figure 28 illustrates the extruded ring section which was required to be roll formed and infiltrated. Figure 29 illustrates the extruded ring section that is positioned at the termination point of the load transfer plate; at each end of the shell. Figure 30 illustrates the details of the joint splice at 90^{o} and 270^{o} for each of the two ring designs; being steel plates and angles riveted to the rings and designed to minimize as much as possible the change in flexural stiffness. Attachment of the rings to the shell is shown in Figure 31, in general using .396 cm (.156 in) diameter Cherry-Lock rivets at 1.905 cm (.75 in) spacing except as shown in the area of load transfer and splice plates.

Stringers - Figure 31 presents the as extruded and chemical milled stringers to be used on the top compression surface (21 stringers covering approximately 1/3 of the circumference). These stringers are spot welded to the skin at 1.27 cm (.5 in) spacing (inter-fastener buckling controlled) between rings and load transfer plates--as shown on Figure 32. The exception to spot welding of the stringers occurs at the skin splice areas where an .081 cm (.032 in) splice doubler is inserted between the skin and stringers. Here the skin, doubler and stringer is riveted on final assembly with .396 cm (.156 in) diameter Cherry-Lock rivets.

Load Transfer Area - The load transfer area consists of the first 35.56 cm (14 in) of each end of the shell, made up of a stepped steel plate, an aluminum doubler and special profiling of the stringers to accept large diameter bolts. Figures 33 and 34 illustrate the various details covering the upper, lower, and skin splice areas. The steel plate is attached to the NASA fixture by 1/2 inch bolts, and bolted to the shell. To effectively accomplish load transfer, the steel plate is stepped tapered over a length of 10.8 cm (4.25 in) so as to reduce stress concentration. A further tapering effect is accomplished by an aluminum doubler that projects further into the body of the shell. The aluminum doubler [.101 cm (.040 inch) thick] is sandwiched between steel plate and the skin, and also the end aluminum hat ring. A primary objective of the aluminum hat ring and doubler is to provide maximum membrane restraint to reduce the effect of the eccentric loading.

The detail design of the transfer bay was based on a limit load of 5253 N/cm (3000 lbf/in) and an ultimate load of 7880 N/cm (4500 lbf/in). Using a reserve factor of 1.5, a failure in the shell and not the load transfer area is ensured.

Using an ultimate design load of 7880 N/cm (4500 lbf/in), each 10.2 cm (4.03 in) stringer bay is required to react a total load of 80,953 N (18,200 lbf). Assuming that the total load is transferred into the stiffener, plus doubler, plus skin (with a stress concentration factor of two (2) to satisfy possible stress concentrations) 14 - .475 cm (.187 in) diameter close tolerance bolts, (NAS 464 Type--F_{su} = 95 ksi) provide sufficient single shear strength.

A reserve factor of 0.86 is predicted for the total bearing area (skin, plus doubler, plus stringer flange). This was accepted considering the conservative reserve factor imposed on the design. Additional precautions were observed by spot welding the skin to the stringers between bolts so as to ensure adequate transfer of load to the stiffer boron stringer. The proportion of load conservatively assumed (by ratio of material thickness) to be present in the doubler is transferred to the skin stringer combination via the surrounding 28 - .394 cm (.156 in) diameter rivets. Following conventional practice, the end bolt is increased from .475 cm (.187 in) to .635 cm (.25 in) in diameter. Stress levels in the steel doubler are 24,130 N/cm^2 (35,000 lbf/in^2)

Assuming the full load is transferred into the stringer over an 20.32 cm (8 in) length, the shear stress in the flange of stringer is 31,024 N/cm^2 (45,000 lbf/in^2) and at the interface between the boron and aluminum the shear stress is 1000 N/cm^2 (1450 lbf/in^2). The F_{su} for 7075-T6 boron is 29,645 N/cm^2 (43,000 lbf/in^2) and the ultimate block shear strength at the interface is approximately 2068 N/cm^2 (3000 lbf/in^2).

SUB-ELEMENT TESTING

Evaluation of Slit Extrusions

Due to practical limitations at the time of shell fabrication, the only method by which a hollow hard aluminum stringer could be extruded was in an open condition, to be subsequently folded to shape by a drawing/folding operation. As shown in Figure 31, this fabrication technique produced a longitudinal slit in the wall of each void of the hat stringer; running the whole length of the extrusion. Prior to commitment to fabrication it was required to prove that this slit was not detrimental to the strength of the section.

The first assessment for slit extrusion was the compression test of simple infiltrated tubes, with and without one slit in the wall. The infiltrated tubes were 1.524 cm (.60 in) long, .635 cm (.25 in) OD, and .47 cm (.187 in) ID. The slit was .25 cm (.010 in) wide, cut through the aluminum after infiltration of the boron epoxy. Figure 35 presents the results of the compression tests, where the tube was compressed between two diboride platens. Comparing results between the reference and slit tubes, it is seen that only one of the "slit" tubes exhibited a failure load which was outside the range of scatter in the test loads for the reference. Hence it was concluded that the ultimate (maximum) strength of the tubular area of stringer would not be affected by the slit.

The next series of tests conducted were designed to ascertain the effect of the slit on the typical stringer section where the failure mode would be by local crippling of the flanges. Four, six inch long tri-element specimens were tested in compression with the results as shown in Table 9, and typical failure modes illustrated in Figure 36. One section was tested without slits, the other three sections were slit with .010 inch wide saw through each wall of each void (after infiltration). As shown in Table 9, one "slit" section failed at a boron filament stress in excess of the non-slit section while the remaining two failed at 87% and 77% respectively. The failure mechanism for the slit specimen was a local opening of the slit in each case while for the non-slit section the failure was crippling of the wide flange.

The strictly comparative tests described above indicated that the strength of the infiltrated extrusion is not dependent upon the circumferential homogenity of the aluminum that surrounds the boron. As a result, sufficient confidence in the design was achieved to warrant the procurement of slit extrusion for the boron reinforced stringers. Crippling tests on the slit hat stringers were scheduled as first priority.

Stringer Crippling Tests

To evaluate the ultimate strength of the boron epoxy reinforced hat stringer, two lengths of the extruded stringer were infiltrated and chemically milled in preparation for test. The sections were infiltrated with 325 .014 cm (.0056 in) diameter boron filaments in each void and then chemically milled to a stringer web thickness of .101 cm (.040 in) and .063 cm (.025 in) for each stringer respectively.

The test sections consisted of a 11.43 cm (4.5 in) long section of the stringer, spot welded to a section of a .081 cm (.032 in) 2024-T3 sheet that represented the shell skin. Each end was ground square and parallel and the skin was cut off in line with the edge of the stringer flange. The total width of the specimens were 5.08 cm (2.0 in) for the specimen Number 1 (.040 inch web thickness) and 4.52 cm (1.8 in) for the specimen Number 2 (.025 inch web thickness). The weld spacing for specimen Number 1 was 1.58 cm (.625 in) and 1.27 cm (.5 in) for Number 2. Each specimen was "potted" at each end, in a .95 cm (.375 in) thickness of cerrobend, for support of the thin material while subjected to the compressive load. Axial strain gages were mounted on the exterior surface of the skin, side stringer web and top stringer web, at mid length of specimen and mid width of skin and webs. For each compression test the specimen was mounted in a FGT test machine between two 3.81 cm (1.5 in) thicknesses of diboride. The diboride thicknesses (platens) are required so as to enforce plane strain at the abutted faces--steel platens are too soft with the result that the aluminum is deformed while the boron presses into the steel. The selected load rate was .127 cm (.05 in)/min.

Figure 37 presents the load strain history recorded for test specimen Number 1 and as can be seen the skin buckled at a strain of 2500 μ cm/cm (μ in/in). At this time the stringer flange buckled in sympathy with the skin in wave lengths of approximately the same distance as the width of the specimen. This failure mode was expected for the critical buckling strain for the skin between spot welds is calculated to be 3140 μ cm/cm (μ in/in) (long sides simply supported - short sides clamped) which, of course, is further reduced by free flange buckling effects. Comparisons of the measured and calculated axial stiffness are excellent. The measured EA for the initial section of the load strain curve (up to a level of approximately .4%) was 23 N x 10^6 (5.16 lbf x 10^6). Using a modulus of 20.1 x 10^6 N/cm^2 (30 x 10^6 lbf/in^2) for the boron epoxy, x 10^6 for the 7075 aluminum extrusion and areas measured from enlarged photographs, the axial stiffness (EA) was calculated to be 22.5 x 10^6 N (5.07 x 10^6 lbf) or nearly identical to the measured value. Failure occurred at an axial load of 164,131 N (36,900 lbf) and was precipitated by a compressive failure in one of the reinforced rods near the skin line. An examination of the failure indicated that the boron epoxy rod failed at the location where the skin and flanges were buckled most severely. There was also a slight amount of opening up at the longitudinal slit in this region. At failure the stress

levels were 45,500 N/cm^2 (66,000 lbf/in^2) in the aluminum and 165,470 N/cm^2 (240,000 lbf/in^2) in the boron epoxy. No sign of stringer web buckling was observed in any portion of the test specimen.

The crippling specimen Number 1 (see Figure 38), successfully withstood a compressive load that was in excess of twice the maximum load computed for the stringer when assembled in the shell at a spacing of 10.2 cm (4.03 in). The stringer also remained free of distortion with a near linear load/strain curve up to failure. This test was considered a success, predicting a large level of confidence for the "slit" design and the concept where the stringer is expected to remain unaffected by the highly buckled skins.

Figure 39 illustrates the compressive load versus strain curve for test specimen Number 2, which was chemically milled to a (web) thickness of .063 cm (.025 in). As shown, all curves are indicative of an axial stiffness (AE) of 20.2 N x 10^6 (4.55 lbf x 10^6). If the stiffness of the .081 cm (.032 in) skin is subtracted, this reduces to 17.34 N x 10^6 (3.86 lbf x 10^6) for the boron epoxy reinforced stiffener alone. The calculated AE, (for the stiffener above) using 325 .01424 cm (.0056 in) filaments in each void, is 17.69 N x 10^6 (3.86 lbf x 10^6). Failure in the specimen occurred at a load of 124,544 N (28,000 lbf) with prior local buckling of the skin flange. The skin deformed (buckled) at an approximate load of 48,928 N (11,000 lbf). However, as shown in the post test photographs, Figure 40, the webs of the stiffener between the "lumps" of boron (although starting to yield at 80,064 N (18,000 lbf) remained elastic with no sign of permanent set. The final failure of the hat section occurred at .065% strain, with a "load drop-off" as the skin buckle enlarged to include the stringer flange. The stringer itself remained undamaged whereas shown in Figure 41 (a section through the test specimen) the hat section is intact with no sign of failure in the boron or sign of opening of the slits.

It is concluded that the boron reinforced hat section as designed either with a .063 cm (.025 in) or .101 cm (.040 in) web thickness, is satisfactory for inclusion in the shell design--having exhibited failure strain and failure loads in excess of the design load.

Load Transfer

At each end of the test shell a load introduction mechanism is employed to transfer the load from the test fixture into the body of the shell. The transfer design consists of NASA supplied ring attachment fixture, bolted to a stepped tapered plate and a doubler, that are in turn bolted and riveted

directly to longitudinal stringers and skin. Figure 42 is a pictorial presentation of the load transfer area, being a typical cross-section at each end of the shell. At the top and bottom centerline of the shell there is calculated to be an axial load of 5253 N/cm (3000 lbf/in), derived from the design bending load of 157 N-cm x 10^6 (13.96 in-lbf x 10^6). With a stringer spacing of 10.25 cm (4.03 in) it is implied that the test specimen must withstand an ultimate load of 80,064 N (18,000 lbf).

As shown in Figure 42 the load transfer mechanism consists of a number of separate elements spliced together, with the result that there exists an obvious load eccentricity that is difficult to model in a test specimen, while at the same time maintaining the correct shell restraint and hence the correct load distribution. By virtue of the rigidity of the NASA test fixture the load path originates at the median of the test fixture ring flange, which is offset from the shell at the neutral axis of the shell/stringer combination. An eccentricity of 1.01 cm (0.4 in) results, and as discussed previously the resultant bending moment is intended to be reacted principally by local shell membrane forces and ring restraint. Characteristically, the eccentricity "decays" within a few inches of the end of the shell, where the combined membrane reaction of the shell skin, the stepped steel ring and the hat ring will significantly reduce the bending loads. With the sub-element test of a short segment of the shell, the membrane restraining forces will not be evident; hence non-representative bending forces will be present throughout the length of the test specimen.

In an effort to reduce the effect of the eccentric load, the first test specimen was modeled as shown in Figure 43. The fixed end was intended to represent a position just inside the hat ring stiffener, where it was considered that a plain strain condition would exist in the shell. In lieu of representing the ring attachment fixture at the other end of the specimen a simple support was specified, for any fixation (such as attachment by the double line of bolts through the stepped plate and ring) would induce a severe bending stress in the plate such that without the membrane restraint, an early failure would occur. The length of the specimen was specified so that the selected length 'a' (Figure 43), would theoretically enforce a zero bending moment at the fixed end. This was calculated from the simple static equilibrium equation, using the relative stiffness of the plate and stiffener. The resultant test was intended as the first of several where the bending moment at the fixed end would be varied (by changing length 'a') from zero to positive and negative. In this manner it was intended to examine the two possible extremes of stress distribution.

The detail design of the first test specimen is presented in Figure 44. The width of the stepped plate was equivalent to the 10.16 cm (4.0 in) stringer spacing and the length 'a' was set 6.35 cm (2.5 in). At the stringer end of the specimen the stringer and skin were cast in a 3.3 cm (1.3 in) length of cerrobend, and the end ground square and parallel. The thickness of the stringer web was chemically milled to .101 cm (.04 in).

Load strain curves for the first specimen are presented in Figures 45 and 46. Figure 45 presents strain readings for a pair of back strain gages (Number 4 and Number 8) mounted on the steel tabs just short of the hat section stiffener. Bending of the tab was expected and is in evidence from inception of the load. The load strain behavior of the stringer at the potted end is presented in Figure 46. Back to back gages (Number 1 and Number 5) were used and the results show that bending is occurring. These gages were located 1.4 inches from the potted end, and if the initial results (to 40,000 N [9,000 lbf] axial load) are extrapolated to the end of the specimen, one would predict that the bending stresses at the potted end are essentially zero as planned.

The test specimen behaved as desired up to an axial load of 40,000 N (9,000 lbf) where stresses in the stringer flanges were approximately 18.6 $N/cm^2 \times 10^6$ (27 $lb/in^2 \times 10^3$). At this stress level the stringer flanges and the skin between the flanges buckled locally in the area adjacent to the potting (see Figure 43), imposing a shift in the neutral axis towards gage 1. This is evident by the sudden reversal of gage 1 shown in Figure 46, implying a change from compression to tension due to an increase in bending. Gage 5 cannot be relied upon above 40,000 N (9,000 lbf) because of the local skin buckling. Upon unloading, the specimen returned to its original shape and suffered no permanent damage with the exception of minor buckling of the stringer flanges and skin at the potted end (see Figure 43).

As shown in Figure 43 the condition of the first specimen at the termination of the test was such that the excessive bending of the stepped plate was resulting in an undesirable and non-representative test condition. It was impossible to achieve the ultimate design load of 80,064 N (18,000 lbf) unless modifications were incorporated. Accordingly the specimen was retrieved for further tests with the steel plate reduced in length (length 'a', Figure 42) from 6.35 cm (2.50 in) to 2.54 cm (1.0 in), with the minor flange buckling at the potted end "dressed" out.

In the retest of the first load transfer specimen (without instrumentation) the test load reached a level of 93,408 N (21,000 lbf) prior to failure. This corresponds to an equivalent running load of 9106 N/cm (5200 lbf/in); well above the design ultimate load of 7880 N/cm (4500 lbf/in) required for stringer spacing of 10.23 cm (4.03 in). Very little bending was in evidence in the tab during the test and the failure was primarily a shear crippling in the stringer near the potted end (see Figure 47). At the maximum load, calculated axial stresses in the stringer were in the order of 32.4 $N/cm^2 \times 10^3$ (47 $lbf/in^2 \times 10^3$) in the aluminum and 97.2 $N/cm^2 \times 10^3$ (141 $lbf/in^2 \times 10^3$) in the boron epoxy. Since no instrumentation was used for this test the additional bending stresses were not obtained. The slitted section of the extrusion was slightly deformed, opening approximately .05 cm (.02 in).

As a result of the first two tests of load introduction specimen, it was concluded that the specimen had successfully demonstrated the capability for sustaining the maximum load. With non-representative and certainly conservative test boundary support conditions, one specimen had withstood 83% of the design ultimate load and the other 116%. However, further tests were required for the stringer was subsequently required to be chemically milled to a web thickness of .063 cm (.025 in) and there was some concern for the skin buckling causing early failure.

For the next test specimen the stringer web thickness was chemically milled to a thickness of .063 cm (.025 in) and the flange of the stringer trimmed back to a total width of 5.08 cm (2.0 in)--so as to be more representative of the final design. The test procedure was as for the previous specimens, using a simple support at the stepped plate end and fixed at the other end. As in the previous tests, the steel plate flexed away from the stringer and there was skin/flange buckling adjacent to the cerrobend. However, unlike the previous two specimens this specimen failed by tearing the stringer away from its flange as shown in Figure 48, at a load of 73,392 N (16,500 lbf).

As recorded in Figure 49, the readings for the back to back gages on the steel plate follow the pattern as indicated for the first two tests, recording bending but with a lower magnitude flexure in this test because of the reduction in length of the steel plate. The gages positioned at the top of the specimen (just inside the cerrobond) indicated some section bending - however, significantly less than the first test specimen. The axial stiffness curve (AE) calculated for the section is shown on Figure 49, and is reasonably close to gage Number 3 which was placed at the neutral axis. Gage 3 reached a strain level of 3,400 μ cm/cm (μ in/in) prior to failure. Gage Number 6 indicated non-linear behavior subsequent to a strain level of 2,400 μ cm/cm (μ in/in) due to elastic buckling of the skin between stringer flanges. Dial indicator readings at midway between the two last bolts (see Figure 48) indicated a maximum deflection of .058 cm (.023 in).

As a result of this test, some doubt was expressed as to the strength of the .063 cm (.025 in) thick flange of the stringer. Although the failure load was in excess of the shell test load, it was considered advisable to continue the test series, with a support condition that is more representative of the membrane restraint.

Figure 50 illustrates the test fixture fabricated to facilitate the "buttressing". The fixture is mounted on the base of the test machine with a "vee" groove to support the steel plate and a clamped "round nosed bar" to provide the buttress. Installed as shown in the fixture is test specimen Number 4 which was tested to failure at a load of 73,392 N (16,500 lbf). Failure was indicated by a load drop off, precipitated by a permanent skin/stringer buckle between the end of the steel plate and the "potting". In the failure area the flanges had not been cut down to the minimum width, for the design now called for rivets with large edge

distances. As seen in Figure 51 the deformation pattern is similar to the previous test with reduced bending in the steel flange and a maximum deflection at the dial gage of .109 cm (.043 in) (away from the test fixture). All gages except that on the aluminum skin and one of the side web gages read off values that were very close to the previous test. The skin gage (Number 3) indicated buckling at a strain level of 3100 μ cm/cm (μ in/in), suggesting that the buttress support had precluded some of the excessive deformations as compared to the previous specimens where buckling occurred at lower total strains.

Test Number 4 was considered a partial success, at least precluding the "tear away" failure mode, but not reaching the ultimate design failure load. Failure occurred in the stringer flange with no sign of deformation in the area of the boron rod. The maximum test load sustained (using a stringer which was chemically milled to .063 cm (.025 in) web thickness) was still only 73,392 N (16,500 lbf). A further test was planned with additional buttressing.

Test Number 5 is shown in the sequence of photographs of Figure 52. Two buttress positions were employed and a failure of 82,288 N (18,500 lbf) was recorded. Again the failure was precipitated by the flange/skin buckling but this time a permanent "bow" was induced along the total length of the stringer. The top dial indicator measured a maximum deflection of .119 cm (.047 in) at 80,064 N (18,000 lbf) load, recovering to an approximate permanent deformation of .076 cm (.030 in)--away from the fixture. However, the boron rods and the slits were unaffected. Figure 53 illustrates the strain gage reading for the steel plate, which when compared to the previous tests indicate a reasonable success in reducing the bending stresses. However, it appears that the induced bending was still sufficient to cause tensile stresses on one surface. Gage readings for the aluminum area were disregarded due to erratic readings. Unfortunately, the coating provided was insufficient to protect the gages from being affected by the cerrobond casting.

As a result of the five load introduction tests conducted, it is concluded that the design is satisfactory for inclusion in the test shell. Of the five tests conducted three were representative of the final shell design, with representative rivet and bolt spacing, and stringer geometry. Of these three tests the lowest failure load was 73,392 N (16,500 lbf) and the highest 82,288 N (18,500 lbf). The first is representative of a shell line load of 7179 N/cm (4100 lbf/in) and 18,500 lbf is representative of 8055 N/cm (4600 lbf/in). That is 91% and 102% respectively of the 7880 N/cm (4500 lbf/in) load set as the ultimate design value for the load transfer for design. The actual maximum line load expected in the test shell is 5253 N/cm (3000 lbf/in) - so it is evident that failure in the joint will not occur prior to an instability failure. Other points in favor of accepting the design are: first, the test boundary conditions imposed are in excess of the support condition expected in the shell; second, the failure always occurred at the unsupported flange area which in the shell will

be supported by the Number 1 and Number 4 ring stiffener; last but not least, at no time was there any evidence of boron rod pull out or any indication of a shear failure between the boron and the aluminum or any shear failure in the aluminum stringer.

FABRICATION OF THE TEST SHELL

Fabrication and assembly of the test shell was completed by Avco, using Alcoa produced extrusions and Avco boron filament. The various tasks involved in the shell completion are discussed as follows:

Extrusions

There were four aluminum extrusions purchased from Alcoa, two for the stringers and two for the ring stiffeners. The solid extrusions (end hat ring and hat stringers for the lower surface) were no problem to fabricate being of conventional design. The hollow ring stiffener (Figure 31), although unconventional in general industrial practice was by now common practice for Alcoa using the softer alloy 6005-T6, however, the hollow 7075-T6 hard aluminum extrusion required was still considered to be in the "research and development" stage.

The requirement for the hollow 7075-T6 stringer, in term of thicknesses, etc., have been outlined previously being a relatively slim cross-section, web thicknesses as thin as .063cm(.025in), and minimum volume of material around the voids. Alcoa could not promise a seamless extrusion as they were producing for the ring stiffener and in lieu of undertaking the further development necessary to produce a seamless extrusion, it was decided to use a "slit" extrusion--produced by extruding the shape "open" and subsequently draw folding the shape closed. Figure 31 was the result of a number of changes in thicknesses and tolerances required by Alcoa in order to satisfactorily produce the basic hat stiffener, which was to be chemically milled to the final thickness. The disappointing requirements from Alcoa were the thicknesses of material required to ensure a satisfactory folding of section--to obtain the required roundness of the hole and minimum width of the slit. A groove in the section was required at each fold line and a certain thickness of material around the hole required to ensure correct folding. As shown in the photograph, Figure 41, the section is obviously heavy, and as subsequently proven by Alcoa, a seamless hard aluminum extrusion would be of more uniform thickness and hence produce a lighter weight shell.

The two extrusions required to be infiltrated were prepared for installation of the boron epoxy. The six semi-circular tee rings were roll formed to the required radius and, as shown in Figure 54, clamped to the accurate profile on an aluminum plate assembly. 425, .014cm(.0056 in) diameter filaments were installed in each void of the tee section, infiltrated with epoxy resin and cured. The cure cycle followed the conventional Avco procedure of four days at room temperature (clamped to the plate assembly) and four hours at 388.8°K(240°F). This cure cycle was a procedure developed to minimize residual stresses in the constituent parts. The hollow hat extrusions were prepared for infiltration and chemical milling by sealing the "slits" with an epoxy (Figure 55). Many fillers were evaluated as well as flash welding (Figure 56), however, an epoxy system proved to be more acceptable. Twenty-one stringers were installed with 325 filaments in each of the four holes. The epoxy resin was infiltrated simultaneously into the four holes, and cured as per the normal procedure. Each of the 21 extrusions (plus spares) were chemically milled by the requirement of Figure 31. The four half ring, all aluminum, extrusions were roll formed to shape. All roll forming operations required the fabrication of special steel rolls for each shape.

Stepped Taper Load Transfer Ring

The 30.4cm (12 in) wide 195.6cm (77 in) diameter steel load transfer ring was fabricated. A 30.4cm (12 in), 1.58cm (.625 in) thick steel plate was purchased and rolled into semicicular sections. The half circles were welded together and further rolled to accomplish a near as possible circular shape. Subsequent machining in a large vertical turret lathe (See Figure 57) on both the inside and outside surfaces accomplished the required thicknesses and dimensions ready for assembly to the end ring fixture.

Test Shell Assembly

The assembly procedure adopted for the shell was: the subassembly of five segments of the shell skin and stringers, subassembly of the rings in a special circular jig, install the steel load transfer rings onto the NASA attachment rings, and then install the components in a special steel fixture that would ensure straightness and roundness.

The 5 skin segments were assembled by spot welding the stringers to the skin, (Figure 58). A special fixture was fabricated to hold the panels in a circular shape to avoid problems with subsequent forming. The end steel rings were bolted to the NASA rings and assembled in the steel rig, jigging them horizontal, square, and parallel using optical equipment (See Figure 59). The 5 rings were subassembled on special aluminum forms to ensure the correct profile.

The final assembly was accomplished by pilot drilling in place all 5 skin quadrants with the splice plates, doublers, and rings in position. After de-burring all elements, the final assembly was accomplished without problem except for a shimming requirement on the compression surface. A maximum bow was observed of .152cm (.060 in) over the total length of the shell, measured on the outer surface of the boron reinforced stringers. The bow was corrected by placing tapered shims between the rings and the skin panels.

Figures 60 through 65 illustrate various views of the completed shell in its assembly fixture. The shell and fixture were delivered to NASA Langley for test.

As Measured Weights of Elements of the Shell

Table 10 is a recording of the weights of the rings drilled ready for assembly, including the weight of the splice plates angles and bolts.

The weight of the compression panel (324^{o} to 60^{o}), inclusive of 13 stringers and skin was measured to be 26.7kg (59.06 lbm). Making an allowance for additional material incorporated for skin splices and load transfer, a weight of 26.13kg (57.62 lbm) is calculated for a 285.75cm (112.5 in) by 133.1cm (52.4 in) boron reinforced panel. This reduces to a weight of the compression panel of 6.88kg/m^2 (1.41 lbf/ft^2).

DELIVERABLE SUB-ELEMENT TEST ITEMS

In addition to the shell, Avco was required to deliver to NASA several small sections that are representative of the shell construction. Five 25.4cm (10 in) long x 5 stringer wide boron reinforced panels were fabricated, using the identical construction proposed for the compression surface of the shell. In addition, 2, -5 stringer wide load transfer test sections were fabricated. These were identical in cross-section to the Avco test specimen number five. The seven panels were delivered to NASA for test.

ESTIMATE OF WEIGHT OF FULL SCALE INTERTANK SHELL

Based upon the results of and the experience gained from the design and fabrication of the half scale shell, a preliminary design for the full scale shell was prepared. As in the prototype shell only an even spacing of stringers was considered, with two pitches selected (i.e., 10.23 cm (4.03 in) and 20.5 cm (8.06 in). Using hat stringers spaced closer than 10.23 cm (4.03 in) was not considered practical and the concept of pre-buckled skins precluded stringer spacings greater than 20.5 cm (8.06 in).

Full scale shell designs were generated using the same approach as was employed for the design of the test shell. Parametric results for the two stringer spacings are presented in Figure 66, in terms of shell weight versus skin thickness, and as expected these curves exhibit the same trends as presented earlier--minimum weight for minimum skin thickness. Closer examination of the range of design postulated by these curves led to the selection of the full scale design. The full scale shell consists of shallow boron reinforced hat stringers, (see Figure 67) spaced at 10.23 cm (4.03 in), with a .1016 cm (.040 in) thick skin and rings spaced at 60.96 cm (24 in). In making this selection all designs with 45.7 cm (18 in) ring spacings were eliminated because the stringer depths required were too shallow. The 60.96 cm (24 in) ring spacing designs represented a reasonable lower limit on stringer depth and for ring spacings above 60.96 cm (24 in) stringer section were fabricable but, as shown in Figure 66, they exhibited higher weights.

The curves of Figure 66 indicate that the shell weight is directly related to the skin thickness with the thinner skin gages resulting in the lowest weights. In spite of this trend, a slightly thicker skin thickness of .0106 cm (.040 in) was selected. The rationale for this selection is based upon practical considerations, where it was observed that during the fabrication of the prototype shell (with .081 cm (.032 in) thick skins) difficulty was experienced in preventing oil canning. As a result, thicker skins were recommended for any future shells. The final choice for a respectable skin was either .1016 cm (.040 in) or .127 cm (.050 in) working with standard gages. There was some concern about selecting any standard gage above .127 cm (.050 in) since it would tend to buckle at higher stress levels, such that its buckling could interact with the overall shell buckling. Shell weight considerations finally led to the selection of the .1016 cm (.040 in) skin over the .127 cm (.050 in) thickness.

As for the stringer pitch, the 10.23 cm (4.03 in) spacing with .1016 cm (.040 in) skins was compared to the 20.5 cm (8.06 in) spacing with .127 cm (.050 in) skins, the minimum which appeared acceptable at the larger spacing, and it was observed that the closer stiffener spacing gave the lighter weight. On the basis of cost effectiveness however, the larger stiffener spacing would be less expensive to fabricate with fewer stiffeners as well as containing approximately 18% less boron epoxy reinforcement.

The factor which led to the selection of the closer stiffener pitch was simply some apprehension about using prebuckled skins on an 20.5 cm (8.06 in) spacing.

As shown in Figure 26 the weight of the full scale shell at 5.27 kg/m^2 (1.08 lbm/ft^2) is presented as a function of load/weight index. Note that the point is very close to the all metal sandwich design - exhibiting similar weight savings as the test shell.

APPENDIX A - ANALYTICAL METHODS UTILIZED

The design optimization of the reinforced ring/stringer stiffened shell progressed through three distinctive stages; beginning with stringer design, then to instability of the stringer stiffened shell and concluded with the optimization of the complete ring/stringer stiffened shell. For each stage of the design, computer programs were employed in order to make extensive parametric studies. In the following sections the basic features of the programs are presented accompanied by a brief discussion on the rational behind their selection.

Reinforced Stringer Design Program- Figure A1 illustrates the theoretical stringer geometry considered, being four rods placed at the four nodes of a hat shaped stringer. The section was defined to be 'h' wide and 'h' high with a flange width of h/2. The thickness of the web was a common thickness throughout, such that a common crippling stress would exist for the unattached webs (2 vertical and 1 horizontal). The width to thickness ratio for web instability was considered to be equal to h/t and the skin attachment flange was considered to be unaffected by local considerations.

Using the theoretical section discussed above a computer program was formulated that determines the minimum weight hat section for a given load, length and a volume of boron epoxy equally distributed between the four rods. An equivalent axial modulus was assumed for the aluminum sheathed rod, being directly proportional to the ratio of the axial stiffnesses of the constituent parts (boron epoxy rod and aluminum tube). The boundary conditions imposed were simply supported ends (pin jointed Euler column), and simply supported edges for each section of the stringer webs (local crippling). The pin jointed boundary conditions stipulated for the stringer is acknowledged to be conservative, in the sense that support from the shell skin will increase the critical failure load. However, as in this shell design the skin will buckle at extremely low loads, the transverse restraint (membrane) normally imposed by the skin will be significantly reduced. However, there is a concern for imposed stress levels, where the stress levels predicted for a pin ended simply supported column will be lower than the critical stress for a column with some support from skin membrane effect (column on a spring support). So as to ensure a reasonable stress in the final design, it was decided to ensure that the predicted stress levels in each one of the family of minimum weight stiffeners would have a reasonable margin of safety as compared to the yield stress of the aluminum.

The program was written such that given a design load, column length and allowable aluminum stress level, the computer determines the weight per unit length of the stringer and the volume of boron required. By varying the allowable stress level and plotting the weight versus volume of boron (for each load and length combination) the results may be scanned to determine the actual minimum weight stringer. Also determined by the computer are the respective stiffnesses, areas, etc., in preparation for the input to the shell instability program. Using the computer program described it is possible to generate a family of minimum weight stringers (and their associated properties) that will satisfy a range of end loads expected. It is also possible to evaluate the economical use of the boron epoxy.

Shell Local Instability - Optimization of the basic shell geometry was accomplished using a program developed by J. Dickson and R. Brolliar [A1]. This program treats the general instability under axial compression and lateral pressure of a variety of shell geometries ranging from monocoque, stringer stiffened, ring stiffened, ring and stringer stiffened, and sandwich shells. Since, the program does not specifically handle buckling due to pure bending, the design bending moments were converted to an equivalent axial compressive load at the point of maximum stress, and this was used for design purposes. Normally, knockdown factors of between 40% to 60% are used for theoretical buckling predictions of shells (subjected to axial compression) to bring them in line with test data. However, a lesser factor of 25% was used here, since the available data tends to indicate that the predicted results are in closer agreement for shells when subjected to pur bending.

As with many recent shell codes this program [A1] uses classical small deflection shell theory, accounts for eccentric stiffening by averages the elastic properties, neglects prebuckling deformations and assumes simply supported end conditions. The feature that made this program attractive for the current applications, was that it employed a method for handling local buckling of the skin between adjacent stringers before onset of general instability. This is accomplished by reducing the stiffness properties of the skin as a function of the two principle strains. These reduction factors are determined using the method developed by Van der Neut [A3] for post buckling behavior of simply supported flat rectangular plates. In the program, shell buckling loads as a function of wave number are derived after a series of iterations which adjust the reduction factors, until the principle strains coincide with the calculated buckling load. Reference A2 presents a comparison of predicted and test results for several classes of shells, but of particular interest here are comparisons obtained for shells

with prebuckled skins tested in pure bending in a similar manner to the present design. These results are shown in Table A1 were taken from Reference A2 and are typical of the designs planned for evaluation in this program. The cylinders tested were divided into two groups, differentiated by stringer spacing. The b/t ratios of 125 and 200 for groups I and II respectively were such that local buckling occurred early in the loading history of each shell.

The experimentally determined values are shown in the column labeled N, and represent the average running load calculated at the point of maximum bending stress. Two sets of predicted results are presented; the first set, N (a), were determined without corrections for buckled skins and are well above the experimentally determined values; whereas, the second set of values, N (b), account for the reduced skin stiffness due to local buckling and compare very well with the experimental results. The only exception to this is cylinder 4-1 which is a second analysis of cylinder 4, considering only a shell segment between rings (i.e., 45.7cm (18 in). This analysis was conducted to see if the program would predict the same buckling load for both cases since it was noted in Reference A3 that unlike the others, cylinder 4 failed by panel instability. One reason offered for the higher buckling load predicted for cylinder 4-1 is that in the analysis of this cylinder no allowance was made for ring compliance which if included would reduce the buckling load to some extent. Admittedly, the measured axial loads given in Table II were determined from the applied bending moment using linear theory. In actuality if the shells were treated in pure bending; then at the onset of skin buckling the linear theory should be corrected to account for both the reduced stiffness of the skin and the corresponding shift in the shell neutral axis. This would tend to change the correspondence between the predicted and measured results. However, since the test setup enforced a rotation about the shell major diameter and did not allow for the shift in N. A. the approximation obtained by the linear theory is warranted. Also, since the shell length was only of the order of 2 diameters this end effect cannot be discounted.

Using this program short shell segments, equivalent in length to the ring pitch, were optimized relative to skin gage, stiffener pitch and stiffener size. Stiffeners used in this phase were selected from the array of optimum sections determined from the stiffener optimization program.

Shell General Instability - Due to the inadaquacy of the Dickson and Brolliar code for determination of general instability with discrete rings s computer program developed by L, K. Chang, and M. F. Card (BAMSOC I); was utilized. Although this program was written to predict

the thermal buckling of orthotropic, multilayered, stiffened cylindrical shells , it also has the capability for predicting the buckling loads due to axial compression. In addition to including eccentricity of layers and stiffeners, and prebuckling deformations, this program is sufficiently general to account for discrete rings. With the rather large pitch contemplated for the hybrid shell design the averaging or the ring properties was not considered adequate, consequently the discrete ring theory in this BAMSOC Program provided the needed alternative. This program completed the design cycle by making it possible to combine the previously optimized shell segments with rings and parametrically evaluate the various designs as an integral unit. The one problem with this code was that it did not allow for local panel instability prior to general instability failure. This conditions was corrected by taking the reduction factor obtained from the Dickson-Brolliar Code for local instability and applying these corrections to the skin properties prior to input to the BAMSOC Program.

APPENDIX B

CONVERSION OF U.S. CUSTOMARY UNITS TO SI UNITS

The international system of units (SI) was adopted by the Eleventh General Conference on Weights and Measures, Paris, October 1960 (Reference 7). Conversion factors for the units used herein are given in Table B-1.

Table B-1. - Conversion of U.S. Customary Units to SI Units

Physical Quantity	U.S. Customary Unit	Conversion Factor[a]	SI Unit
Length	Inch (in)	0.0254	Meter (m)
Mass	Pound mass (lbm)	0.4536	Kilogram (kg)
Load	Pound force (lbf)	4.448	Newton (N)
Density	Pound mass/inch^3 (lbm/in^3)	27,680	Kilogram/meter^3 (kg/m^3)
	Pound mass/foot^3 (lbm/ft^3)	16.02	Kilogram/meter^3 (kg/m^3)
Load intensity	Pound force/inch (lbf/in)	175.13	Newton/meter (N/m)
Modulus, stress, pressure	Pound force/inch^2 [psi (lbf/in^2)]	6,895	Newton/meter^2 (N/m^2)
Temperature	Fahrenheit degree ($^\circ$F)	$(t_F + 460)\ 5/9$	Kelvin degree ($^\circ$K)

[a] Multiply the value in U.S. customary units by the conversion factor to obtain the value in SI units.

Prefixes to indicate multiples of units are as follows:

centi	(c)	10^{-2}
kilo	(k)	10^3
mega	(M)	10^6
giga	(G)	10^9

REFERENCES

1. Paul A. Roy, John A. McElman, and Jim Henshaw. "Development of Lightweight Aluminum Panels Reinforced By Boron-Epoxy Infiltrated Extrusions.

2. Shanley, F. R. "Weight Strength Analysis of Aircraft Structures", Second Edition, Dover Publications, Inc.

3. NASA T.N. D-1510, 1962, Van der Neut, "General Instability of Orthogonally Stiffened Cylindrical Shells".

4. NASA T.N. D-3351, David L. Block, "Buckling of Eccentrically Stiffened Orthotropic Cylinders Under Pure Bending".

5. NASA T.N. D-5561, James P. Peterson, "Buckling of Stiffened Cylinder in Axial Compression and Bending - A Review of Data".

6. NASA T.N., 4114, James P. Peterson, "Weight Strength Studies of Structures Representative of Fuselage Construction".

7. Committee On Metric Practices: ASTM Metric Practice Guide, National Bureau of Standards Handbook 102. U.S. Department of Commerce, March 10, 1967.

A1. NASA CR-1280, J. N. Dickson and R. H. Brolliar, The General Instability of Eccentrically Stiffened Cylindrical Shells under Axial Compression and Lateral Pressure.

A2. Card, M. F., and Jones, R. M., "Experimental and Theoretical Results for Buckling of Eccentrically Stiffened Cylinders," NASA TN D-3639, 1966.

A3. Card, M. F., "Bending Tests of Large-Diameter Stiffened Cylinders Susceptible to General Instability," NASA TN D-2200, 1964.

TABLE 1

MINIMUM WEIGHT STRINGER DESIGNS

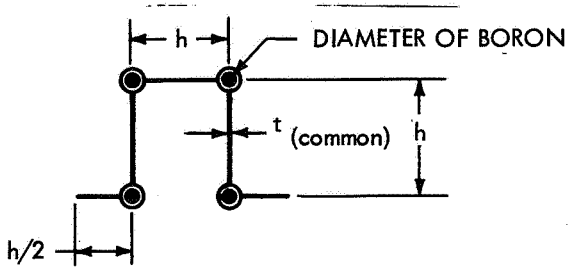

Load	Length		(h)		(t)		Dia. Boron	
Newtons	cm	(in)	cm	(in)	cm	(ins)	cm	(in)
53,000 (12,000 lbf)	46	18	1.90	.75*	.063	.025*	.366	.144
	61	24	2.43	.96	.074	.029	.368	.145
	91.4	36	3.07	1.21	.081	.032	.439	.173
107,000 (24,000 lbf)	46	18	2.14	.84*	.079	.031	.472	.186
	61	24	2.74	1.08	.097	.038	.467	.184
	91.4	36	3.33	1.31	.097	.038	.599	.236
160,000 (36,000 lbf)	46	18	2.34	.92*	.094	.037	.526	.207
	61	24	2.87	1.13	.107	.042	.561	.221
	91.4	36	3.58	1.41	.112	.044	.531	.209

*See Text.

TABLE 2

DETAILS OF SHELLS SELECTED AS PRELIMINARY DESIGNS

	Units	No. 1	No. 2
Shell Thickness	cm	.05	.05
	in	.02	.02
Ring Spacing	cm	61.0	61.0
	in	24.0	24.0
Stringer Spacing	cm	10.2	20.5
	in	4.03	8.06
P (Crit Strg)	Newtons	36,900	85,400
	lbf	8,300	19,200
I_S eg	cm^4	1.99	4.58
	in^4	.048	.110
A_S eg	cm^2	1.70	3.16
	in^2	.27	.49
H_S (1)	cm	2.21	2.67
	in	.88	1.05
DB_S (1)	cm	.314	.43
	in	.125	.17
t_S (1)	cm	.062	.089
	in	.025	.035
Axial Stress in Al. Stringer	N/cm^2	$\simeq$ 24,100	$\simeq$ 27,600
	$lbin^2$	$\simeq$ 35,000	$\simeq$ 40,000
Shell Weight (No Rings)	kg/m^2	4.05	3.66
	lbm/ft^2	.83	.75

(1) See Table 1.

TABLE 3

RING DESIGNS AS DERIVED FROM "SHANLEY AND VAN DER NEUT" EQUATIONS

Ring Spacing (l_R)		Stringer Spacing (S_s)		Shell Thickness t		I_S eg		Van der Neut (1) $A_R = \frac{4\pi^2 R^2 I_{(eg)}}{L^3_R \, 10^7 \, d_s}$				Shanley (2) $I_R = \frac{4\pi C_F \, N_x \, R^4}{L_R \, 10^7}$		Selected Ring Designs							
														I_R		A_R		Apprx $\bar{x}$ (3)		Weight		Ring Design No. (3)
cm	in.	cm	in.	cm	in.	cm^4	$in.^4$	cm^2	$in.^2$	cm^2	$in.^2$	cm^4	$in.^4$	cm^4	$in.^4$	cm^2	$in.^2$	cm	in	kg/cm	lbm/in.	
91.4	36	10.2	4.03	.025	.01	5.74	.138	.25	.04	.974	.151	.56	.014	1.19	.029	.97	.15	2.79	1.10	2.77	.0155	5
				.050	.02	3.83	.092	.126	.02	.645	.100			.58	.014	1.03	.16	1.52	.60	2.32	.013	4
				.081	.032	1.50	.035	.063	.01	.245	.038			.58	.014	1.03	.16	1.52	.60	2.32	.013	4
91.4	36	20.5	8.06	.025	.01	11.6	.28	.27	.043	1.97	.306	.56	.014	1.66	.04	2.32	.36	1.90	.75	5.09	.028	2
				.050	.02	9.2	.22	.215	.034	1.54	.240			.83	.02	1.55	.24	1.90	.75	3.21	.018	3
				.081	.032	6.24	.15	.145	.023	1.06	.164			.83	.02	1.06	.165	1.90	.75	2.50	.014	4
61	24	10.2	4.03	.025	.01	2.66	.064	.38	.067	1.53	.237	1.19	.0287	1.25	.03	1.58	.245	1.90	.75	3.39	.019	3
				.050	.02	2.08	.050	.33	.052	1.19	.185			1.66	.04	1.19	.185	2.79	1.10	2.77	.015	4
				.081	.032	1.50	.036	.23	.037	.85	.132			.83	.028	.97	.150	2.79	1.10	2.77	.015	5
61	24	20.5	8.06	.025	.01	5.41	.130	.27	.068	3.10	.48	1.19	.0287	1.66	.04	3.22	.50	1.90	.75	5.0	.028	1
				.050	.02	4.58	.110	.36	.057	2.64	.409			1.66	.04	3.22	.50	1.90	.75	5.0	.028	1
				.081	.032	3.33	.080	.438	.042	1.74	.269			1.66	.04	2.32	.36	1.90	.75	4.2	.023	2
								(5)		(4)												

1. Van der Neut - Ref. 3
2. Shanley - Ref. 2
3. See Figure 18
4. Modified Results - see text
5. Original Results - see text

TABLE 4

PREDICTED FAILURE LOAD FOR RING/STRINGER STIFFENED SHELLS – 1.82 m (72 in.) LONG. LOCAL INSTABILITY CODE

Ring Spacing		Stringer Spacing		Skin Thickness		Critical Failure Load-Nx		Number of Axial 1/2 Waves	Number of Circumferential Waves
cm	ins	cm	in	cm	in	N/cm	lbf/in	M	N
61	24	10.2	4.03	.025	.01	3,080	1,759	1	3
61	24	10.2	4.03	.050	.02	5,481	3,130 (1)	2	4
61	24	10.2	4.03	.081	.032	7,332	4,187 (3)	2	4
61	24	10.2	4.03	.10	.040	8,067	4,607	2	5
61	24	10.2	4.03	.16	.063	9,752	5,569	1	4
61	24	20.5	8.06	.025	.01	3,061	1,748	1	3
61	24	20.5	8.06	.050	.02	4,546	2,596 (2)	1	3
61	24	20.5	8.06	.081	.032	6,302	3,599	2	4
61	24	20.5	8.06	.10	.040	7,188	4,105	2	4
61	24	20.5	8.06	.16	.063	9,253	5,284	2	5
91.4	36	10.2	4.03	.025	.01	3,810	2,176	1	3
91.4	36	10.2	4.03	.050	.02	5,992	3,422	1	4
91.4	36	10.2	4.03	.081	0.32	8,486	4,846	1	5
91.4	36	10.2	4.03	.10	.040	8,188	4,676	1	5
91.4	36	10.2	4.03	.16	.063	8,128	4,642	1	5
91.4	36	20.5	8.06	.025	.01	3,558	2,032	1	3
91.4	36	20.5	8.06	.050	.02	5,031	2,873	1	3
91.4	36	20.5	8.06	.081	.032	6,938	3,962	1	4
91.4	36	20.5	8.06	.10	.040	12,769	7,292	1	4
91.4	36	20.5	8.06	.16	.063	15,674	8,951	1	4

(1) Preliminary Design No. 1

(2) Preliminary Design No. 2

(3) Reference Design

TABLE 5

RESULTS OF SHELL ANALYSIS USING THE BAMSOC I CODE WITH REDUCED E_x AND E_y

Case	EI (Ring)		EA (Ring)		Critical Failure Load		Failure Mode		
	$MN\text{-}cm^2$	$lbf\text{-}in^2$ 10^{-6}	MN	lbf 10^{-6}	N/cm	lbf/in	N	M	
1	4.3	.15	4.45	1.0	8493	4850	4	4	
2	8.2	.287	6.67	1.5	9543	5450	4	4	Reference
3	17.2	.60	6.67	1.5	9719	5550	4	4	
4	33.0	1.15	10.0	2.25	10944	6250	4	4	
5	82.3	2.87	12.45	2.8	11645	6650	4	4	
6	∞	∞	∞	∞	15322	8750	1	6	

TABLE 6

RESULTS OF SHELL ANALYSIS USING THE BAMSOC I CODE WITH REDUCED E_x, E_y, AND G_{xy}

Case	EI		EA		Critical Failure Load		Failure Mode		
	$MN\text{-}cm^2$	$lbf\text{-}in^2$ 10^{-6}	MN	lbf 10^{-6}	N/cm	lbf/in	N	M	
2	8.2	.287	6.67	1.50	7442	4250	4	4	Reference

TABLE 7

DETAILS OF SHELL REFERENCE DESIGN

Shell Skin Thickness	.081 cm	.032 in (2024-T3)
Stringer Spacing	10.2 cm	4.03 in
Ring Spacing	61 cm	24.0 in
Shell Weight (No Rings)	4.39 kg/m^2	.90 lbm/ft^2
Stringer Details		
Diameter of Boron Epoxy	.286 cm	.1125 in
Depth of Stringer (h)	2.10 cm	.83 in
Thickness of Web & Flange	.057 cm	.0225 in
Aluminum Specification		7075-T6
EI	10.04 x 10^6 N-cm^2	.35 x 10^6 lbf-in^2
EA	9.78 x 10^6 N	2.2 x 10^6 lbf
Ring Details (Theoretical)		
EI	6.02 x 10^6 N-cm^2	.21 x 10^6 lbf-in^2
EA	5.87 x 10^6 N	1.32 x 10^6 lbf
Ring Details (Selected)		
EI	16.29 x 10^6 N-cm^2	.568 x 10^6 lbf-in^2
EA	15.27 x 10^6 N	3.42 x 10^6 lbf
DB	.381 cm	.150"
$\bar{X}$	2.47 cm	.973 in

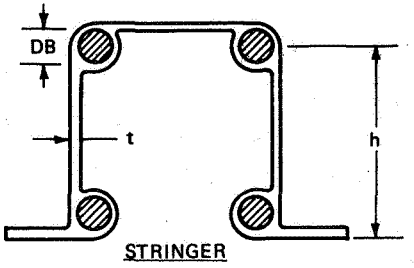

STRINGER

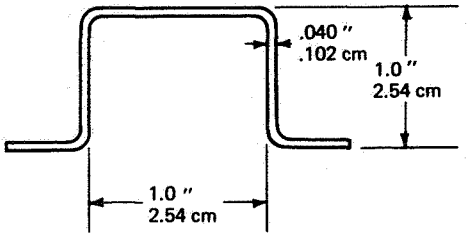

RING
(Theoretical)

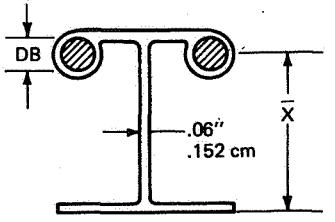

RING
(Selected)

TABLE 8

SHELL DESIGNS AND FAILURE LOADS

Design \ Units	Skin Thickness ④ cm	Skin Thickness ④ in	EI $N\text{-}cm^2 \times 10^{-6}$	EI $(lbf\text{-}in^2 \times 10^{-6})$	EA $N \times 10^{-6}$	EA $lbf \times 10^{-6}$	Stringer Weight. Kg/m	Stringer Weight. lbm/in	Stringer Spacing cm	Stringer Spacing in	No. of Stringers	Nx N/cm	Nx lbf/in	$d\bar{c}/R \times 10^5$ ⑥ $Kg/cm^3 \times 10^{-5}$	$d\bar{c}/R \times 10^5$ ⑥ $lbm/in^3 \times 10^{-5}$	Nx/R ③ KN/cm^2	Nx/R ③ $lbf/in^2 \times 10^{-3}$	Load in Stringer ② KN	Load in Stringer ② lbf	Stress in Stringer N/cm^2	Stress in Stringer lbf/in^2
Reference	.057	.0225	14.06	.49	9.78	2.2	.218	.0122	10.21	4.03	60	7,332	4,187	.448	16.2	.075	.109	75.06	16,873	38,789	56,243
1	.102	.04	17.44	.608	18.99	4.27	.564	.0316	10.21	4.03	60	9,569	5,464	.791	28.6	.098	.142	97.95	22,019	29,952	43,430
2	↑	.04	↑	.608	↑	4.27	↑	↑	11.35	4.47	55	8,900	5,082	.739	26.7	.091	.132	101.0	22,716	30,899	44,804
3	↕	.04	↕	.608	↕	4.27	↕	↕	12.29	4.84	50	8,422	4,809	.697	25.2	.086	.125	103.54	23,275	31,660	45,907
4	↕	.04	↕	.608	↕	4.27	↕	↕	13.97	5.50	44	7,718	4,407	.639	23.1	.079	.114	107.82	24,238	32,970	47,806
5	↕	.04	↕	.608	↕	4.27	↕	↕	15.37	6.05	40	7,241	4,135	.603	21.8	.072	.105	111.28	25,016	34,028	49,341
6	↕	.04	↕	.608	↕	4.27	↕	↕	17.07	6.72	36	6,765	3,863	.567	20.5	.066	.096	115.48	25,959	39,448	57,201
7	↓	.04	↓	.608	↓	4.27	↓	↓	19.18	7.55	32	6,277	3,584	.531	19.2	.060	.087	120.37	27,059	--	--
8	.102	.04	17.44	.608	18.99	4.27	.564	.0316	20.47	8.06	30	6,016	3,435	.509	18.4	.057	.082	123.16	27,686	--	--
9	.0635	.025	14.34	.50	15.61	3.51	.429	.024	10.21	4.03	60	8,934	5,101	.653	23.6	.091	.132	91.45	20,557	32,894	47,696
10	↑	.025	↑	.50	↑	3.51	↑	↑	11.35	4.47	55	8,317	4,749	.617	22.3	.085	.123	94.43	21,228	33,967	49,252
11	↕	.025	↕	.50	↕	3.51	↕	↕	12.29	4.84	50	7,876	4,497	.589	21.3	.079	.114	96.82	21,765	34,826	50,498
12	↕	.025	↕	.50	↕	3.51	↕	↕	13.97	5.50	44	7,226	4,126	.545	19.7	.070	.102	100.97	22,698	36,319	52,663
13	↕	.025	↕	.50	↕	3.51	↕	↕	15.37	6.05	40	6,797	3,881	.517	18.7	.065	.094	104.45	23,480	37,571	54,478
14	↕	.025	↕	.50	↕	3.51	↕	↕	17.07	6.72	36	6,350	3,626	.487	17.6	.059	.086	108.39	24,366	--	--
15	↕	.025	↕	.50	↕	3.51	↕	↕	19.18	7.55	32	5,898	3,368	.459	16.6	.054	.078	113.11	25,428	--	--
16	.0635	.025	14.34	.50	15.61	3.51	.429	.024	20.47	8.06	30	5,687	3,247	.445	16.1	.050	.073	116.41	26,170	--	--

① See figure 26

② Assumes skin between strgrs is inactive

③ Stringer web & flange thickness

④ See table 7

⑤ $\frac{Nx}{R}$ = Predicted failure load ÷ shell radius

⑥ $\frac{d\bar{c}}{R}$ = Average density ÷ shell radius

TABLE 9

TRI ELEMENT COMPRESSION TESTS

Specimen	Length		Max. Boron Filament Stress	
	cm	in	N/cm^2	$\frac{lbf}{in^2}$
Slit	15.2	6	198,559	288,000
Plain	15.2	6	184,080	267,000
Slitted	15.2	6	159,950	232,000
Slitted	15.2	6	141,335	205,000

TABLE 10

WEIGHT OF TEST SHELL RING STIFFENERS

RING NO.	WEIGHT (3)		
	kg	lbm	
1	5.32	11.75	(1)
2	3.76	8.31	(2)
3	3.59	7.93	(2)
4	3.68	8.125	(2)
5	4.98	11.0	(1)

(1) ALUMINUM RING

(2) REINFORCED RING

(3) WEIGHT INCLUDES SPLICE PLATES, NUTS & BOLTS

TABLE A1

RING AND STRINGER STIFFENED CYLINDERS, BENDING LOADS
(Cylinder: Radius to Skin Mid-Plane, 98 cm (38.6 in.), Test Length = 183 cm (72 in.)

Type	Cylinder No.	L_r		L_s		t		$\bar{N}_e$		Predicted						% Error
										N_A		N_B		M	N	
		cm	in	cm	in	cm	in	N/cm	lb/in	N/cm	lb/in	N/cm	lb/in			
I	1	15.2	6	6.23	2.48	.050	.0199	1990	1136	3258	1860	2088	1192	3	6	+4.9
	2	22.9	9	6.23	2.48	.050	.0199	1750	1000	3058	1746	1974	1127	3	7	+12.7
	3	30.4	12	6.23	2.48	.050	.0199	1660	948	2876	1642	1897	1083	3	7	+14.2
II	1	15.2	6	10.26	4.04	.0497	.0197	1271	726	2073	1184	1166	666	1	5	-8.4
	2	22.9	9	10.26	4.04	.0497	.0197	1094	652	1785	1019	1060	605	2	7	-7.2
	3	30.4	12	10.26	4.04	.0497	.0197	1077	615	1625	928	968	553	1	6	-10.1
	4	45.7	18	10.26	4.04	.0497	.0197	795	454	1294	739	806	460	1	6	+1.5
	4-1	45.7	18	10.26	4.04	.0497	.0197	795	454	1689	964	998	570	4	10	+25.4

a - without skin buckling

b - with skin buckling

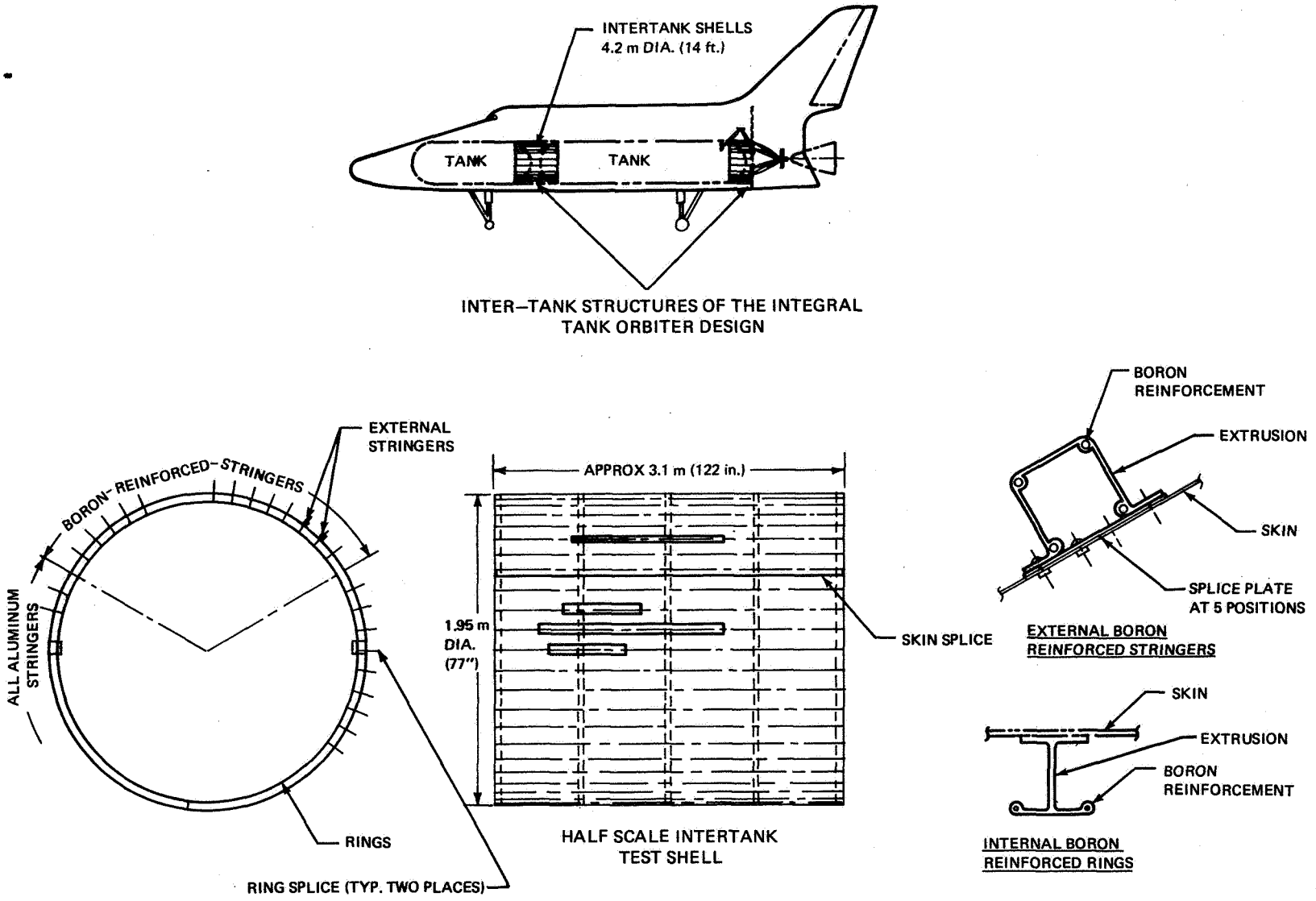

Figure 1 CONCEPTUAL DESIGN OF A BORON REINFORCED INTERTANK SHELL

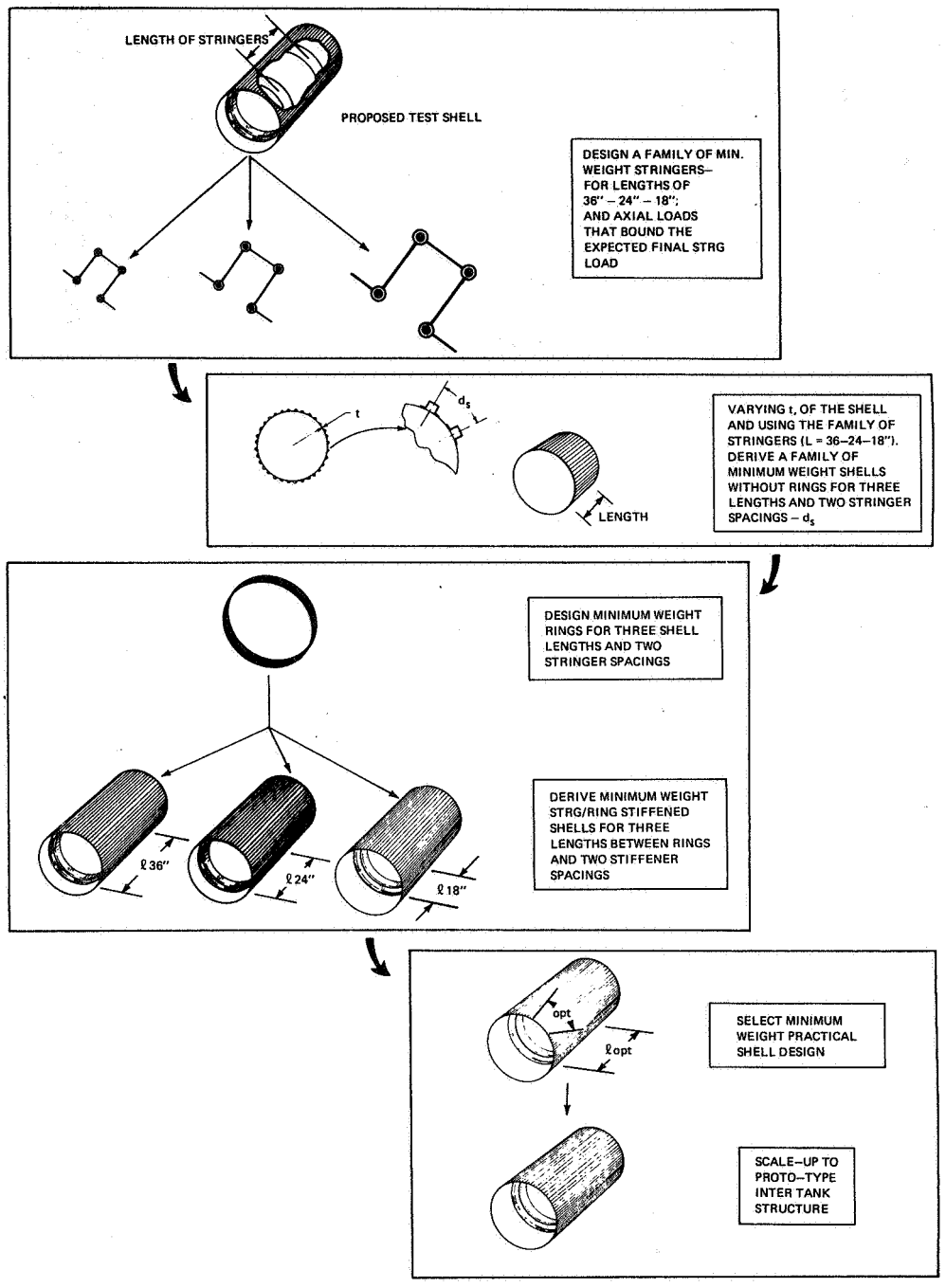

Figure 2 FLOW CHART FOR DESIGN OF MINIMUM WEIGHT SHELL

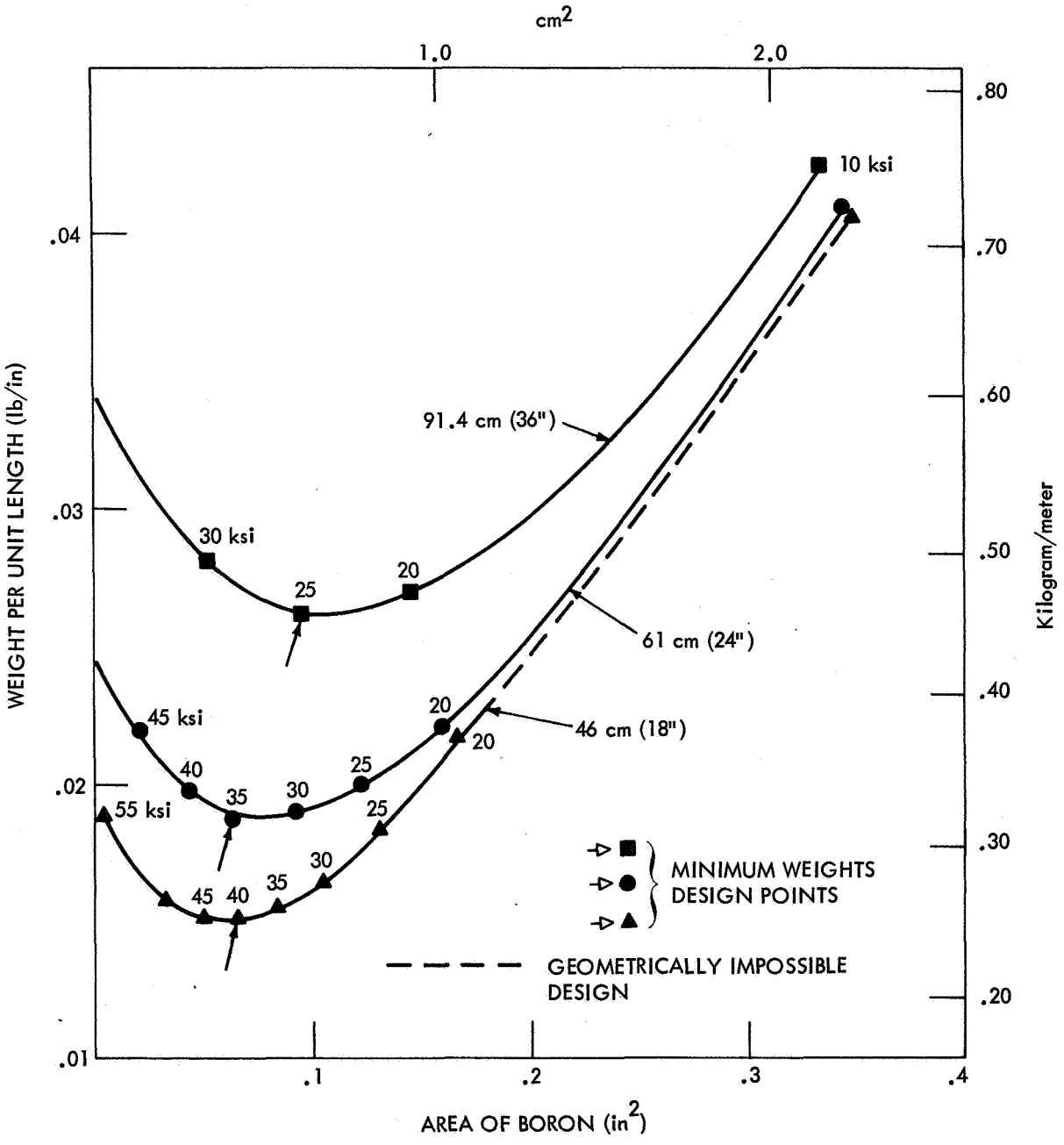

Figure 3 WEIGHT OF REINFORCED ALUMINUM HAT SECTION
VERSUS AMOUNT OF REINFORCEMENT
$P_{[CRIT\text{-}STRG]}$ = 53,000 NEWTONS (12,000 lbf)

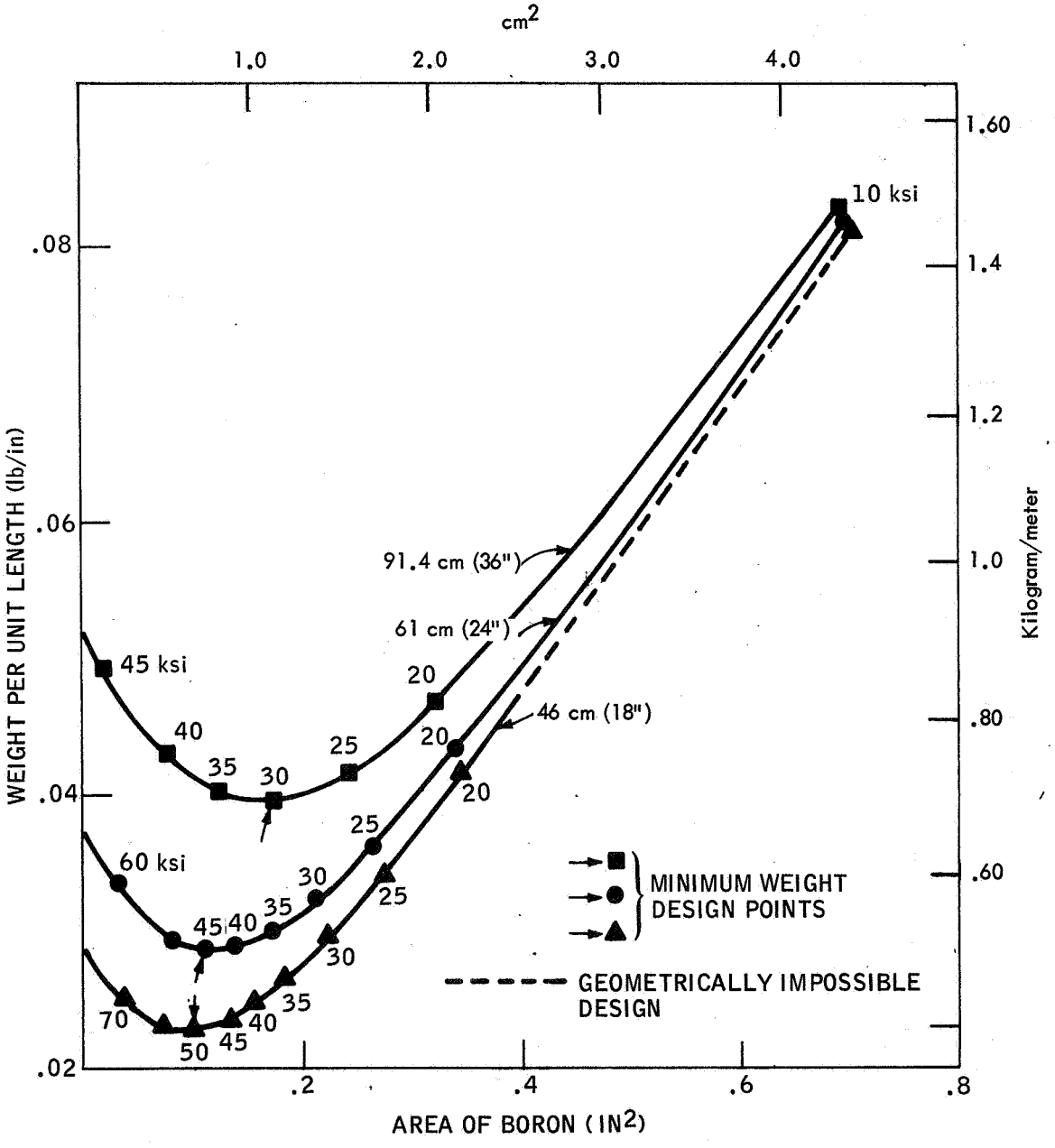

Figure 4 WEIGHT OF REINFORCED ALUMINUM HAT SECTION VERSUS AMOUNT OF REINFORCEMENT $P_{[CRIT\text{-}STRG]}$ = 107,000 NEWTONS (24,000 lbf)

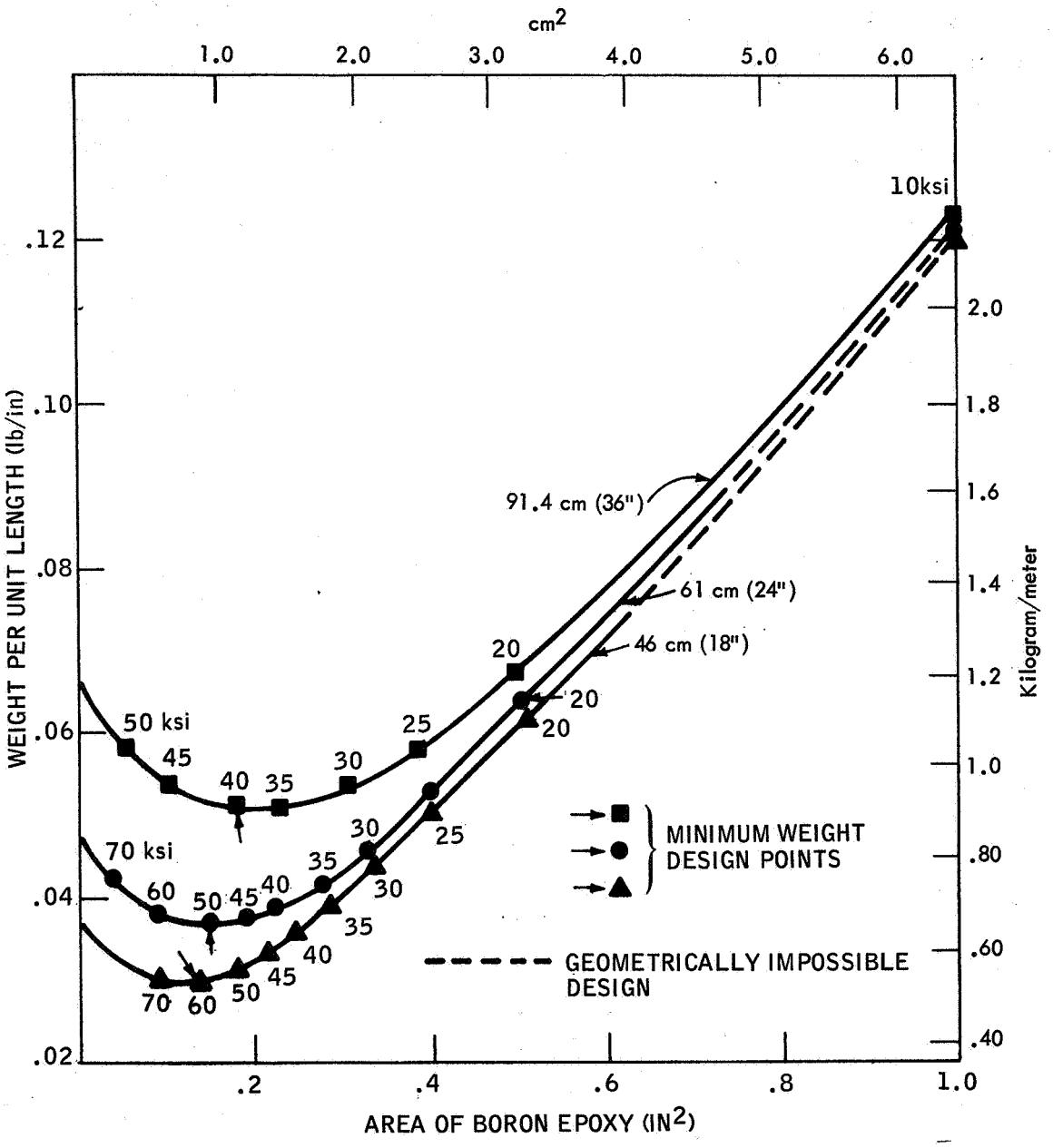

Figure 5 WEIGHT OF REINFORCED ALUMINUM HAT SECTION VERSUS AMOUNT OF REINFORCEMENT $P_{[CRIT-STRG]}$ = 160,000 NEWTONS (36,000 lbf)

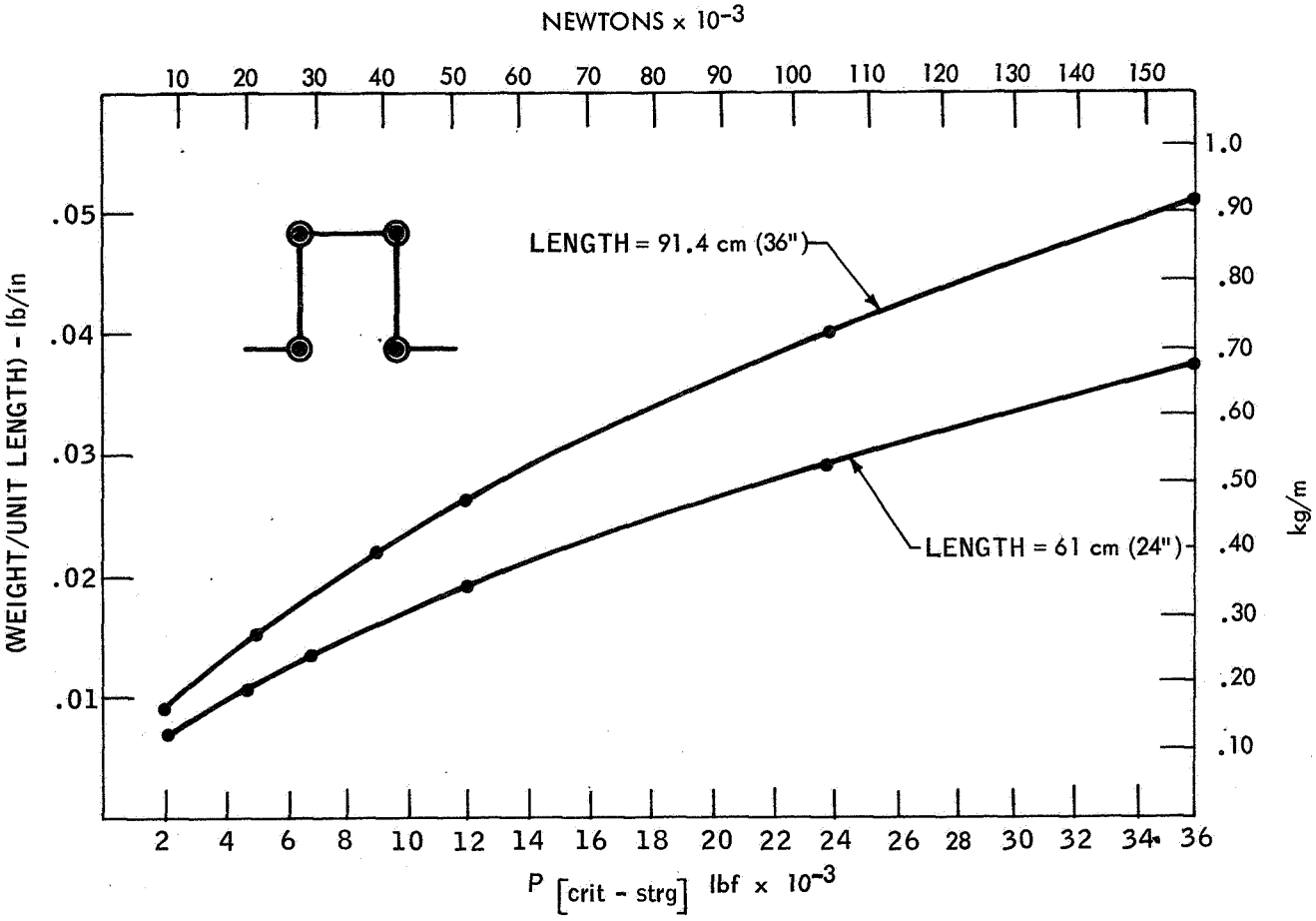

Figure 6 WEIGHT OF MINIMUM WEIGHT HAT STRINGERS VERSUS $P_{[CRIT-STRIG]}$

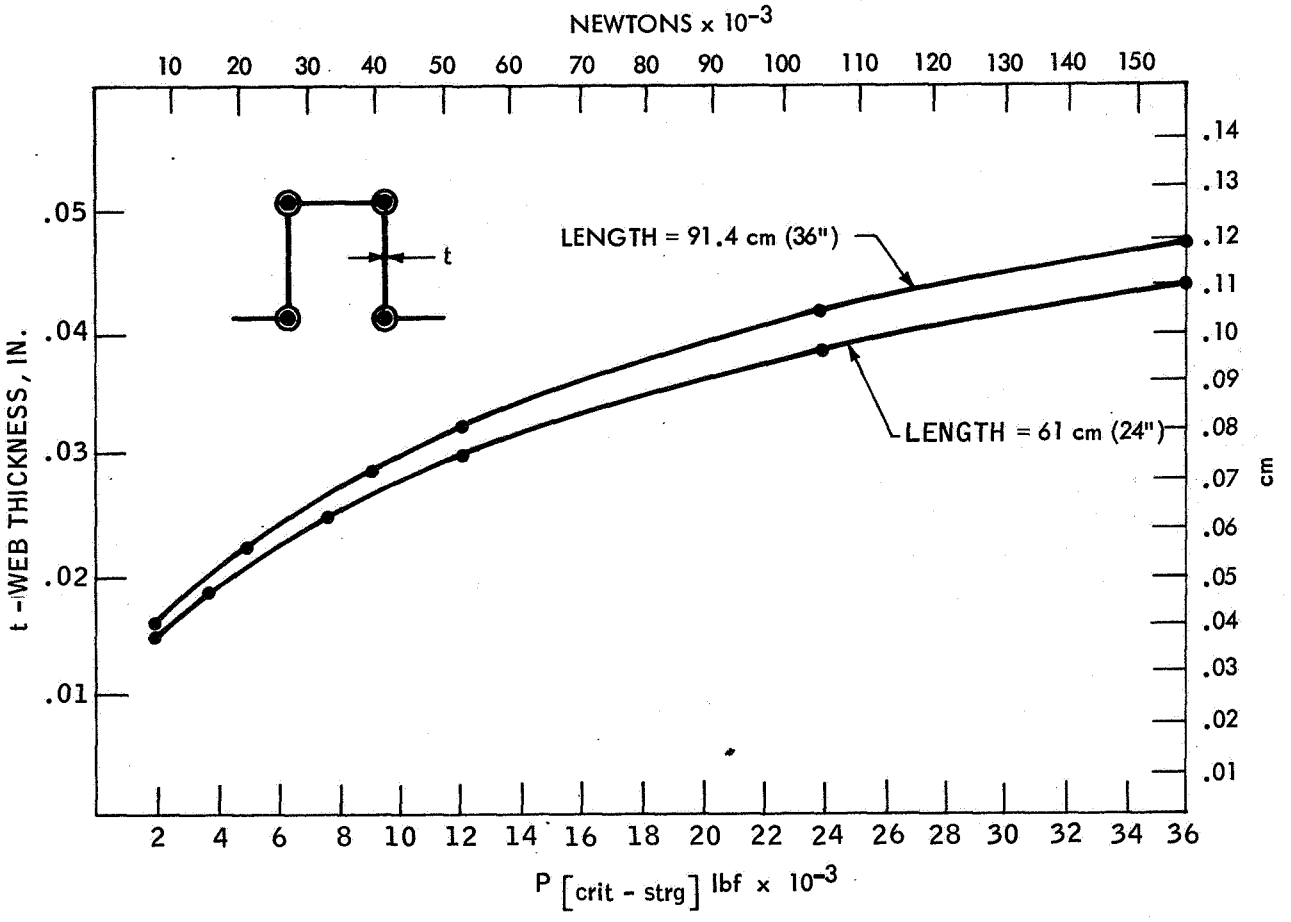

Figure 7 WEB THICKNESS OF MINIMUM WEIGHT HAT STRINGERS $P_{[CRIT-STRIG]}$

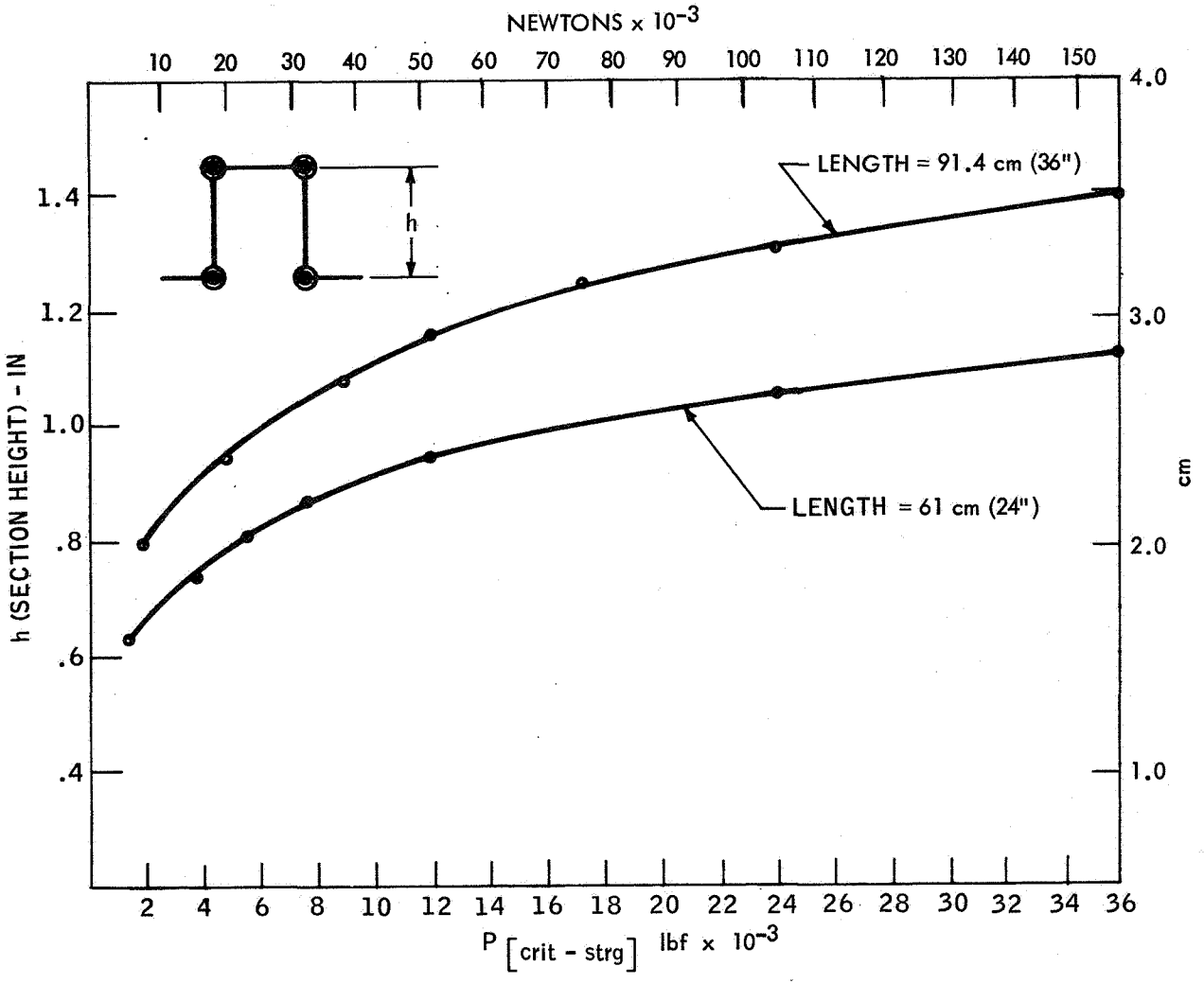

Figure 8 HEIGHT OF MINIMUM WEIGHT HAT STRINGER VERSUS $P_{[CRIT-STRG]}$

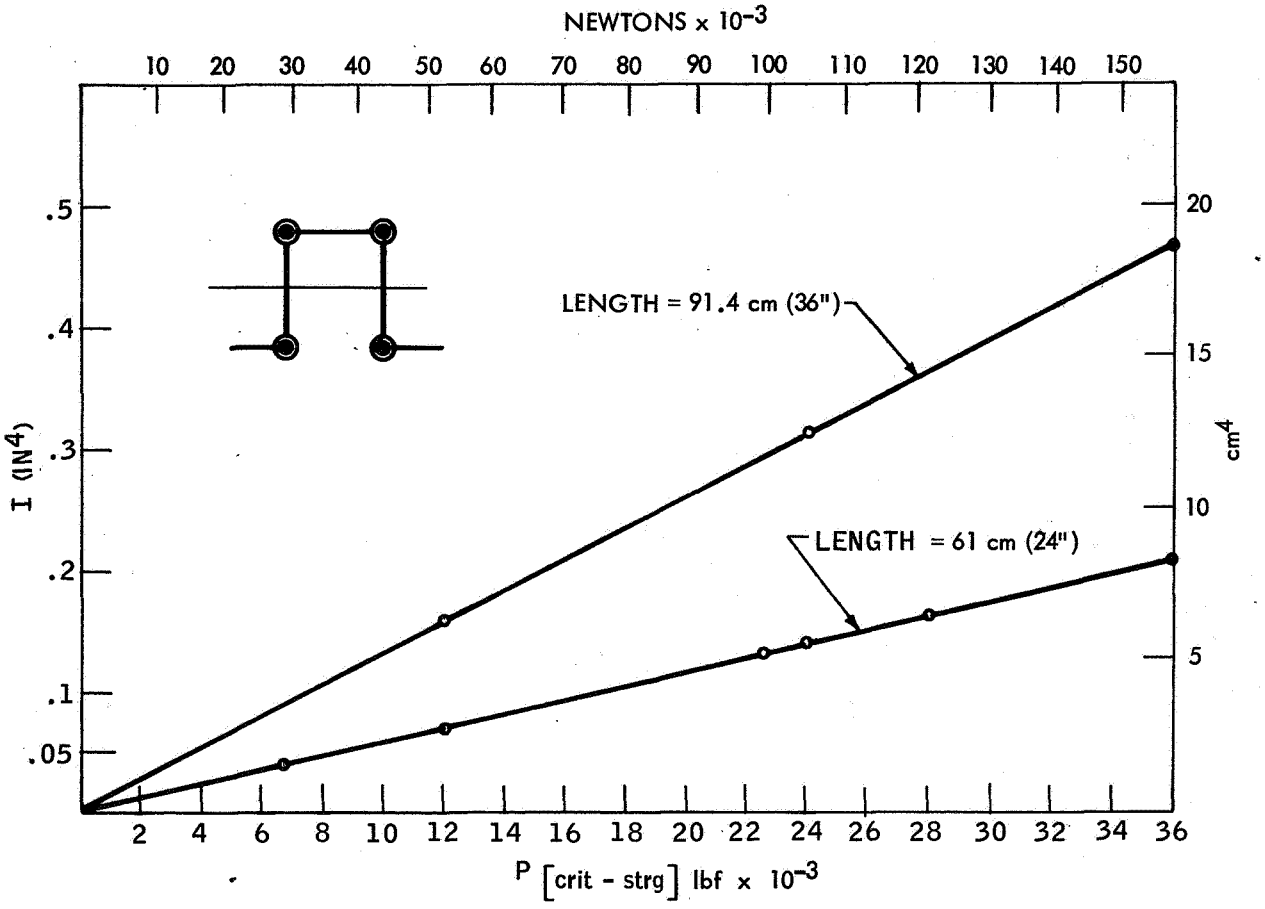

Figure 9 I OF MINIMUM WEIGHT HAT STRINGERS VERSUS $P_{[CRIT-STRG]}$

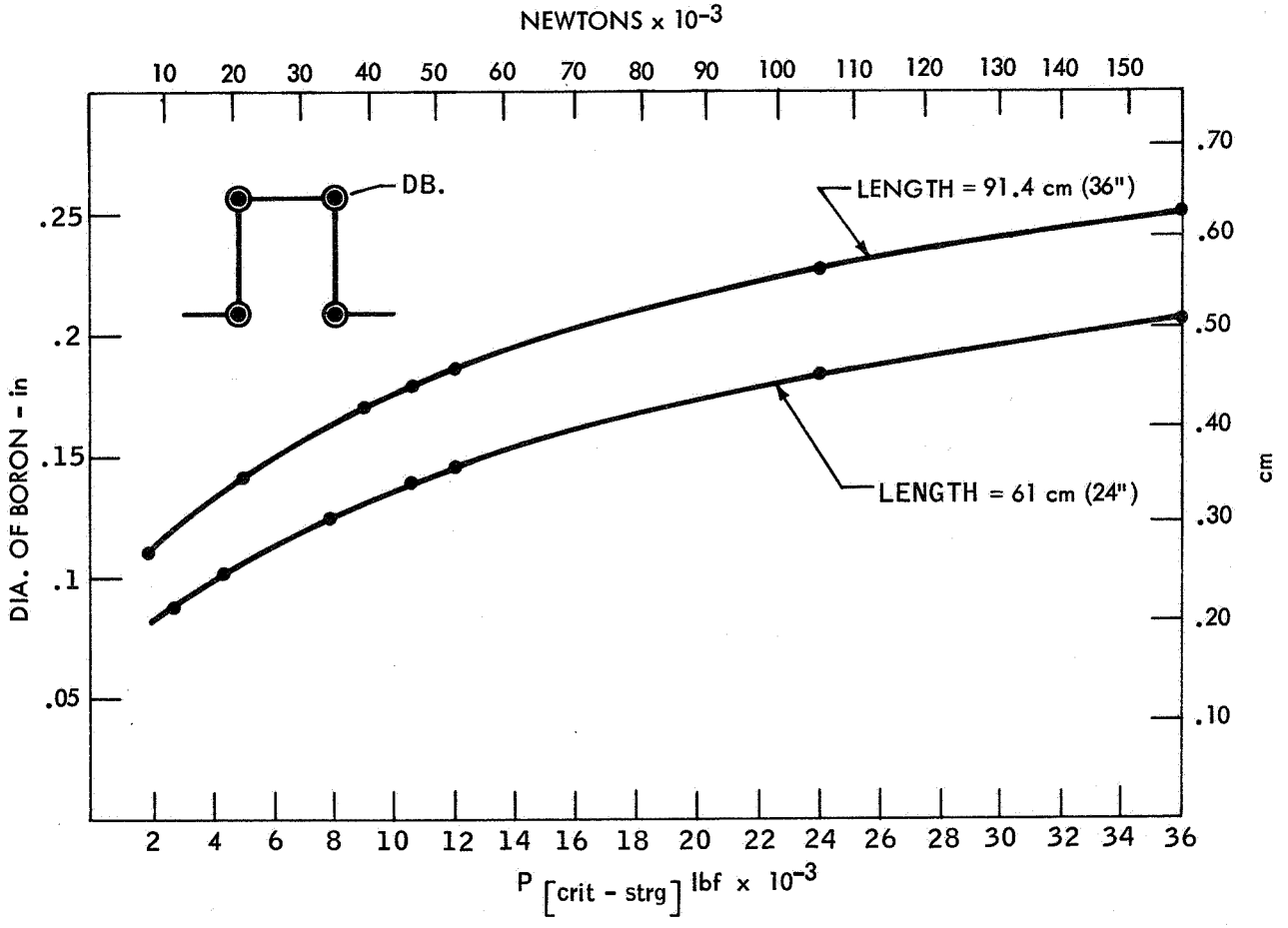

Figure 10 DIAMETER OF BORON FOR MINIMUM WEIGHT HAT STRINGER VERSUS $P_{[CRIT-STRG]}$

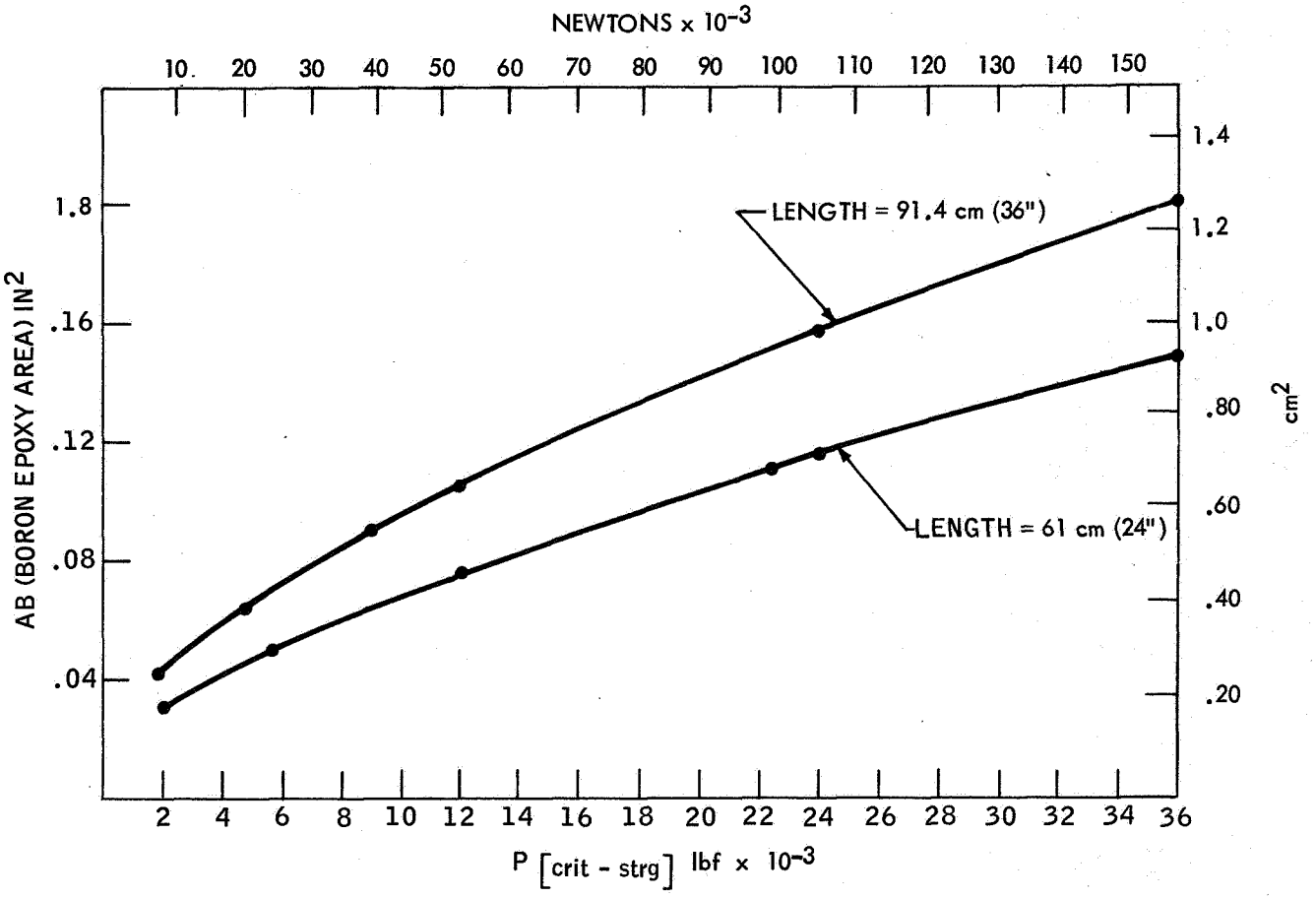

Figure 11 AREA OF BORON EPOXY OF MINIMUM WEIGHT STRINGER VERSUS $P_{[CRIT-STRG]}$

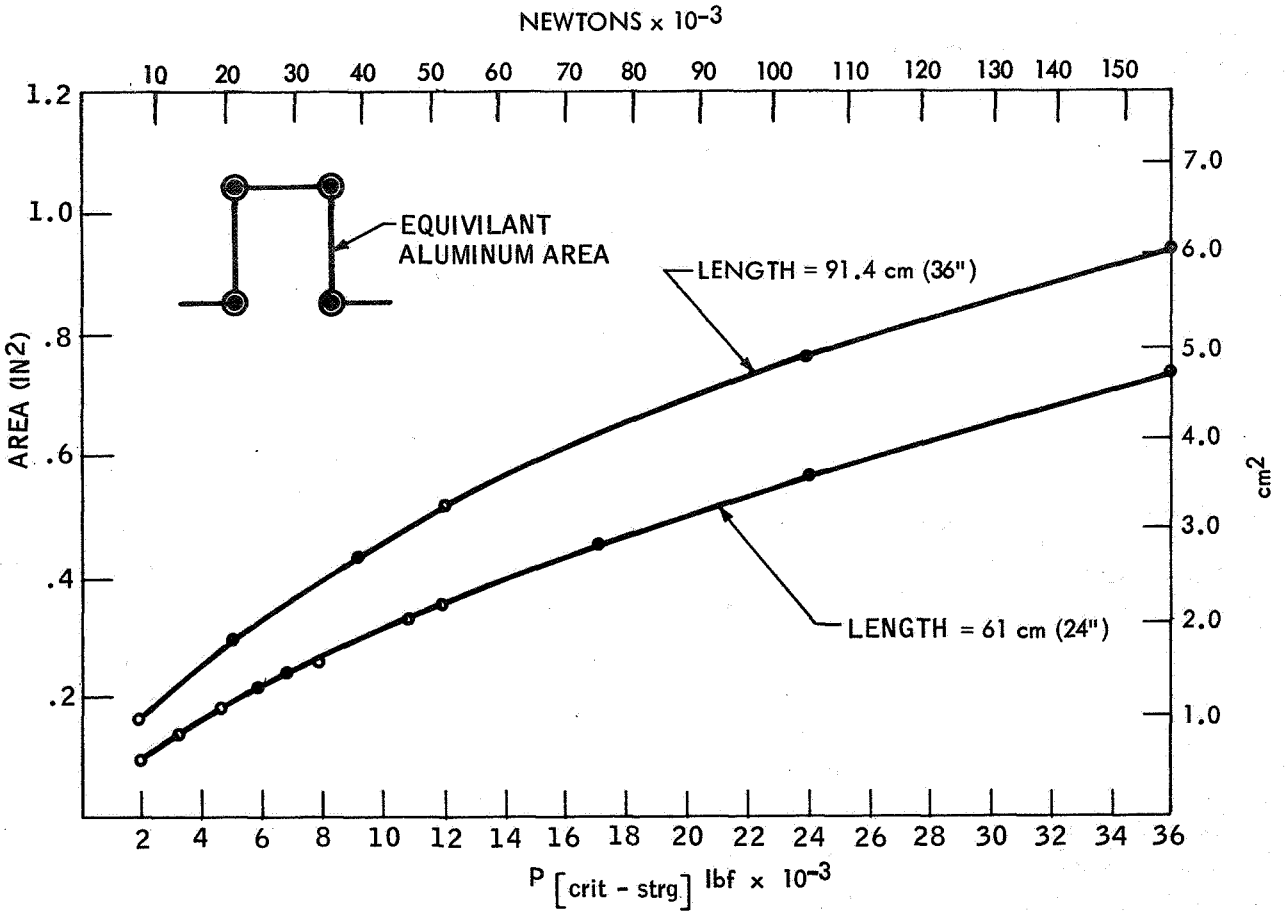

Figure 12 AREA OF MINIMUM WEIGHT HAT STRINGER VERSUS $P_{[CRIT-STRG]}$

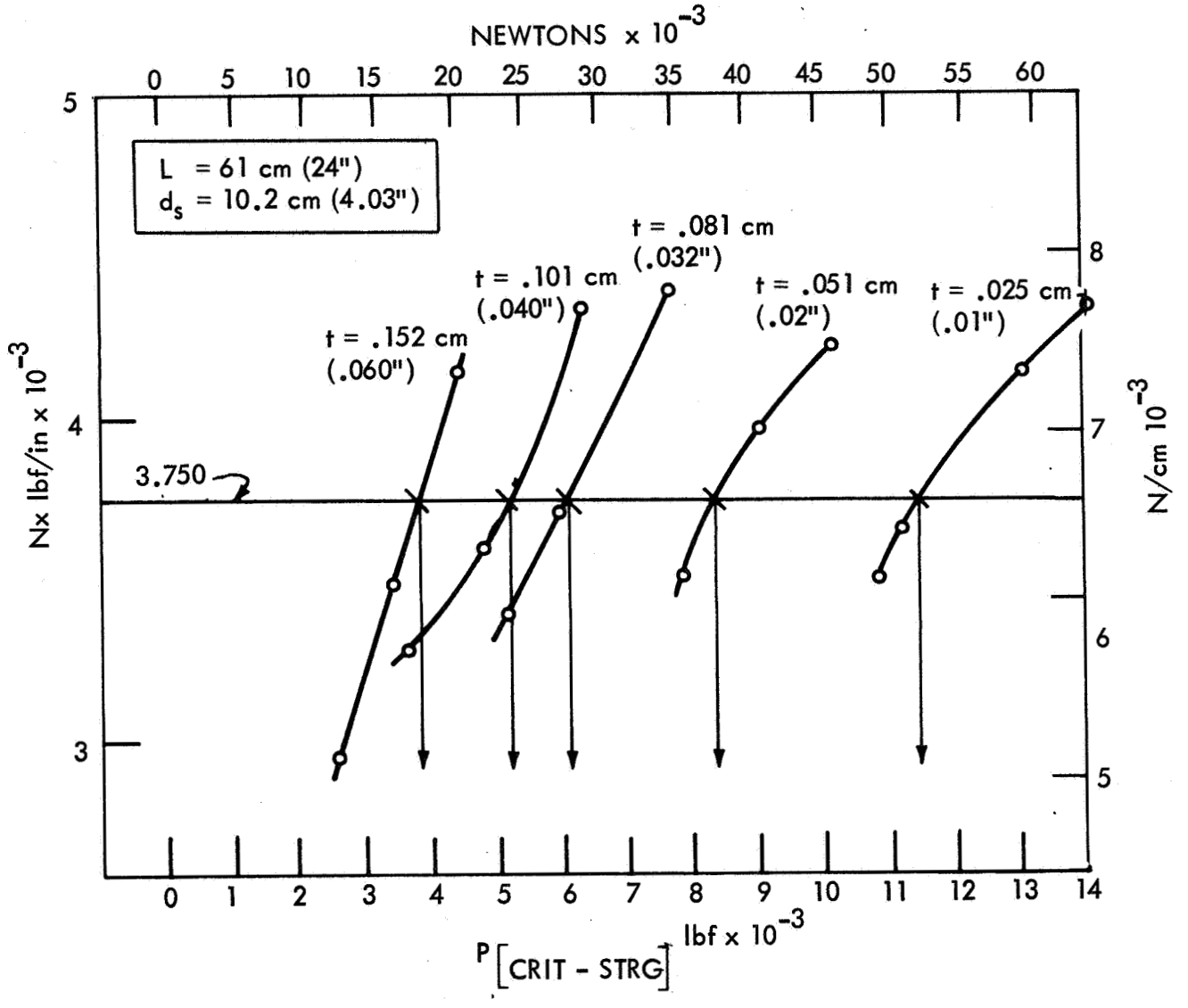

Figure 13 SHELL LOAD (N_x) VERSUS P [CRIT-STRG]

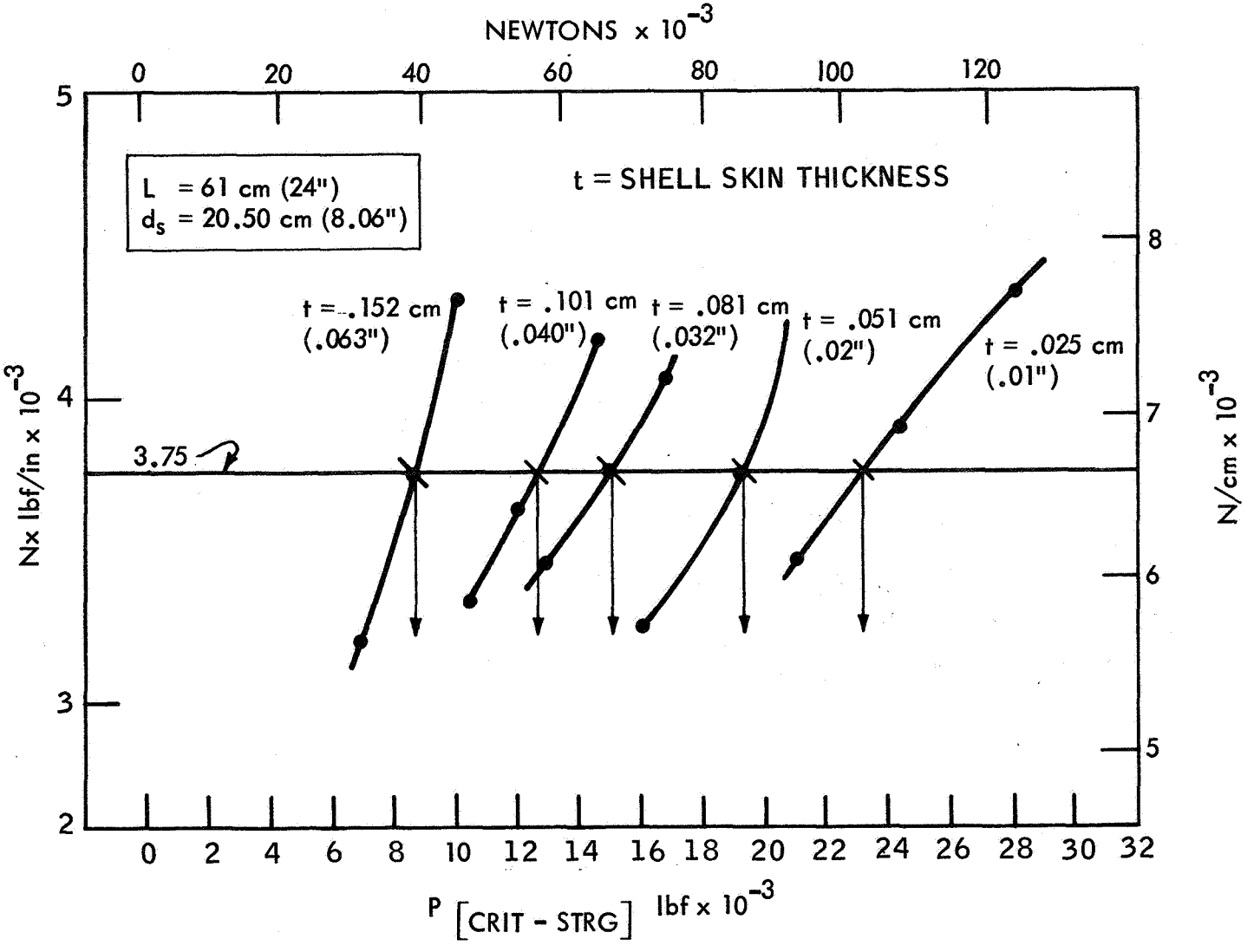

Figure 14 SHELL LOAD (Nx) VERSUS $P_{[CRIT-STRG]}$

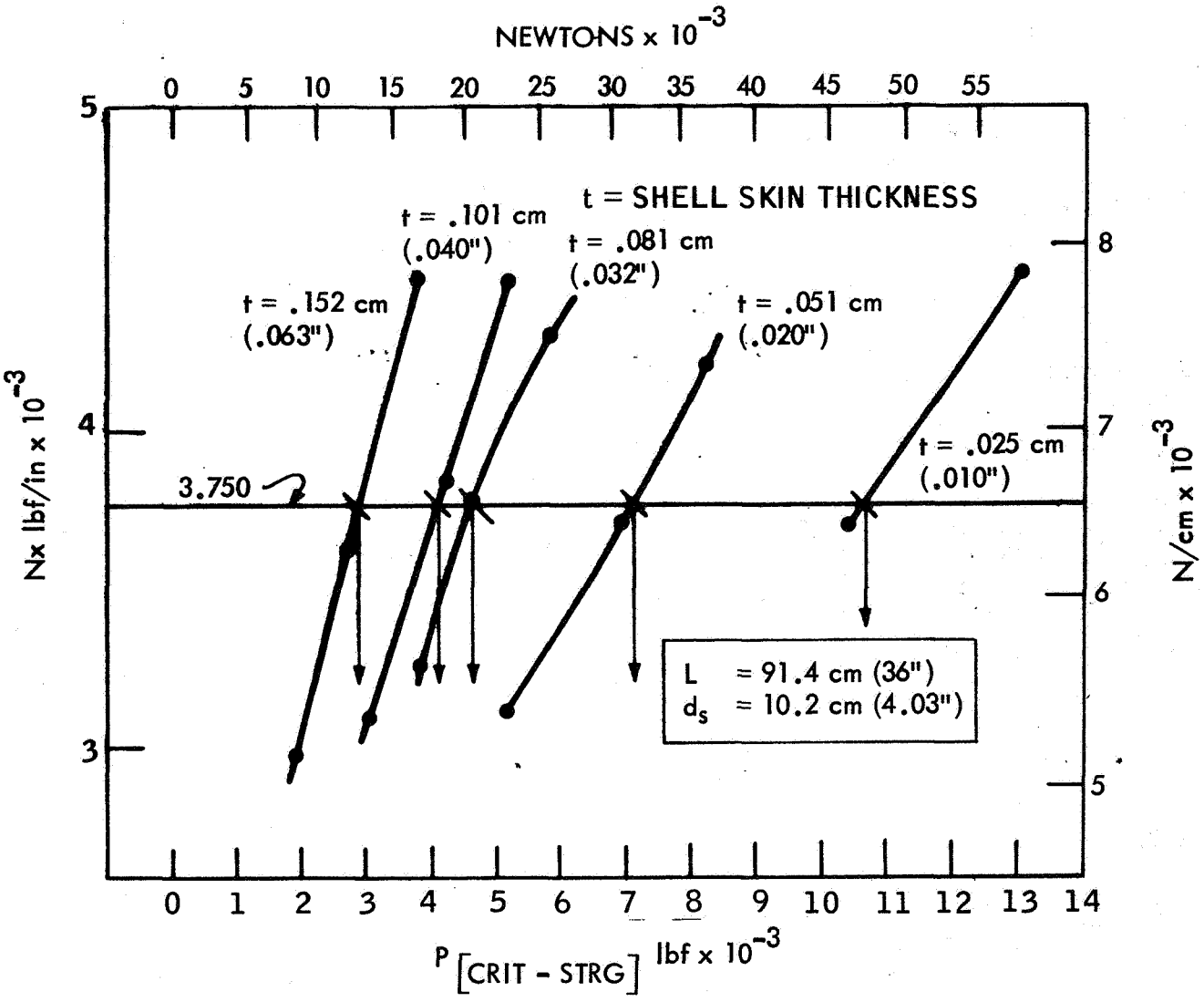

Figure 15 SHELL LOAD PER INCH VERSUS $P_{[CRIT-STRG]}$

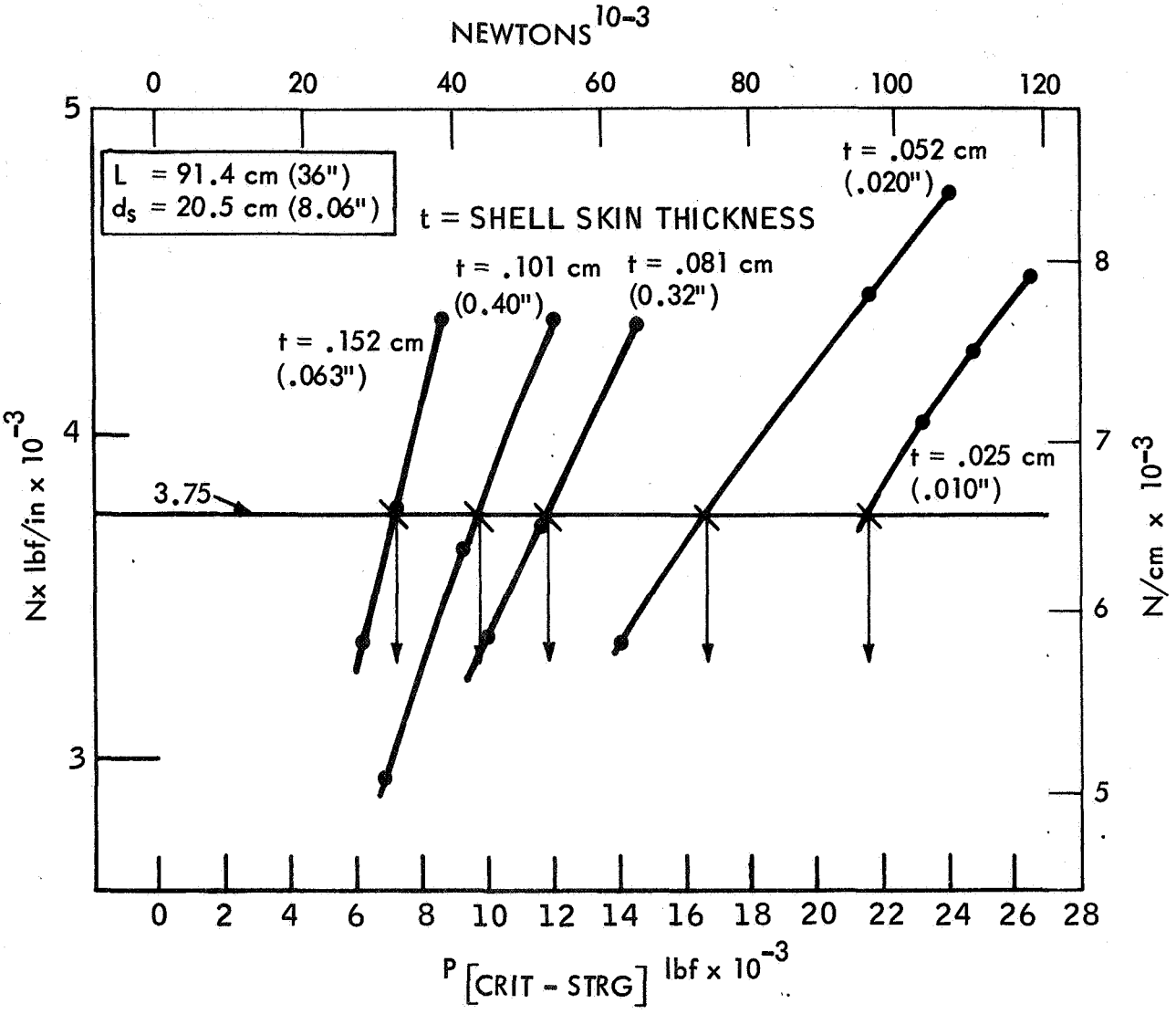

Figure 16 SHELL LOAD PER INCH VERSUS $P_{[CRIT-STRG]}$

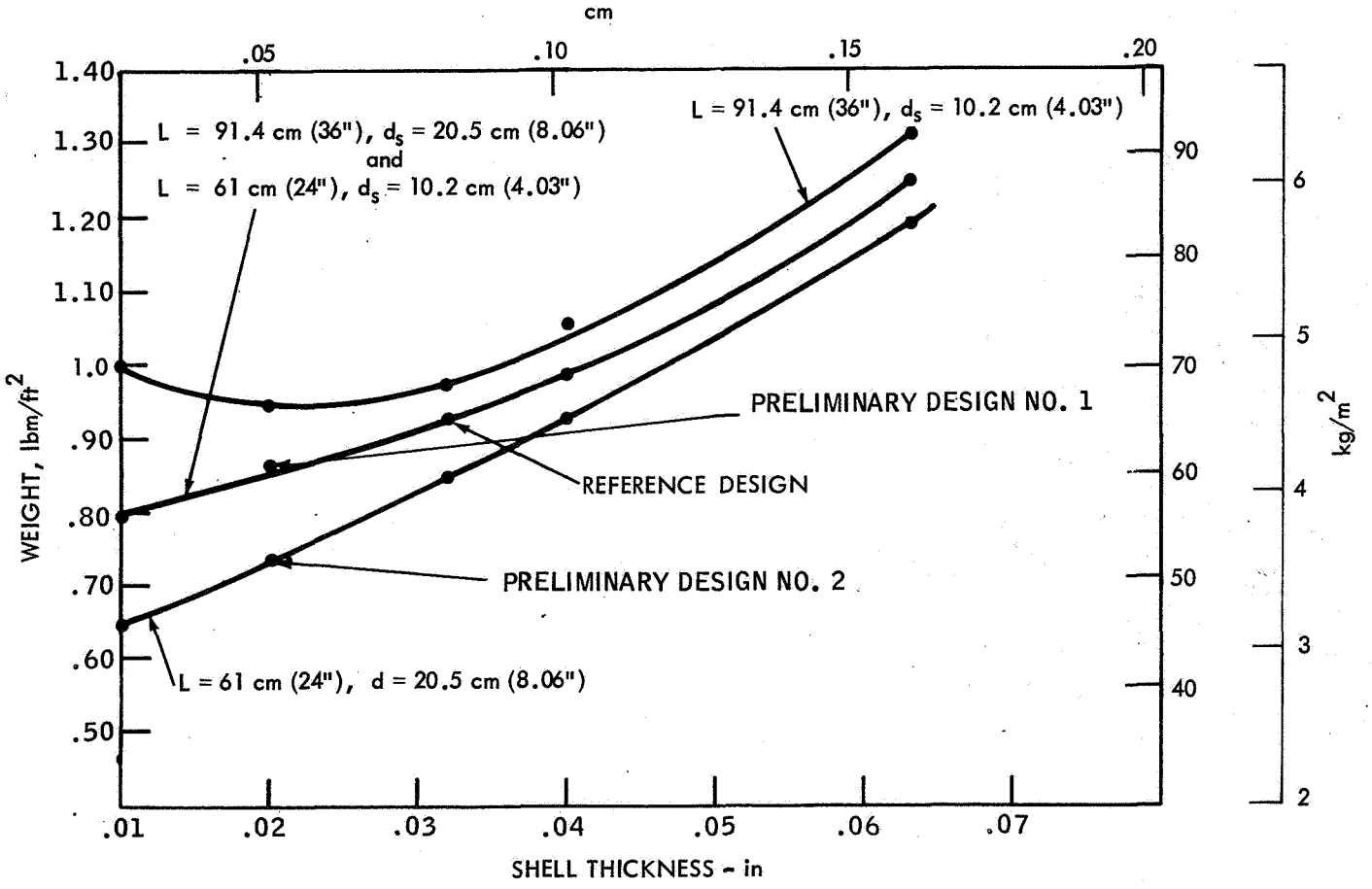

Figure 17 WEIGHT OF STRINGER REINFORCED SHELLS VERSUS SHELL THICKNESS

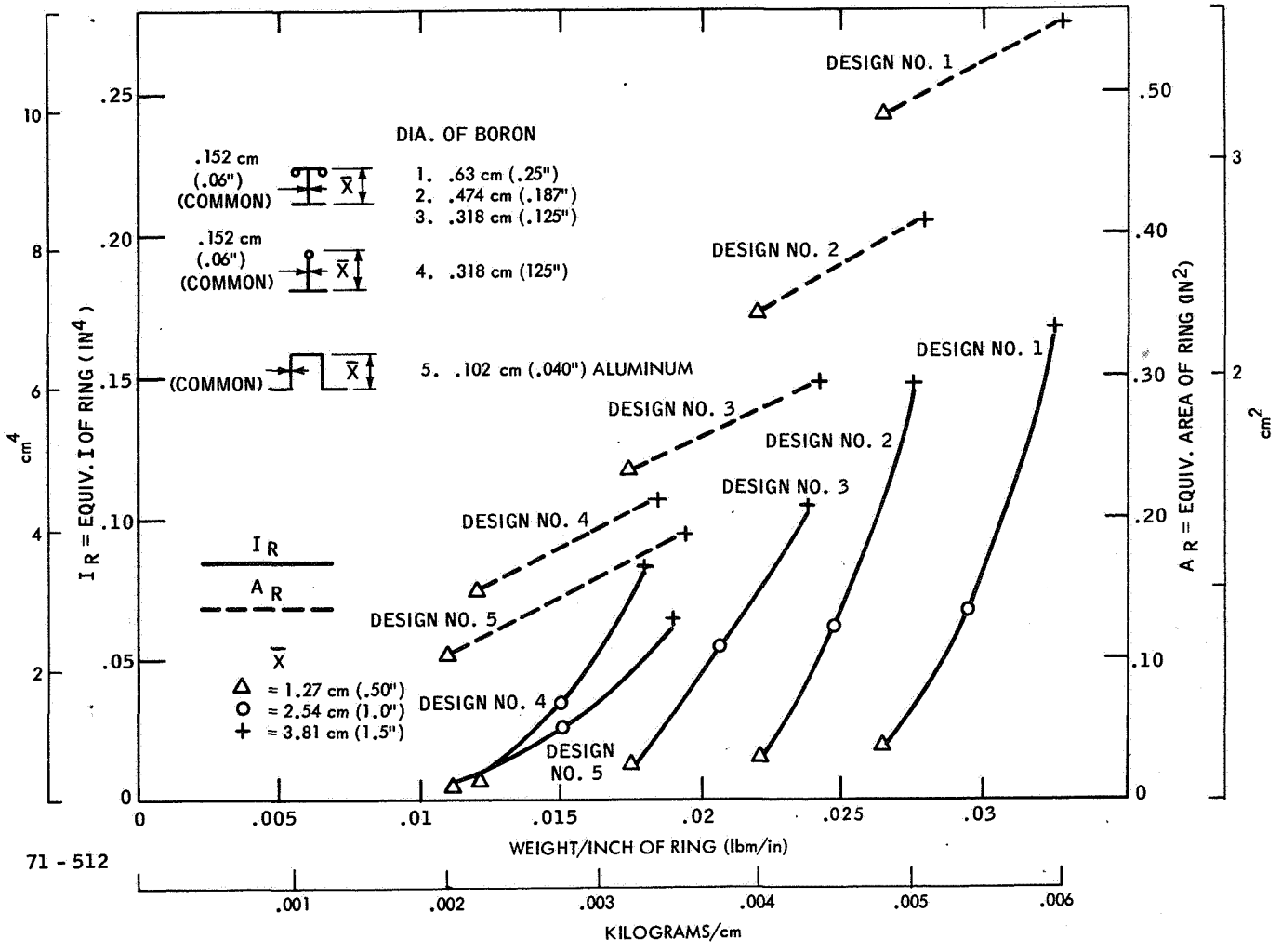

Figure 18 WEIGHT OF RING VERSUS MOMENT OF INERTIA AND AREA

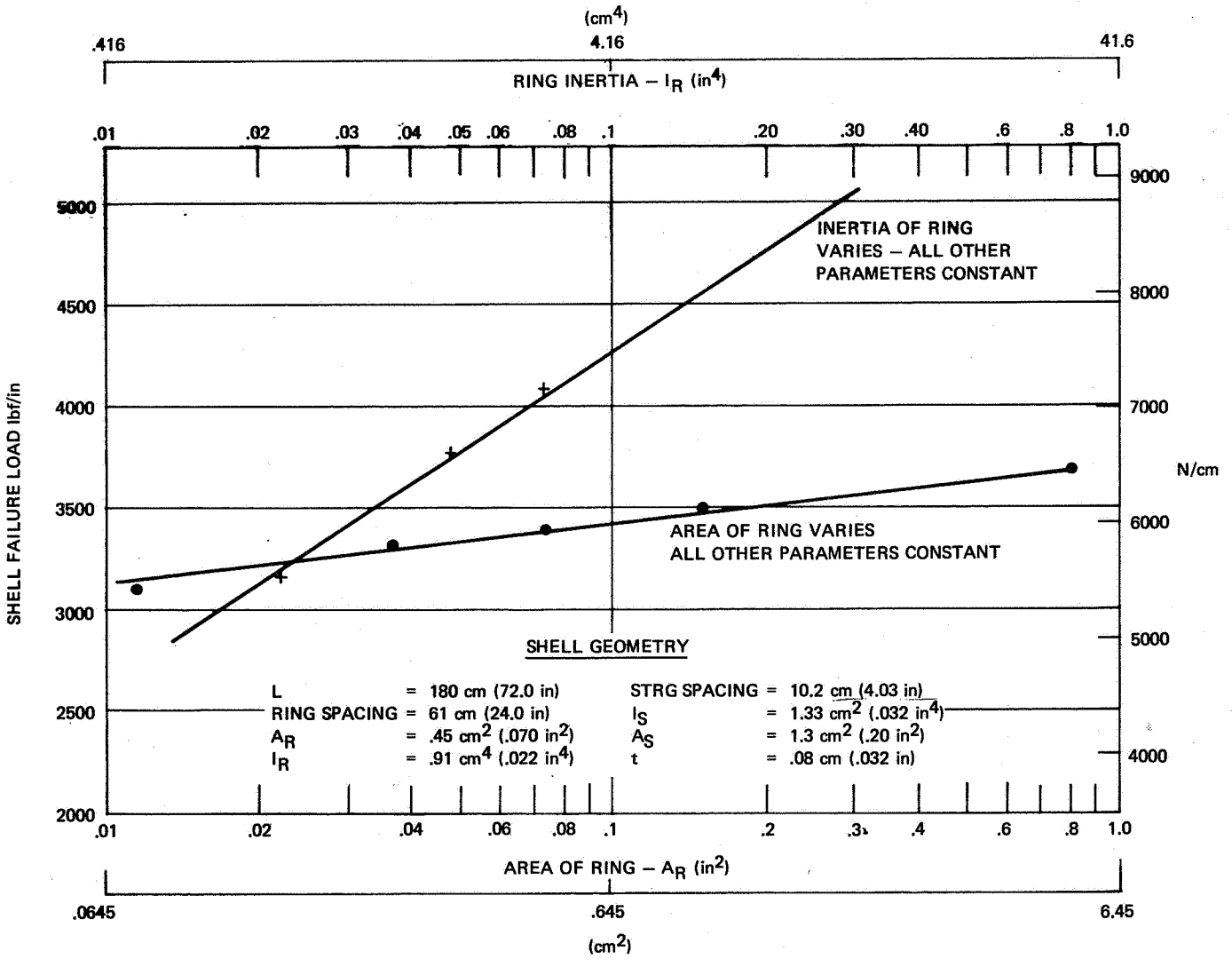

Figure 19 SHELL FAILURE LOAD V AREA AND INERTIA OF RING

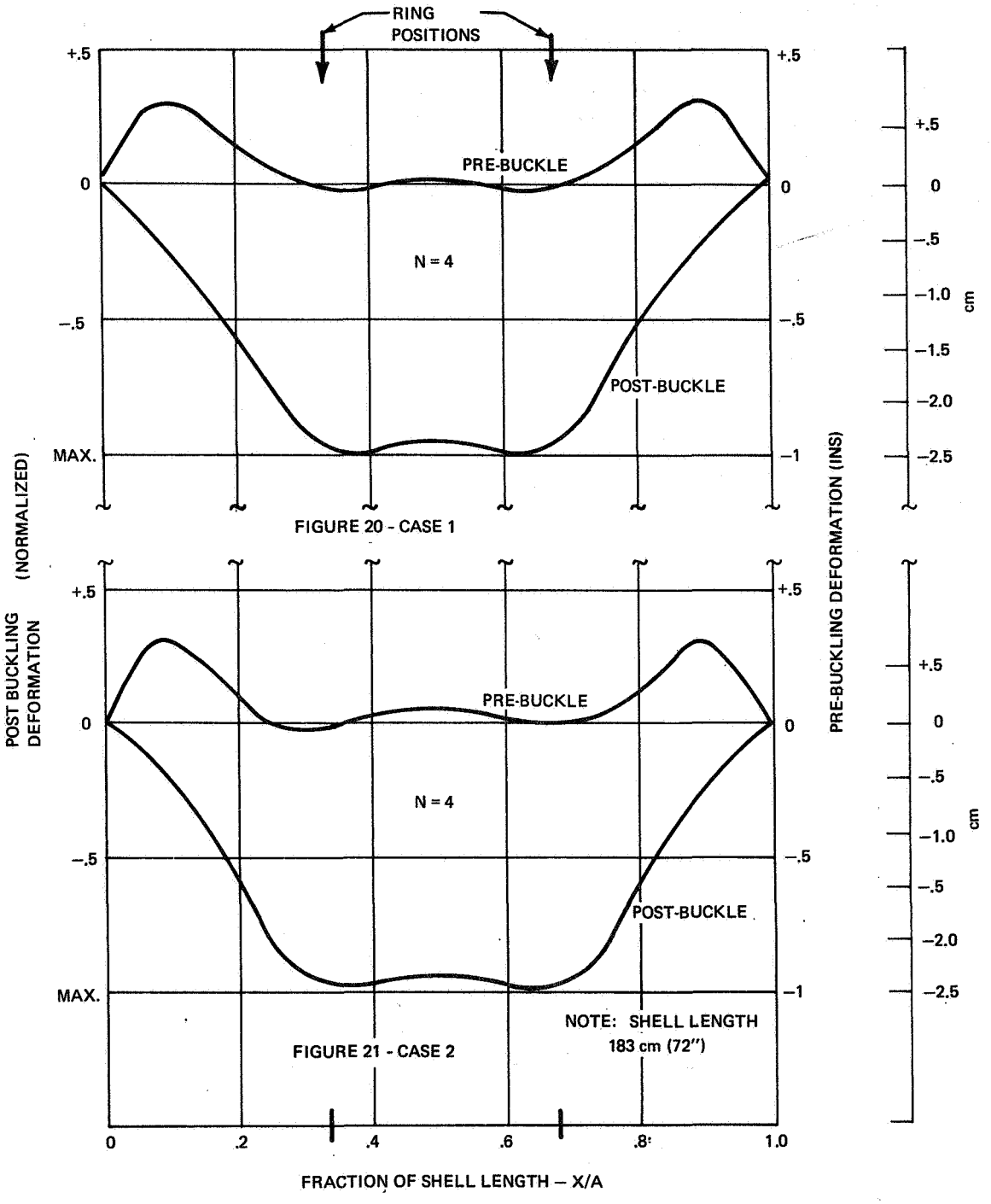

FIGURE 20 - CASE 1

FIGURE 21 - CASE 2

Figure 20 and 21 SHELL RADIAL PREBUCKLING AND POSTBUCKLING DEFORMATIONS

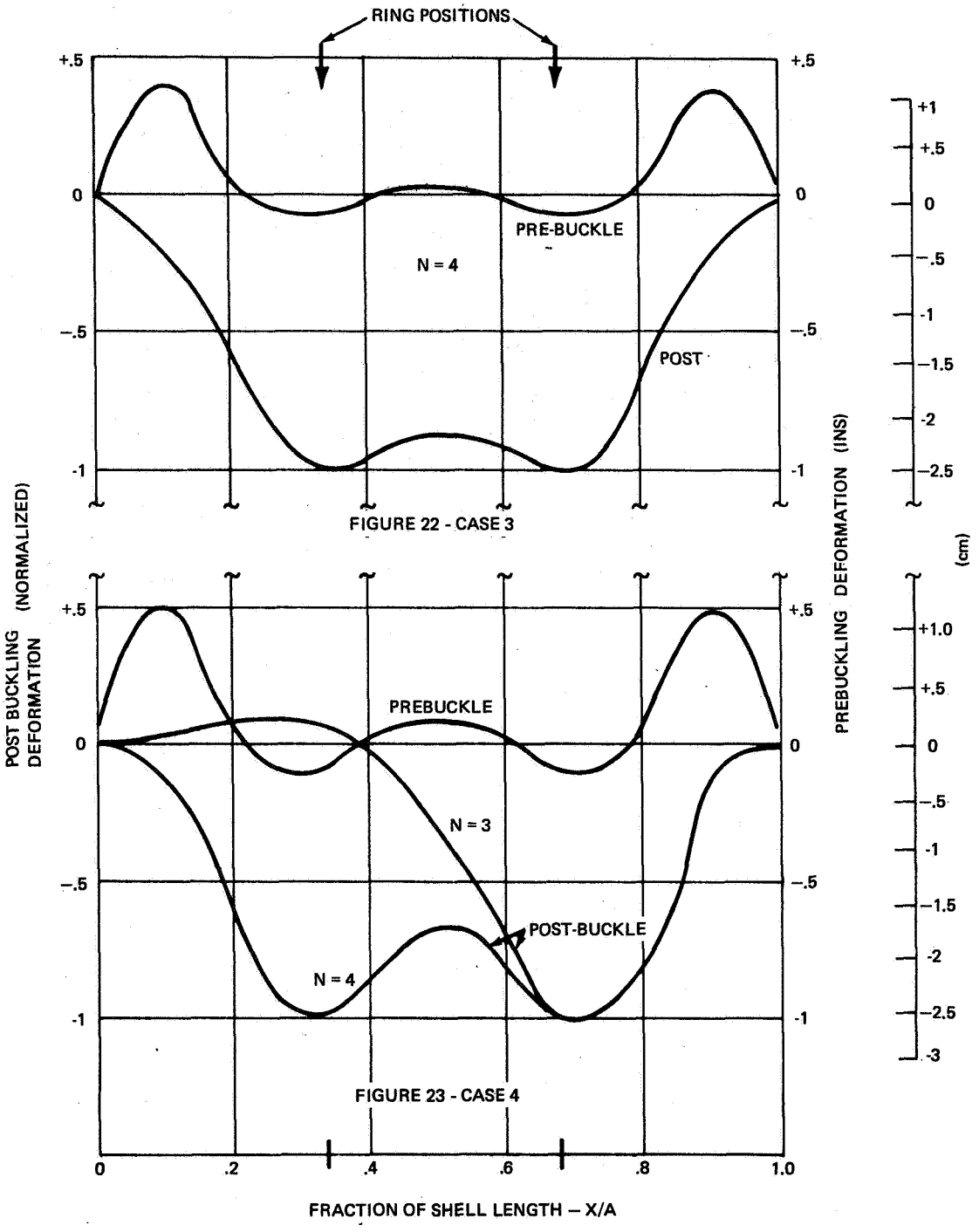

Figures 22 and 23 RADIAL PREBUCKLING AND POSTBUCKLING DEFORMATIONS

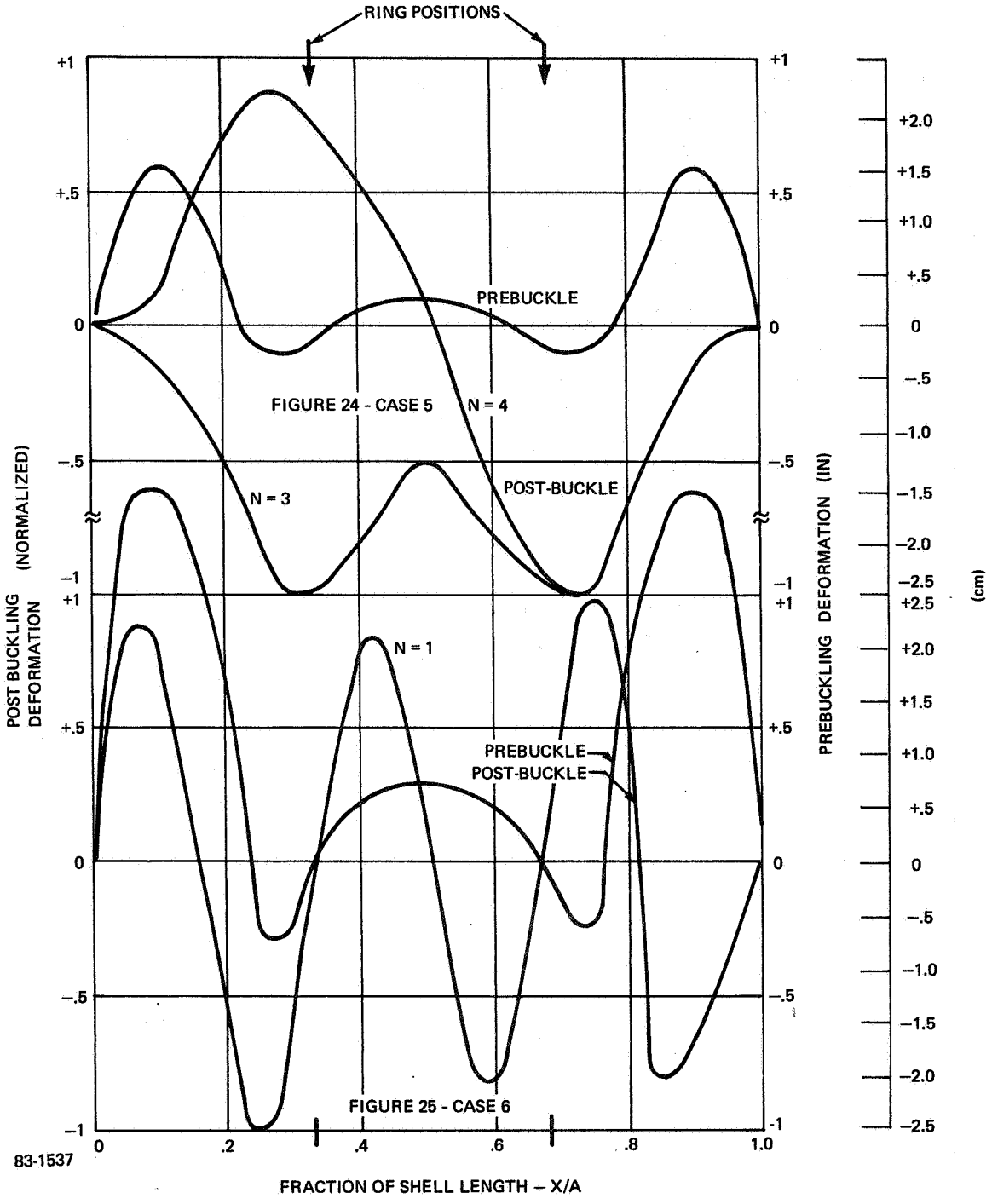

Figures 24 and 25 RADIAL PREBUCKLING AND POSTBUCKLING DEFORMATIONS

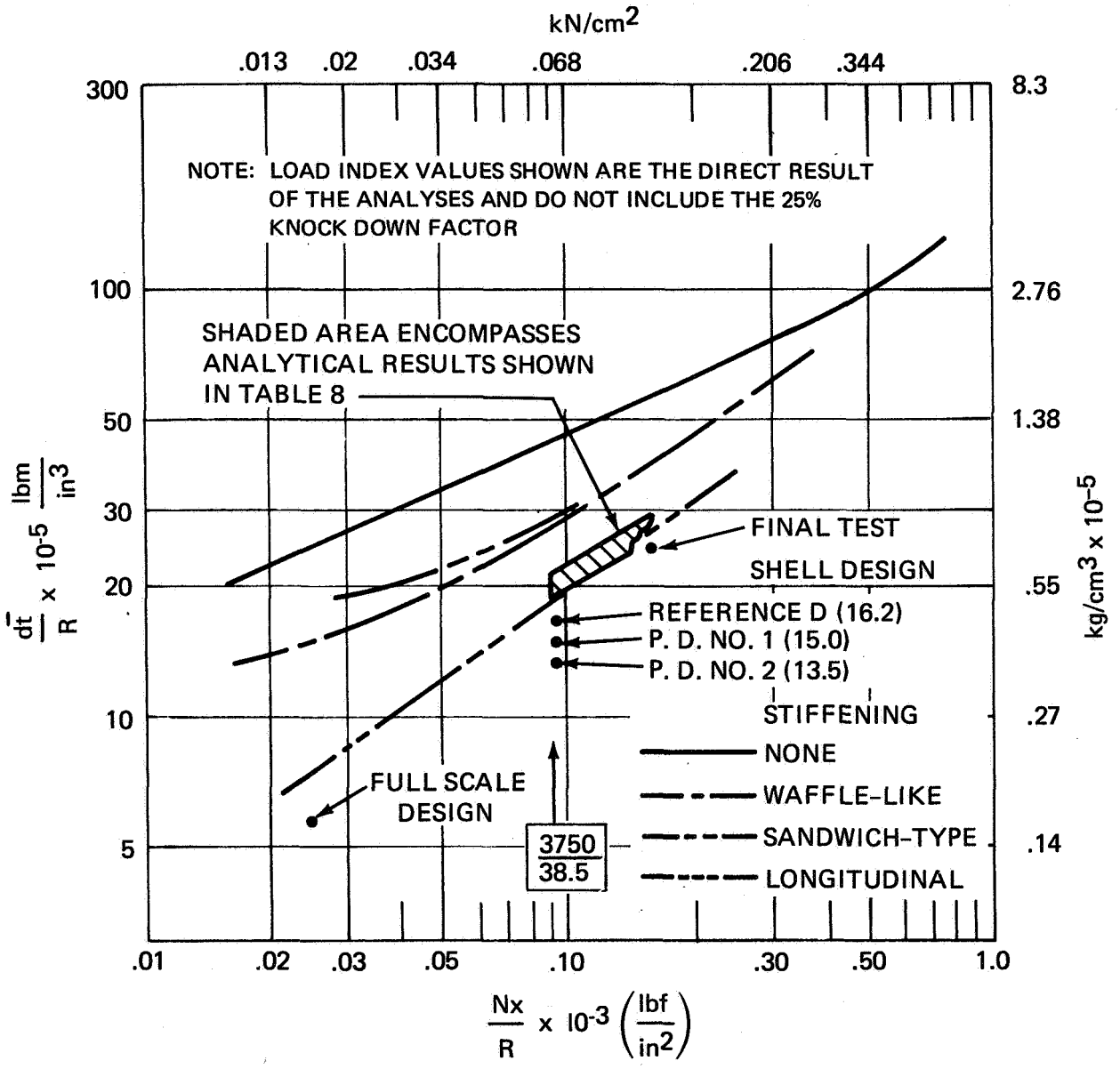

Figure 26 WEIGHT INDEX VERSUS LOAD INDEX FOR SHELL DESIGNS

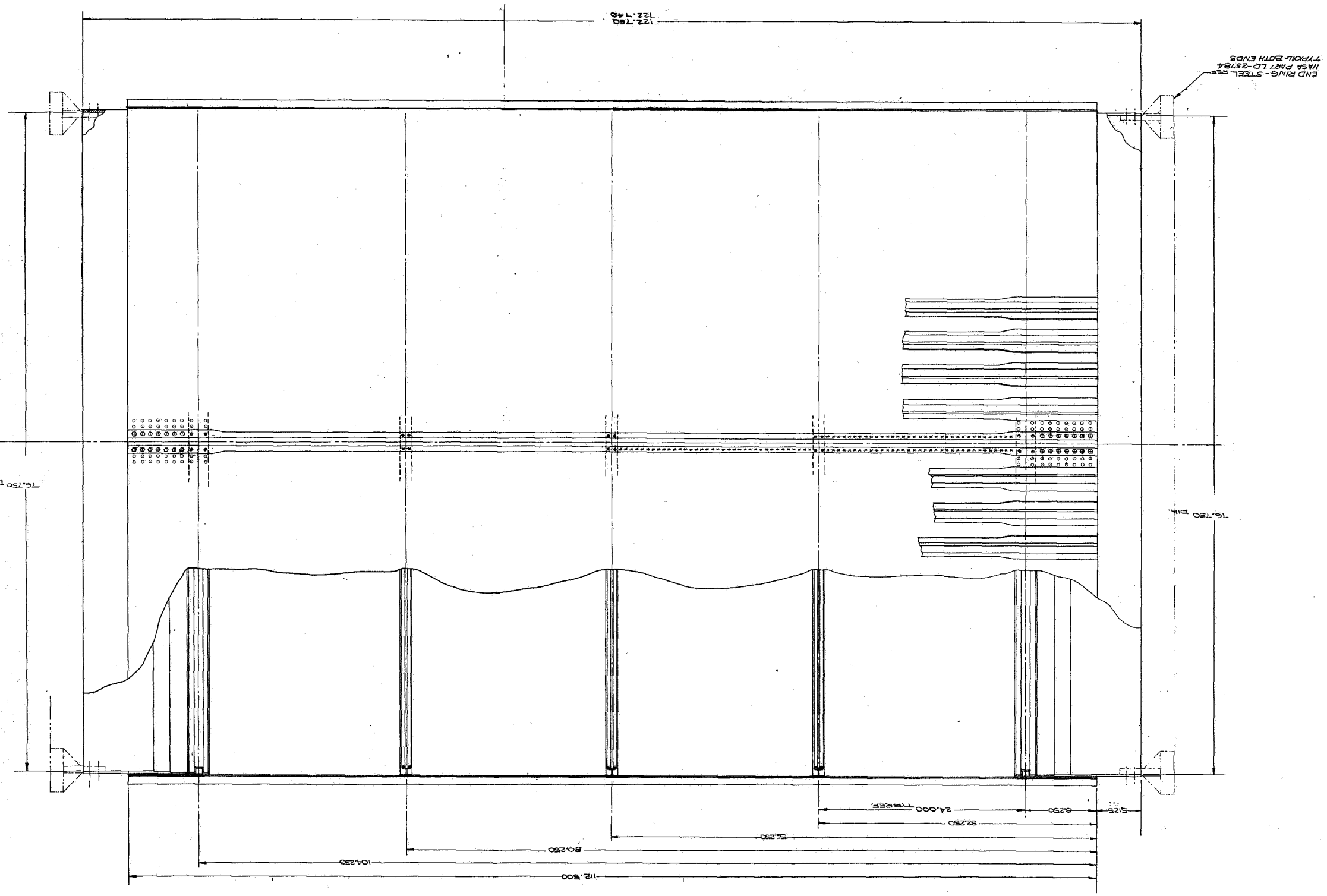
122.760
122.748
END RING - STEEL REF.
NASA PART LD-25784
TYPICAL BOTH ENDS
76.750 DIA.
76.750 DIA.
24.000 THREF.
6.250
SIZE
32.250
52.250
80.250
104.250
112.500

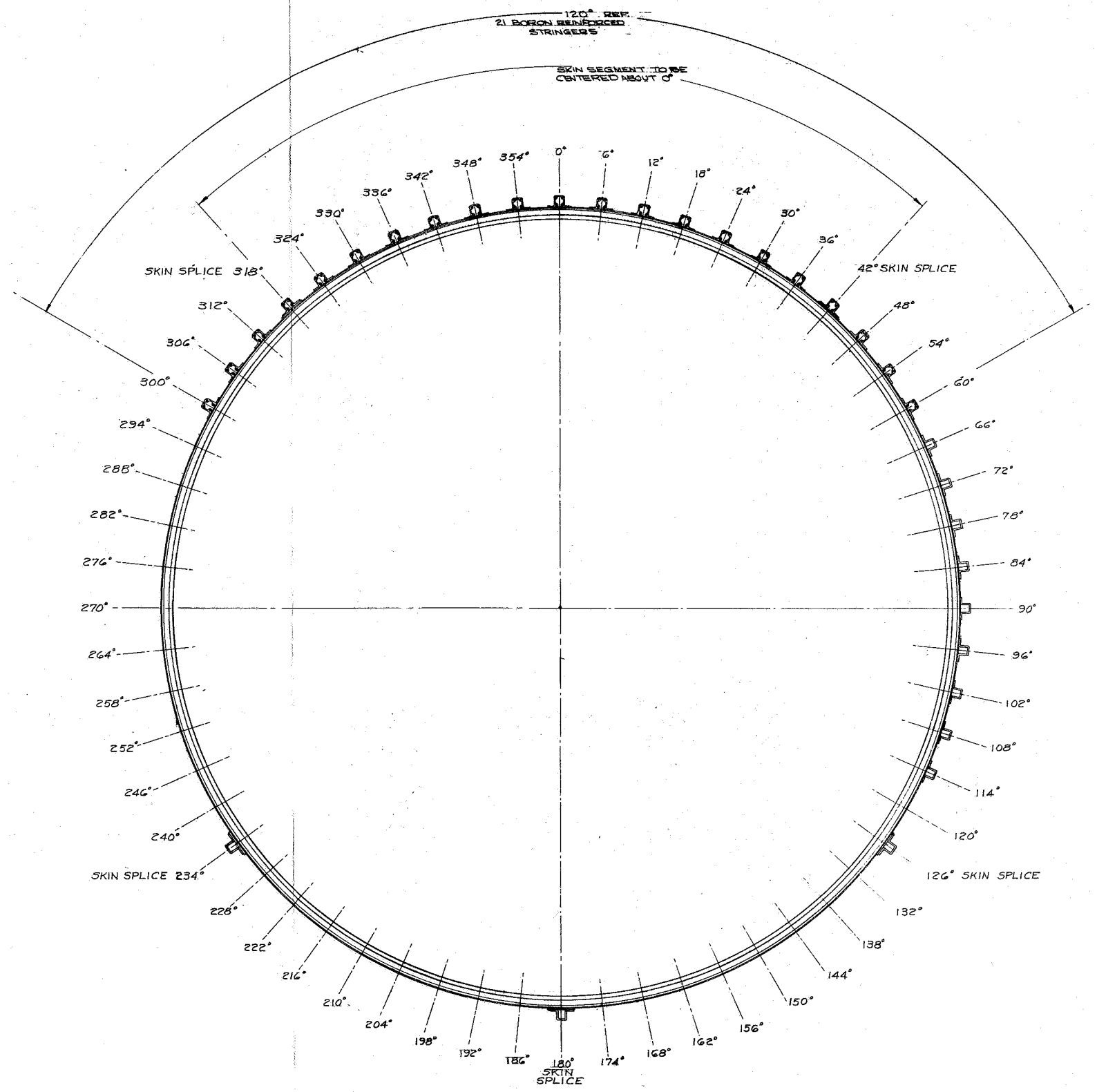

Figure 27 TEST SHELL DESIGN

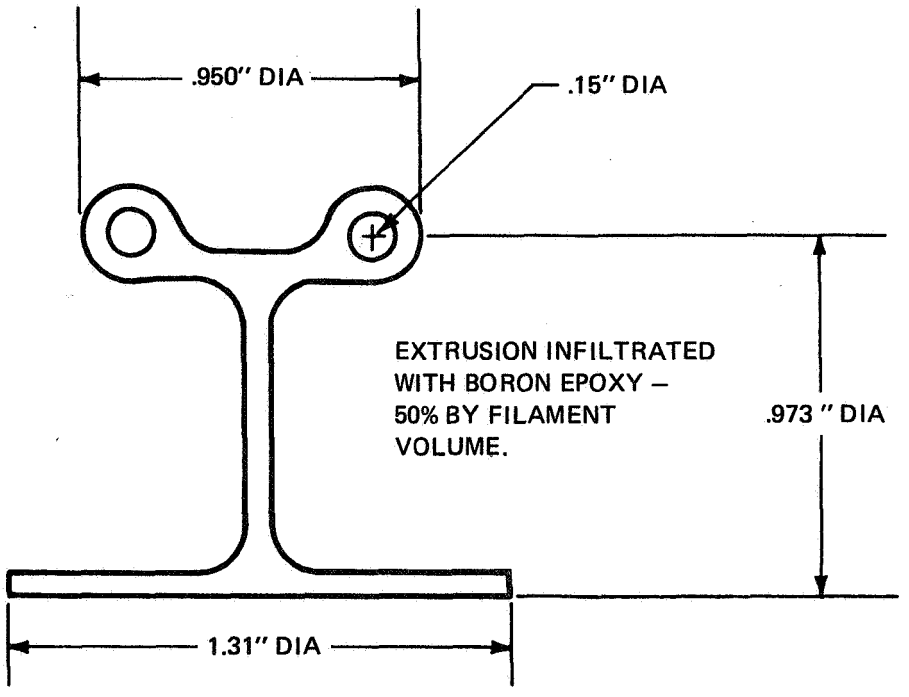

Figure 28 REINFORCED RING SECTION

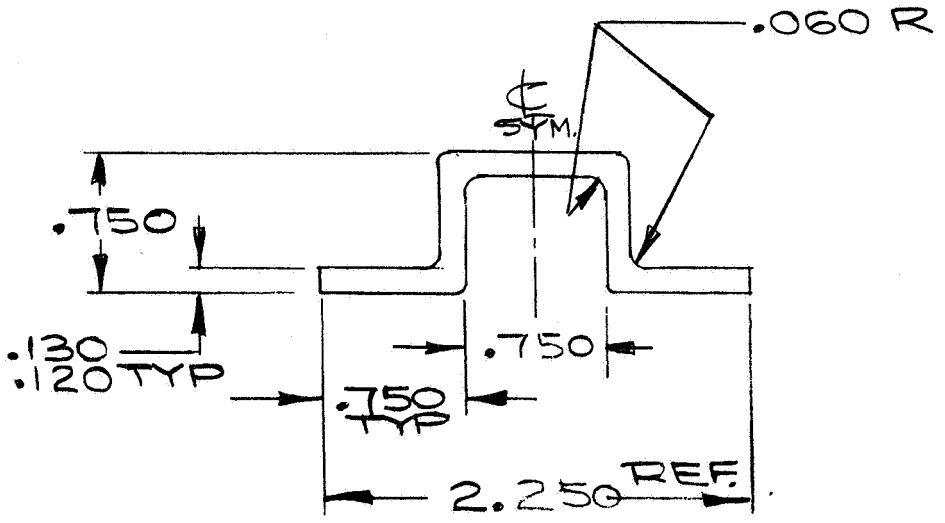

Figure 29 SOLID EXTRUDED RING SECTION

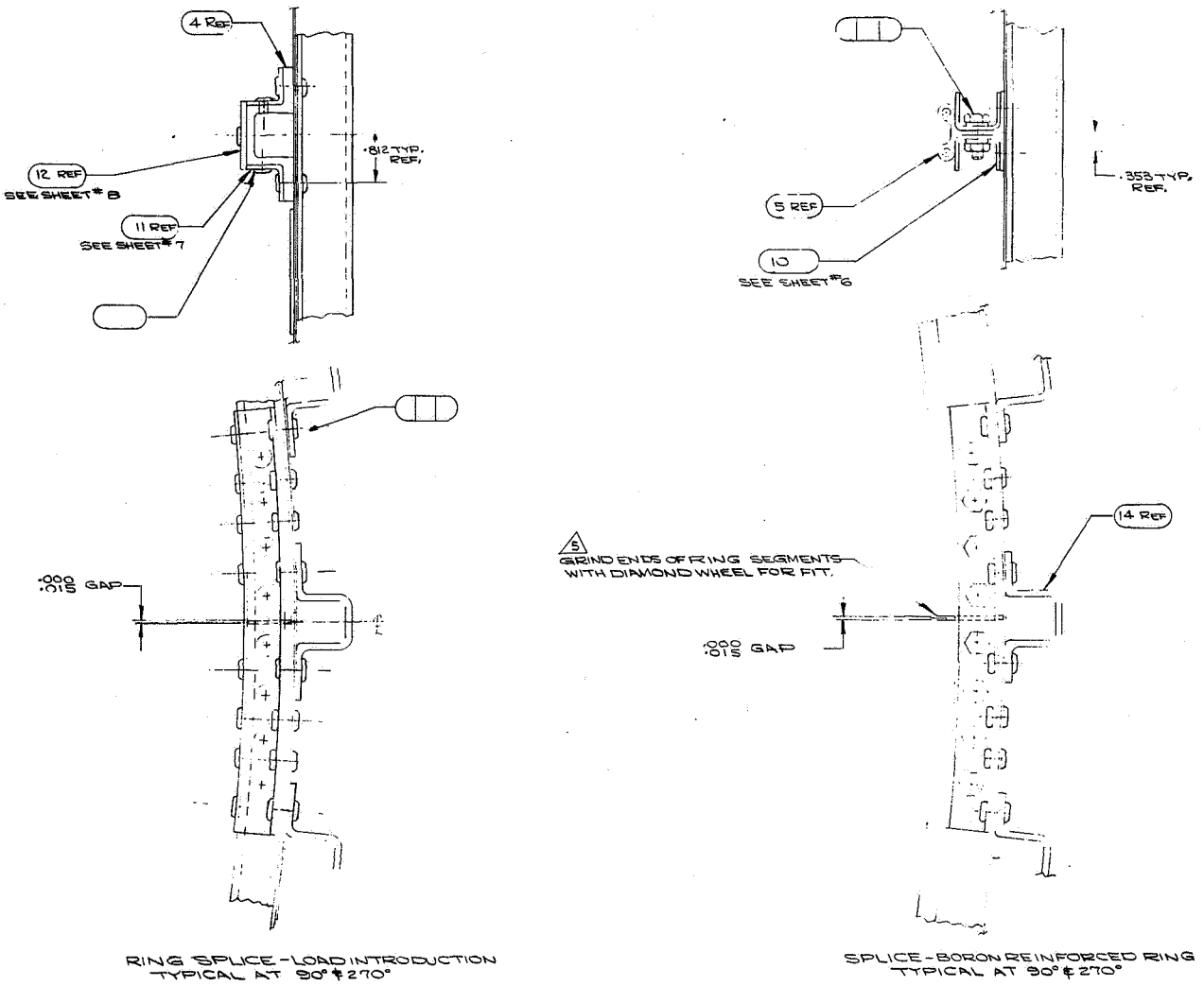

Figure 30 RING SPLICE JOINTS

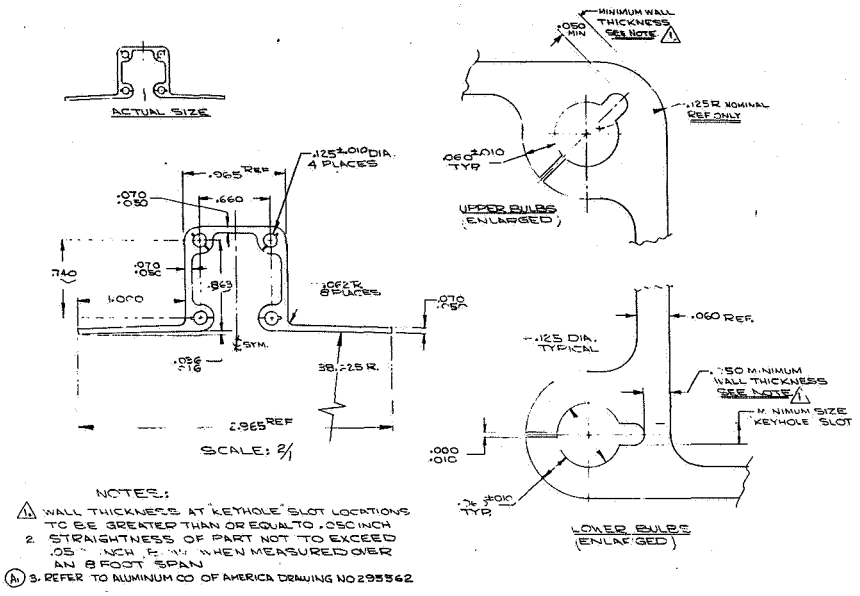

AS EXTRUDED

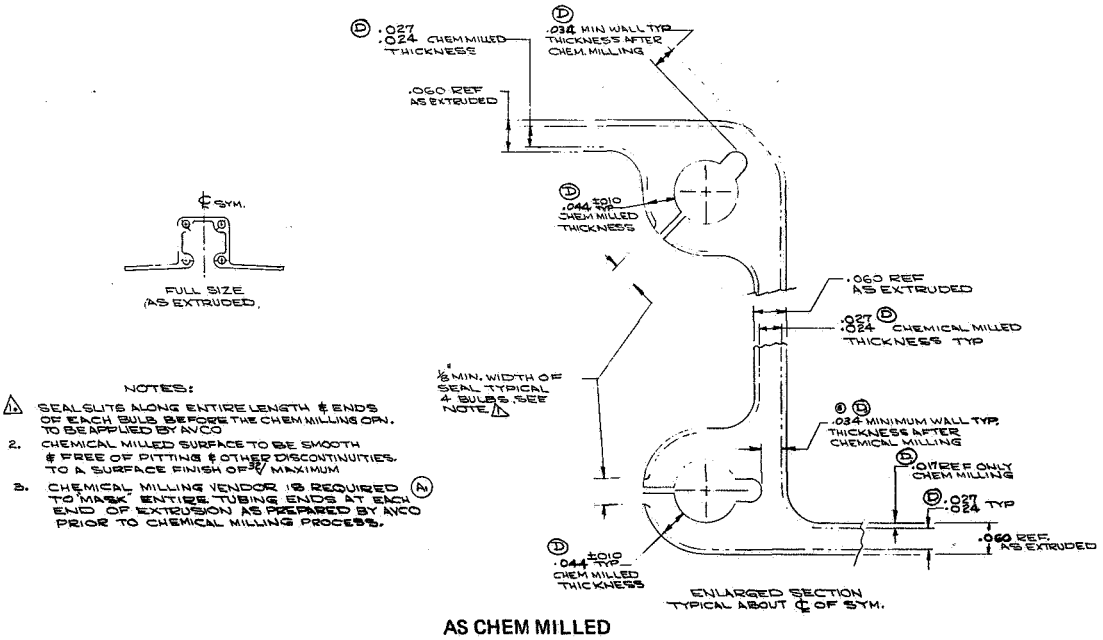

AS CHEM MILLED

Figure 31 HOLLOW STRINGER

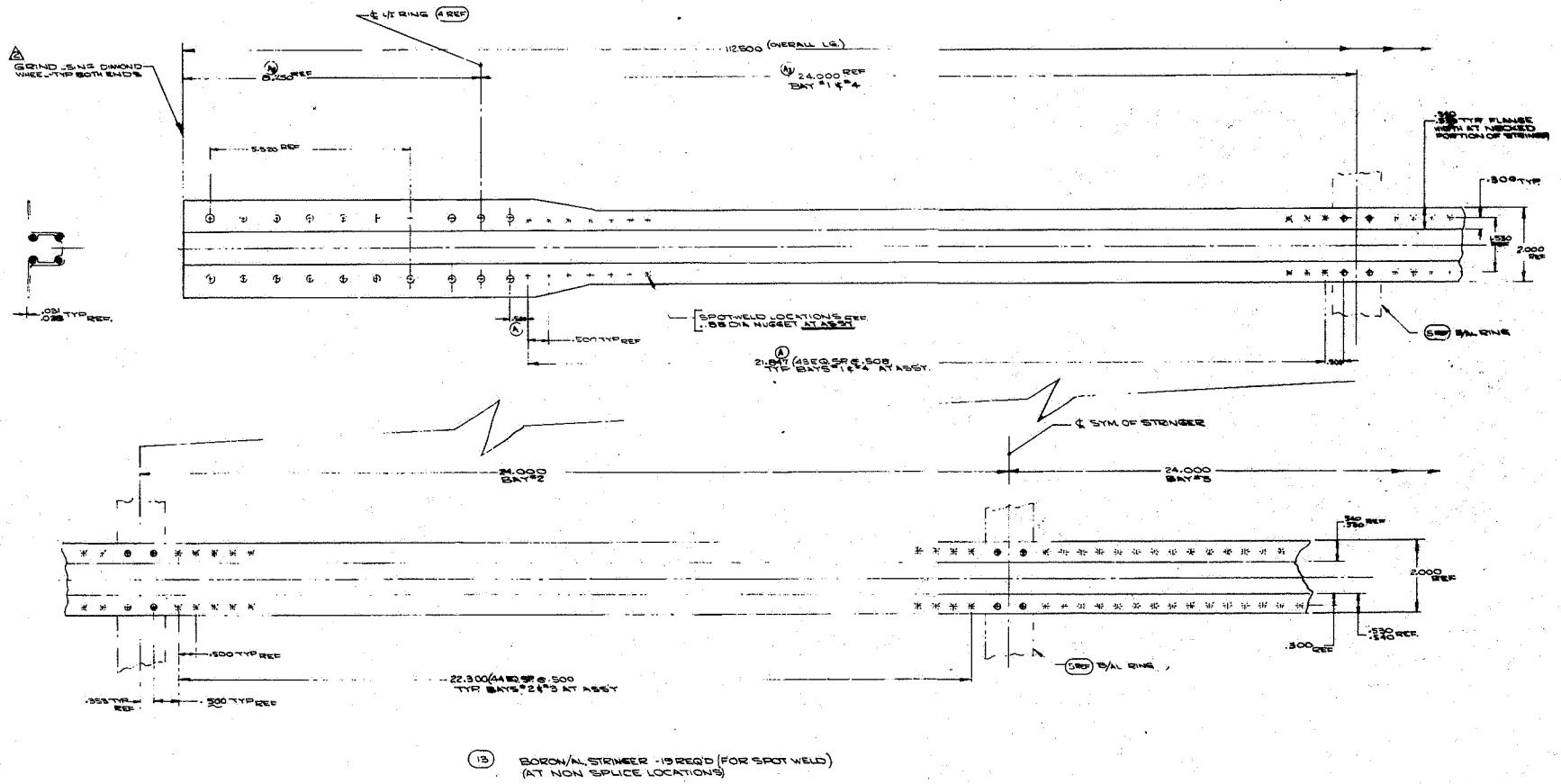

(13) BORON/AL. STRINGER - 19 REQ'D (FOR SPOT WELD) (AT NON SPLICE LOCATIONS)

NOTES:

1. SEE SHEET NO 9 FOR ALL MISSING DIMENSIONS AND NOTES EXCEPT RIVET HOLE ON 21.300 & 22.000 AREA'S.
2. GRIND ENDS OF STRINGERS USING DIAMOND WHEEL ONLY, APPROX. 450 GRIT & LOW FEED RATE. PART TO BE RESTRAINED FROM CHATTERING. BORON ENDS TO BE SMOOTH AFTER FINISHING.

Figure 32 PROFILE AND ATTACHMENT OF REINFORCED STRINGER

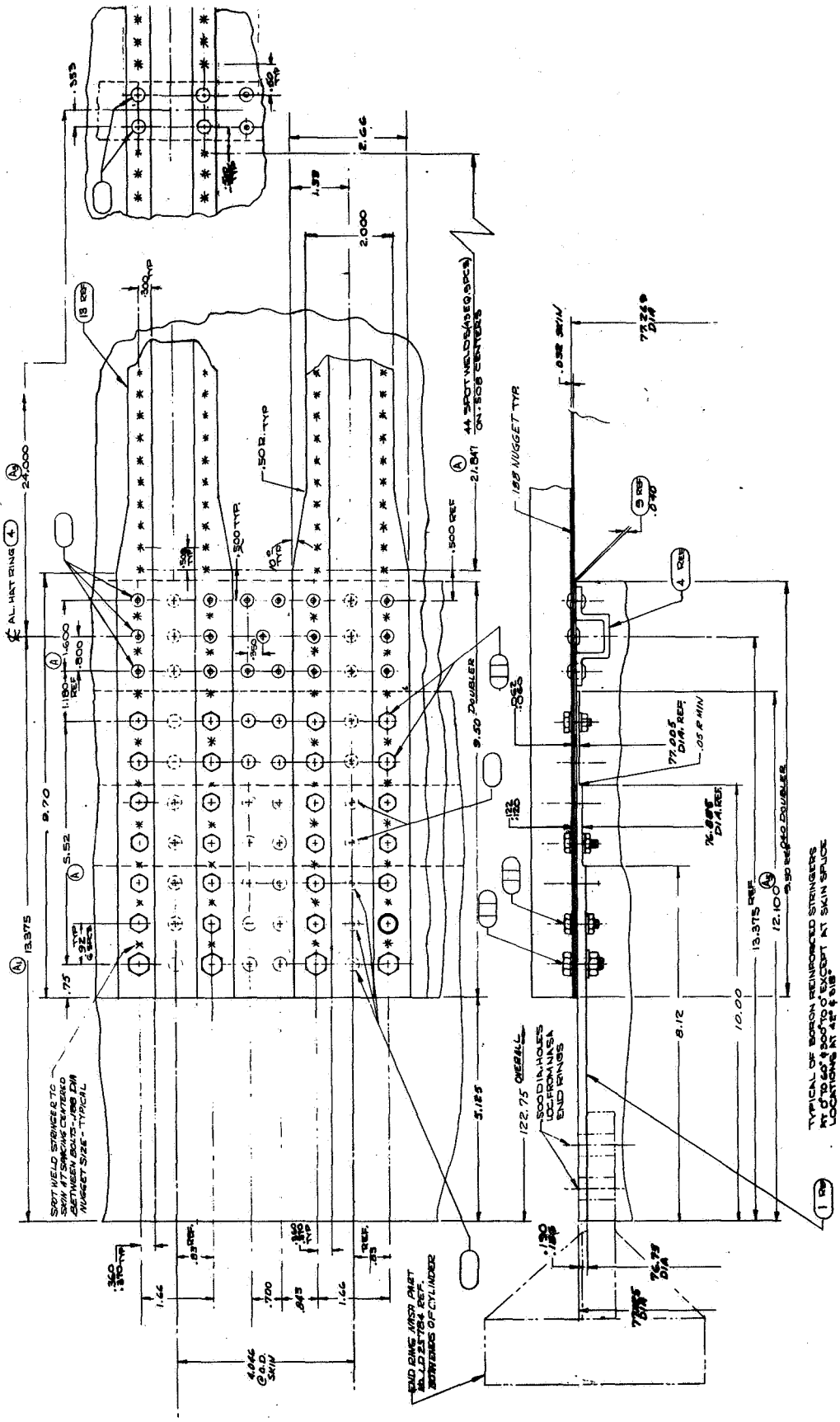

Figure 33 LOAD TRANSFER AREA – REINFORCED STRINGERS

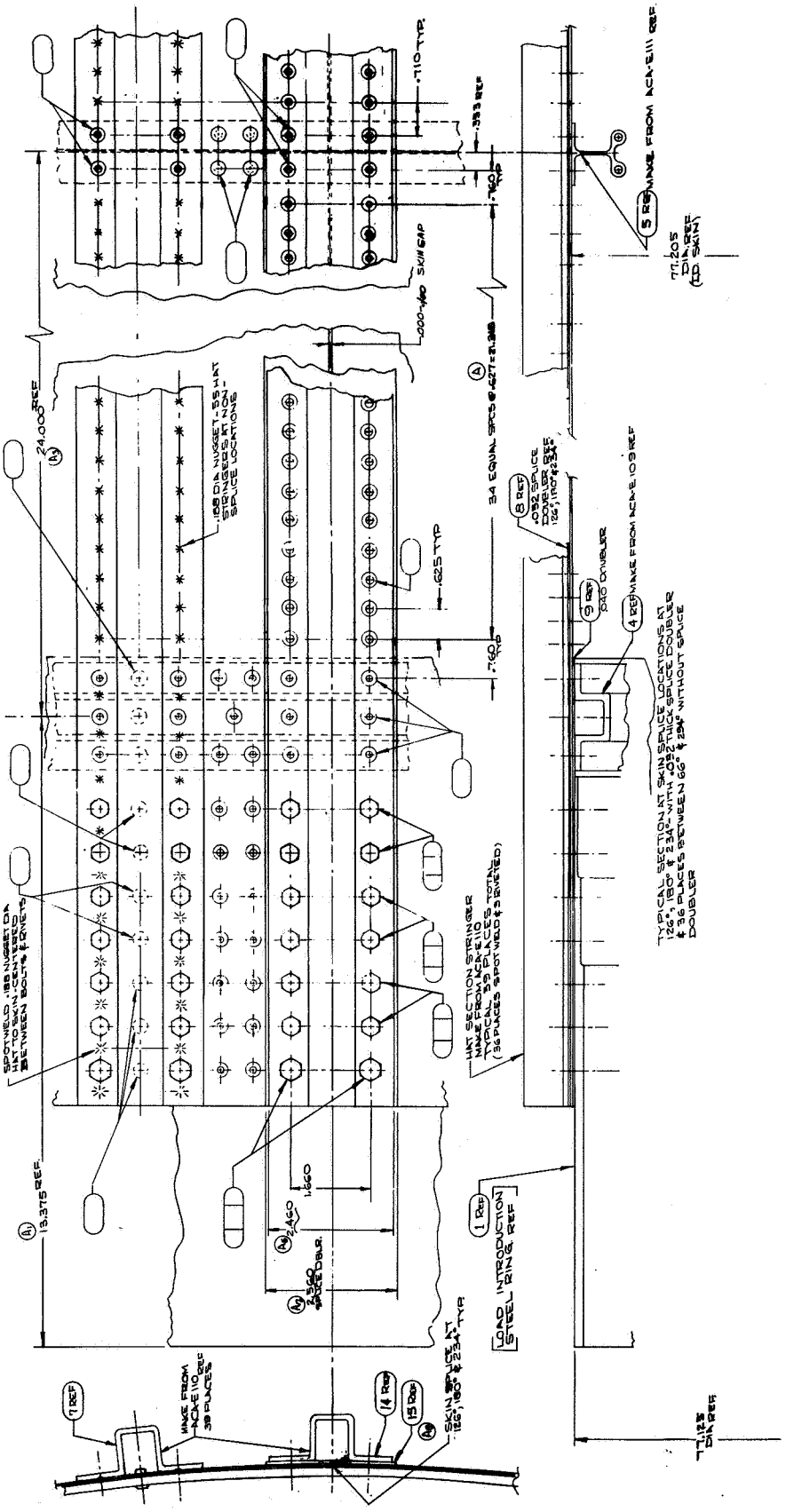

Figure 34 LOAD TRANSFER AREA – NON–REINFORCED STRINGERS

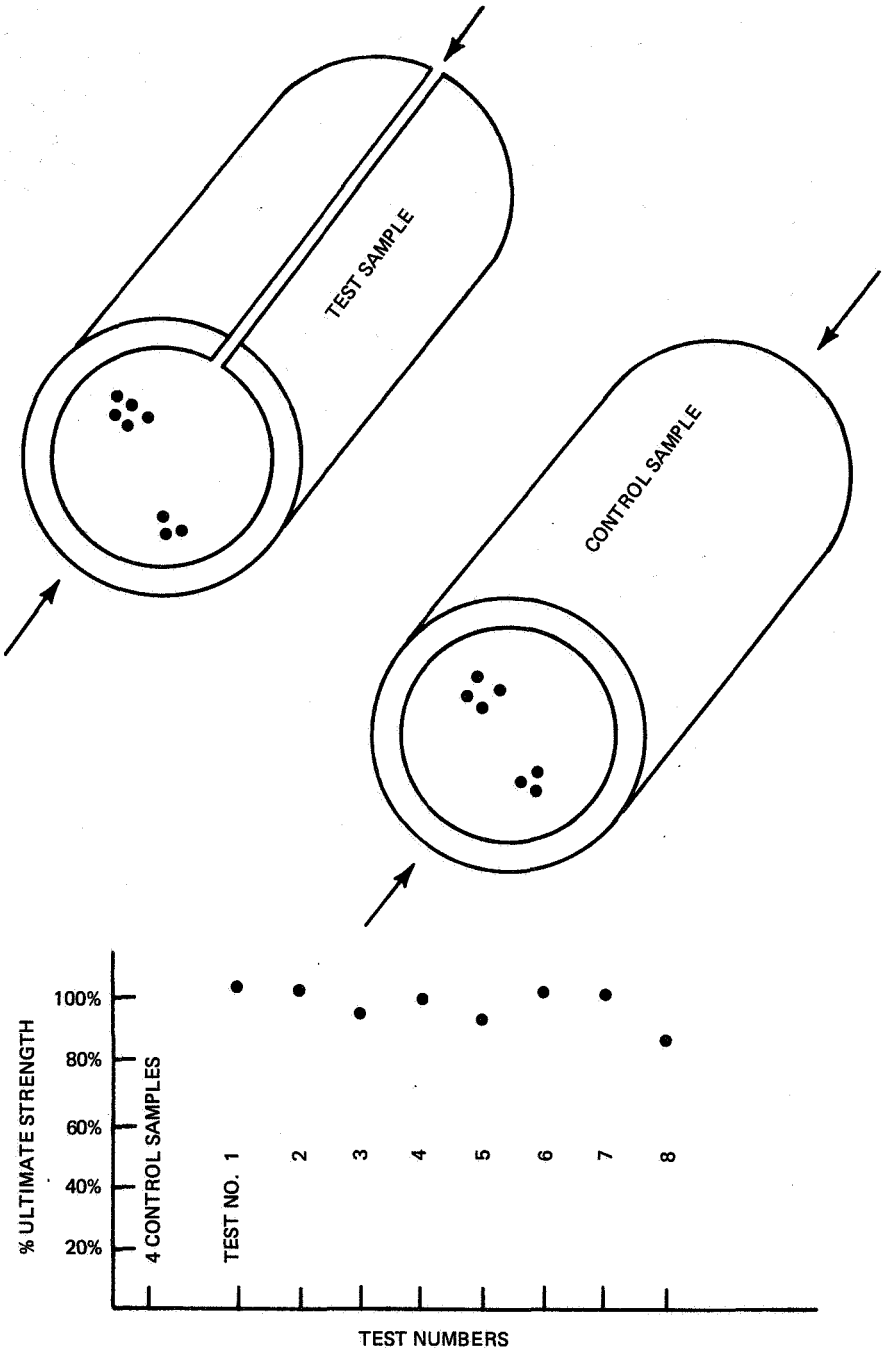

Figure 35 COMPRESSION TESTS ON "SLIT" BORON ALUMINUM RODS

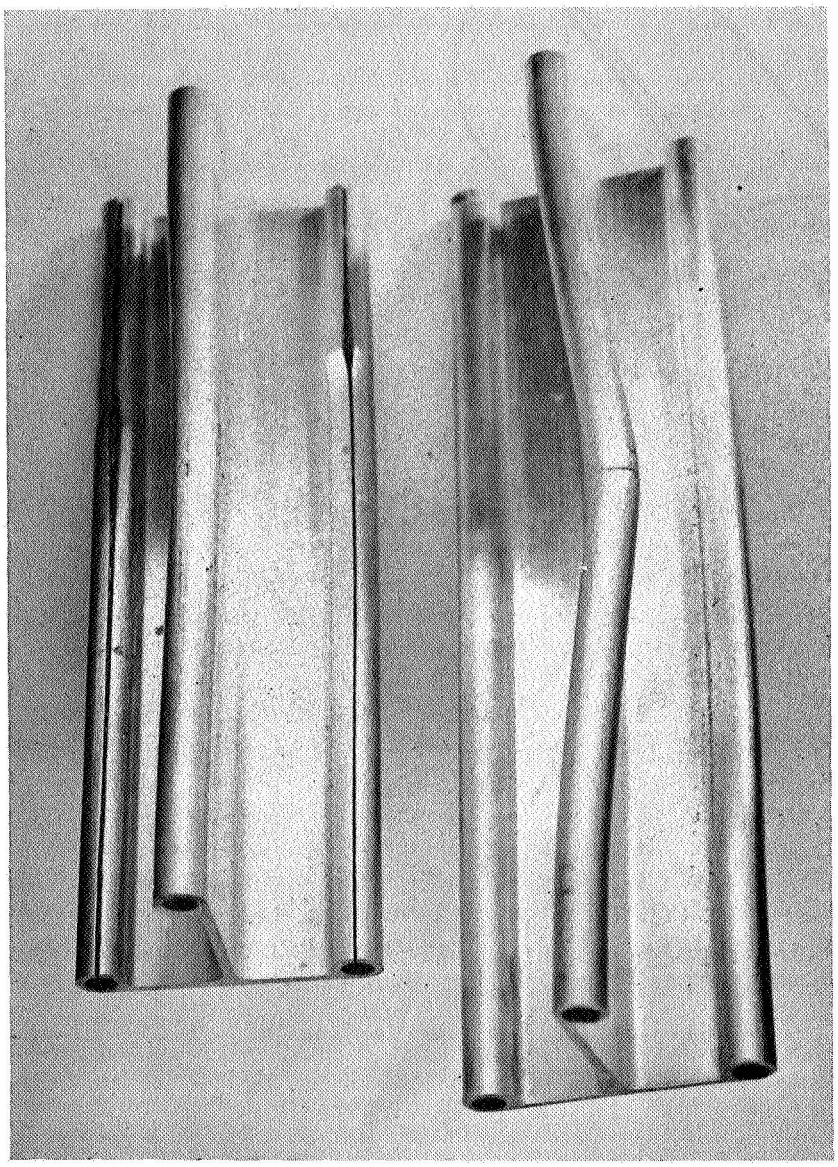

Figure 36 "SLIT" TRI – ELEMENTS TEST SPECIMENS

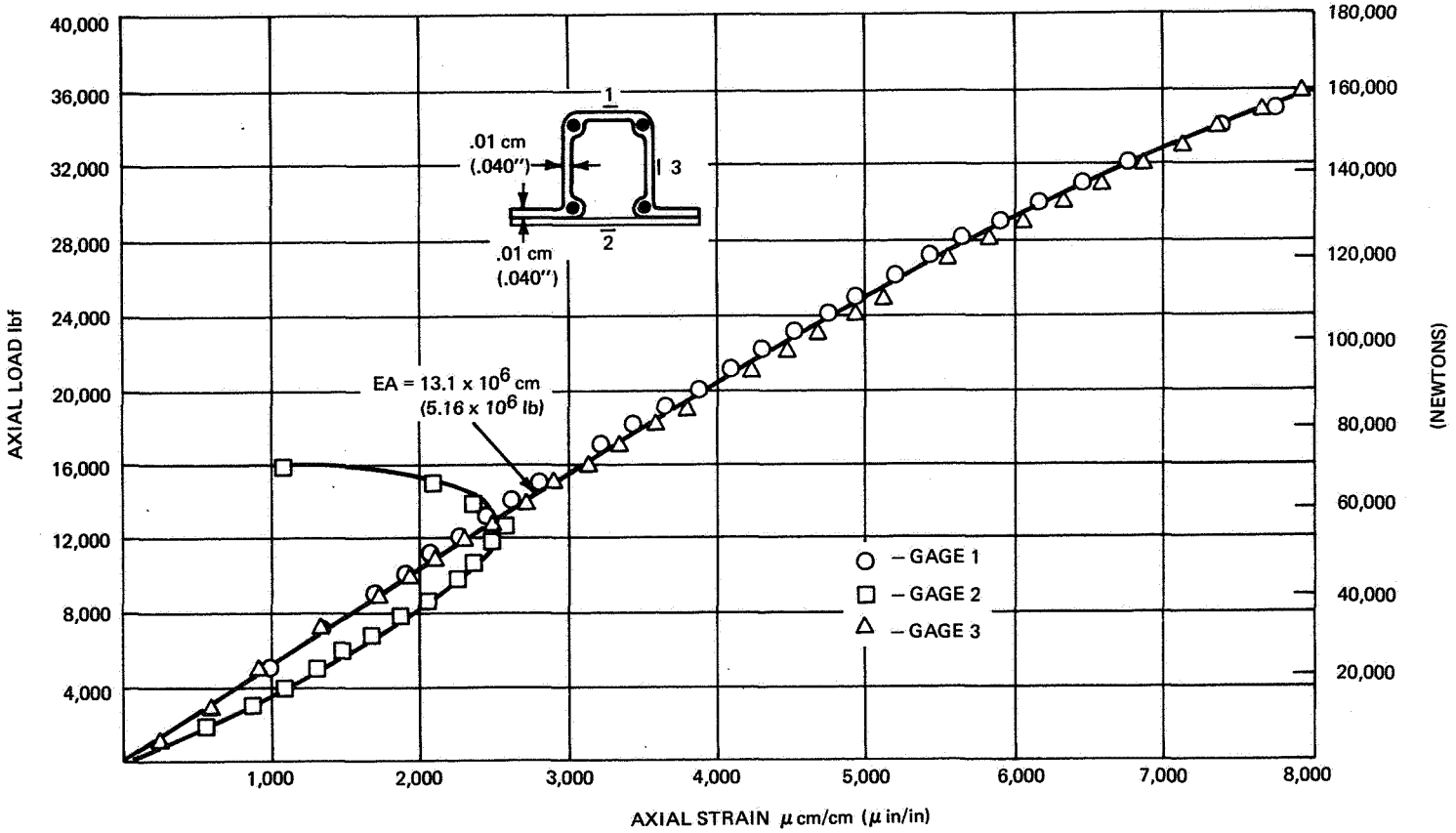

Figure 37 LOAD VERSUS STRAIN HAT SECTION CRIPPLING SPECIMEN NO. 1

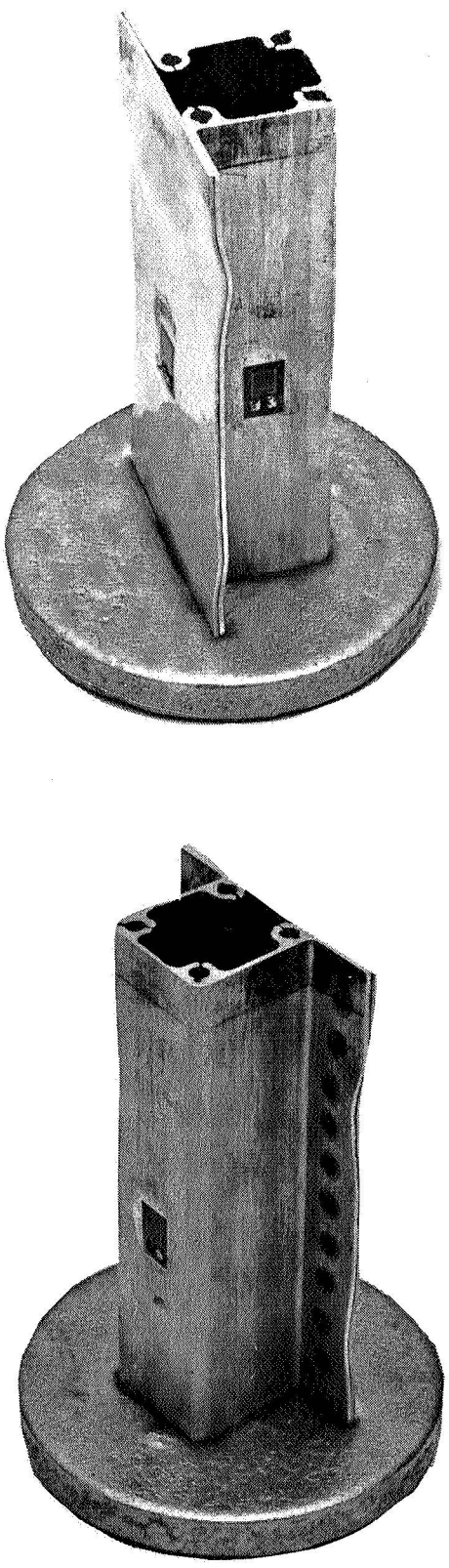

Figure 38 POST TEST – HAT SECTION STRINGER CRIPPLING SPECIMEN NO. 1

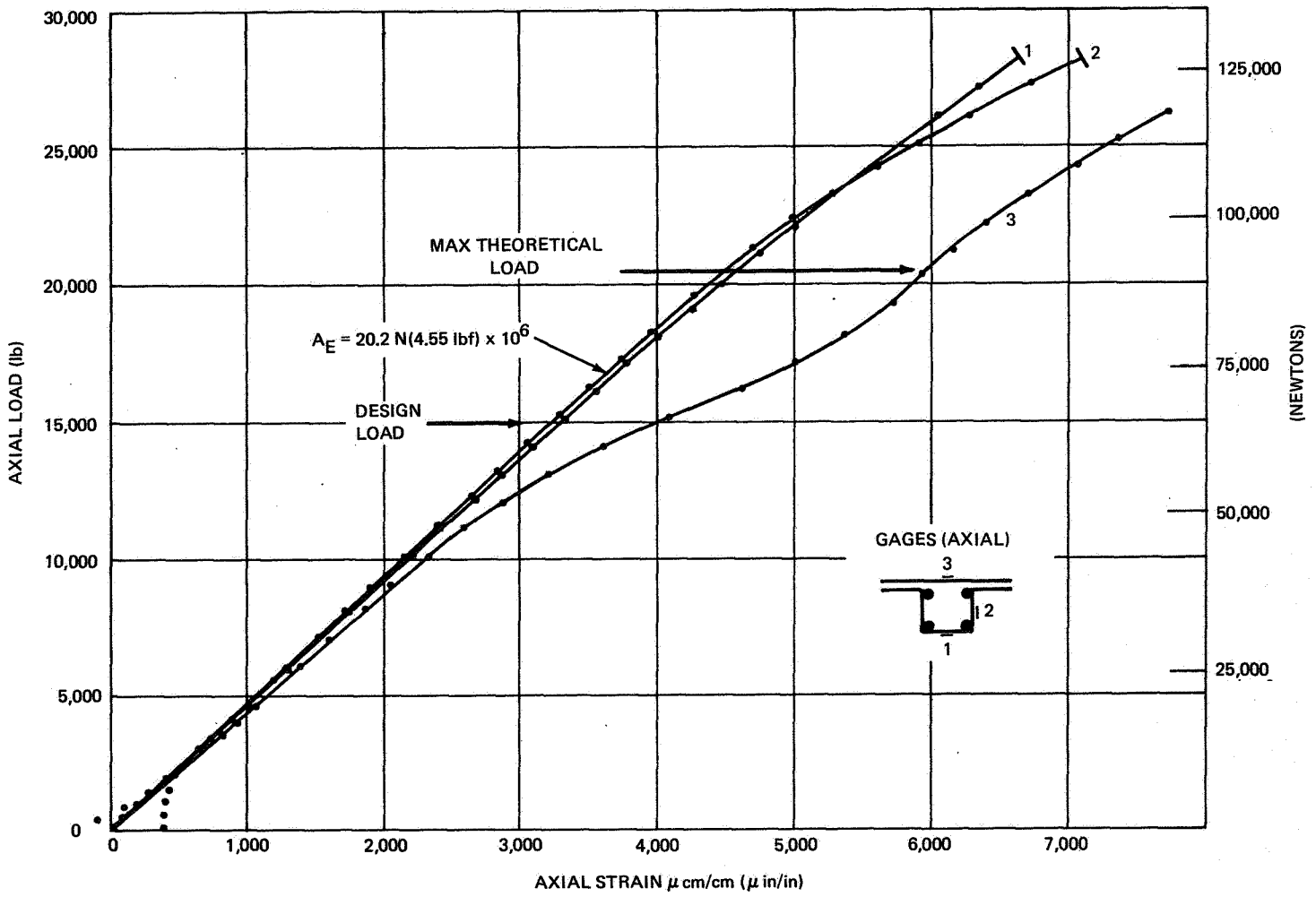

Figure 39 LOAD VERSUS STRAIN HAT SECTION CRIPPLING TEST NO. 2

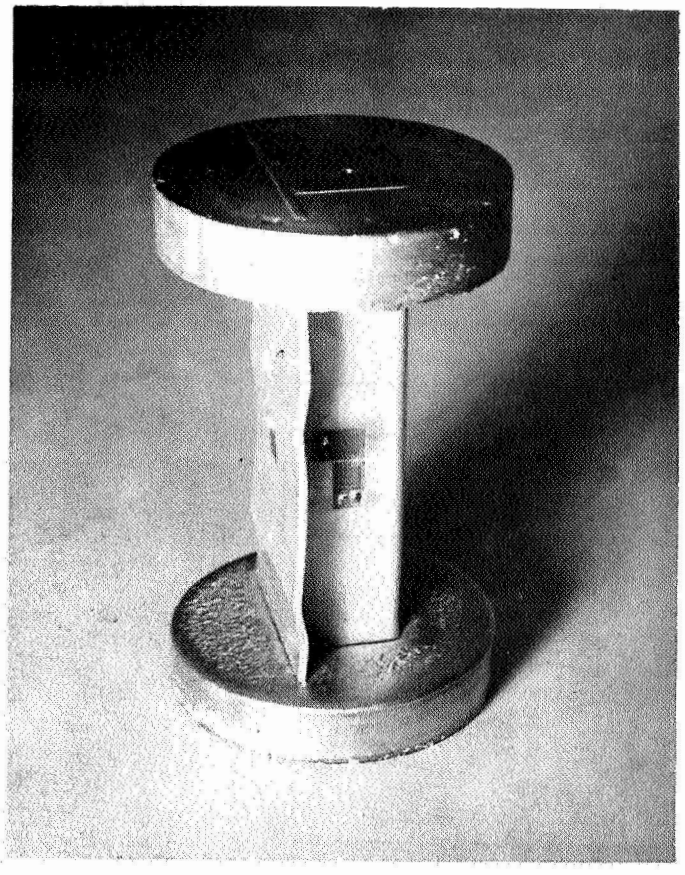

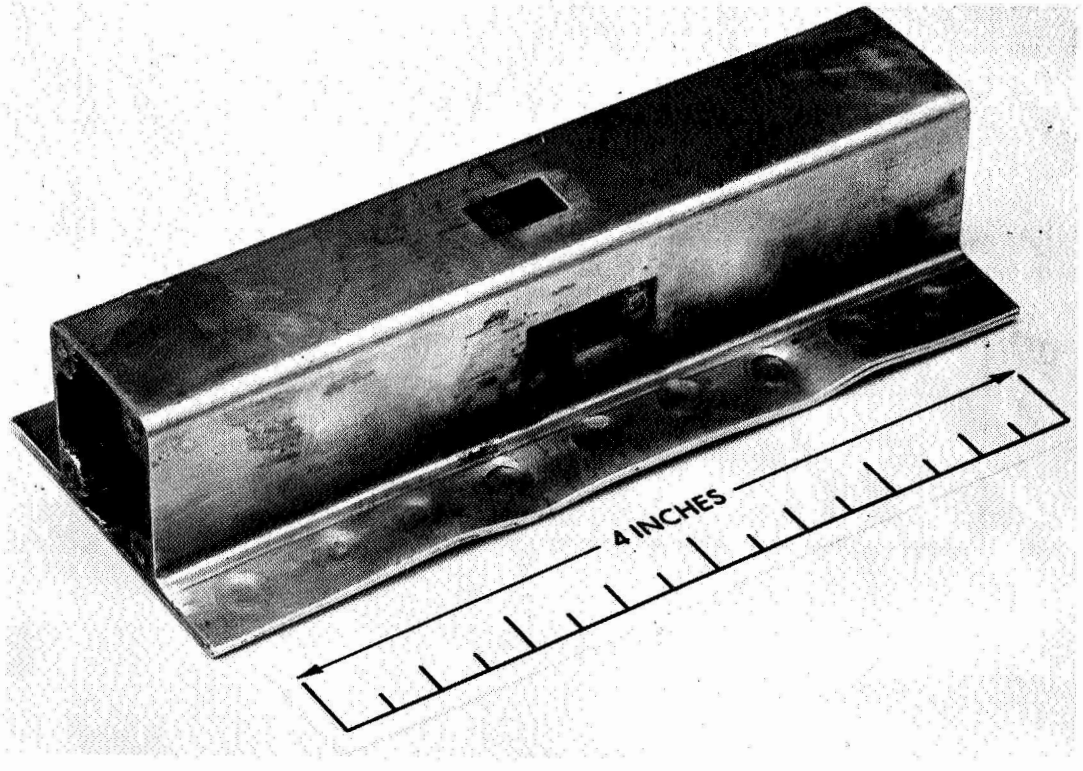

Figure 40 POST TEST – HAT SECTION CRIPPLING TEST NO. 2

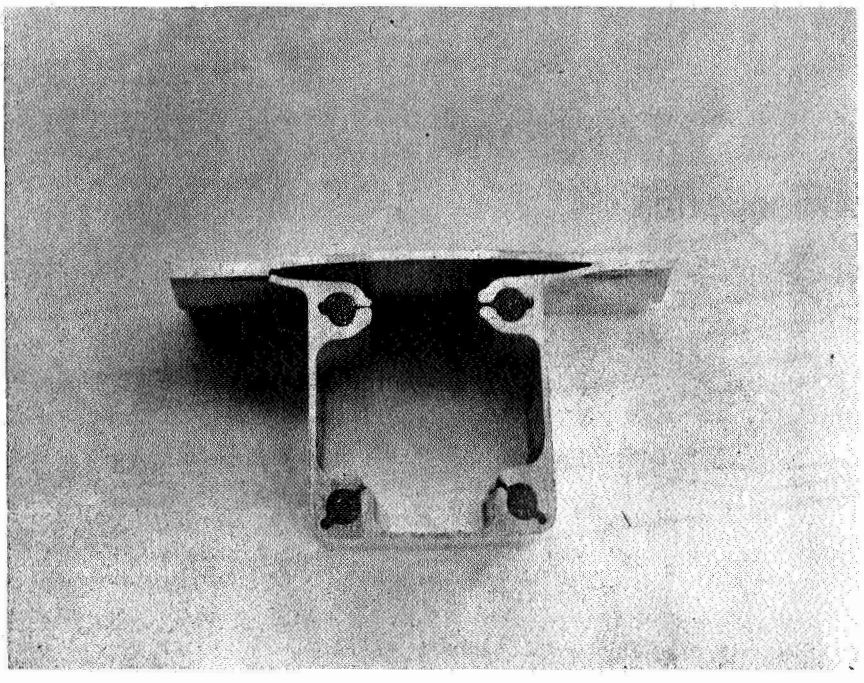

Figure 41 SECTION THROUGH FAILED HAT STRINGER

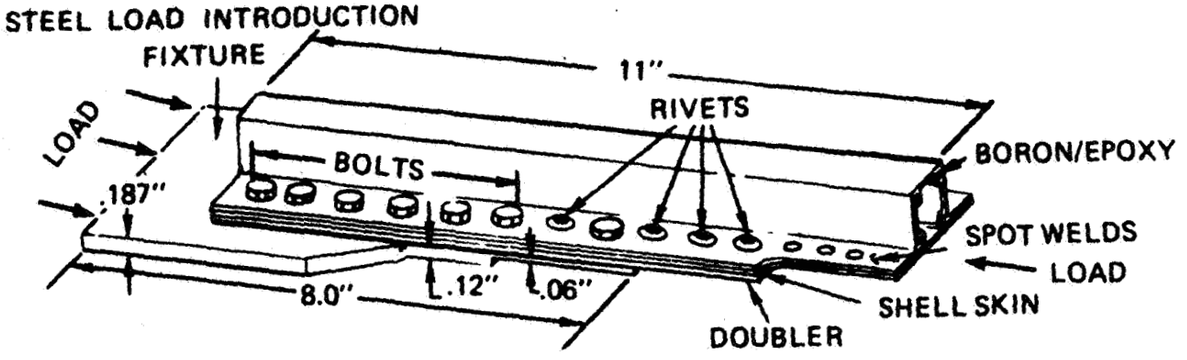

Figure 42 PICTORIAL VIEW OF LOAD TRANSFER TEST SPECIMEN

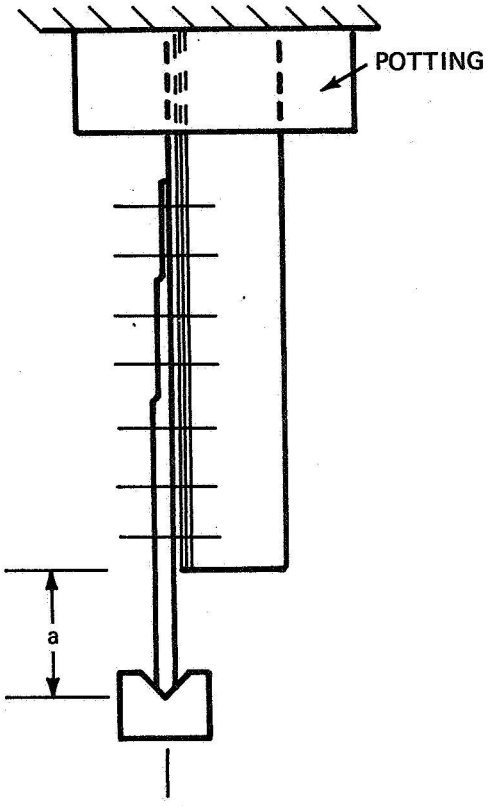

TEST CONFIGURATION

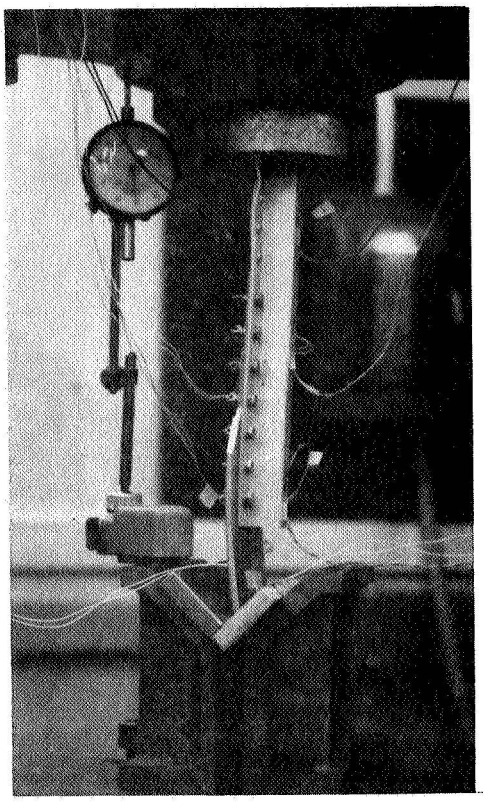

AT 14,800 lb LOAD

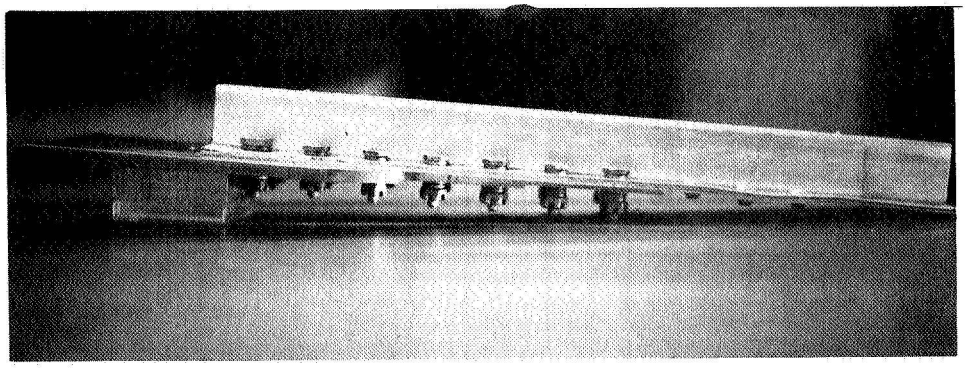

POST-TEST

Figure 43 LOAD TRANSFER SPECIMEN NO. 1

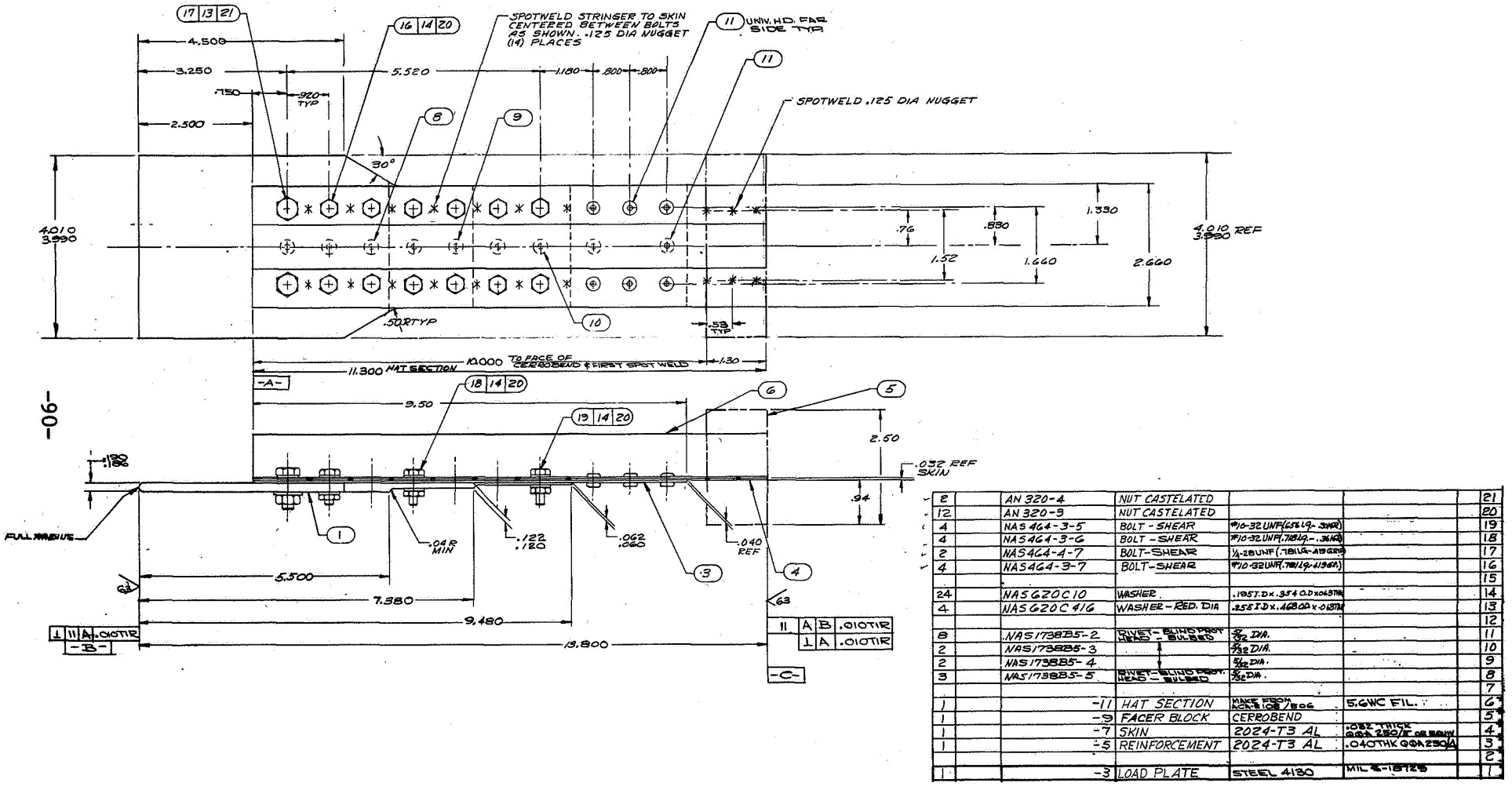

8		AN 320-4	NUT CASTELATED			21
12		AN 320-3	NUT CASTELATED			20
4		NAS 464-3-5	BOLT - SHEAR	#10-32 UNF (.656 LG. - .3962)		19
4		NAS 464-3-6	BOLT - SHEAR	#10-32 UNF (.718 LG. - .3962)		18
2		NAS 464-4-7	BOLT-SHEAR	1/4-28 UNF (.781 LG. - .4159)		17
4		NAS 464-3-7	BOLT-SHEAR	#10-32 UNF (.781 LG. - .4162)		16
						15
24		NAS 620 C 10	WASHER	.195 I.D. x .354 O.D. x .057 THK		14
4		NAS 620 C 416	WASHER - RED. DIA	.255 I.D. x .468 O.D. x .057 THK		13
						12
8		NAS 1738 B5-2	RIVET - BLIND PROT HEAD - BULBED	5/32 DIA.		11
2		NAS 1738 B5-3		5/32 DIA.		10
2		NAS 1738 B5-4		5/32 DIA.		9
3		NAS 1738 B5-5	RIVET - BLIND PROT. HEAD - BULBED	5/32 DIA.		8
						7
1		-11	HAT SECTION	MAKE FROM ACS 1068 / 806	5.6 WC FIL.	6
1		-9	FACER BLOCK	CERROBEND		5
1		-7	SKIN	2024-T3 AL	.032 THICK QQA 250/5 OR EQUIV	4
1		-5	REINFORCEMENT	2024-T3 AL	.040 THK QQA 250/A	3
						2
1		-3	LOAD PLATE	STEEL 4130	MIL-S-18729	1

Figure 44 LOAD INTRODUCTION TEST SPECIMEN NO. 1

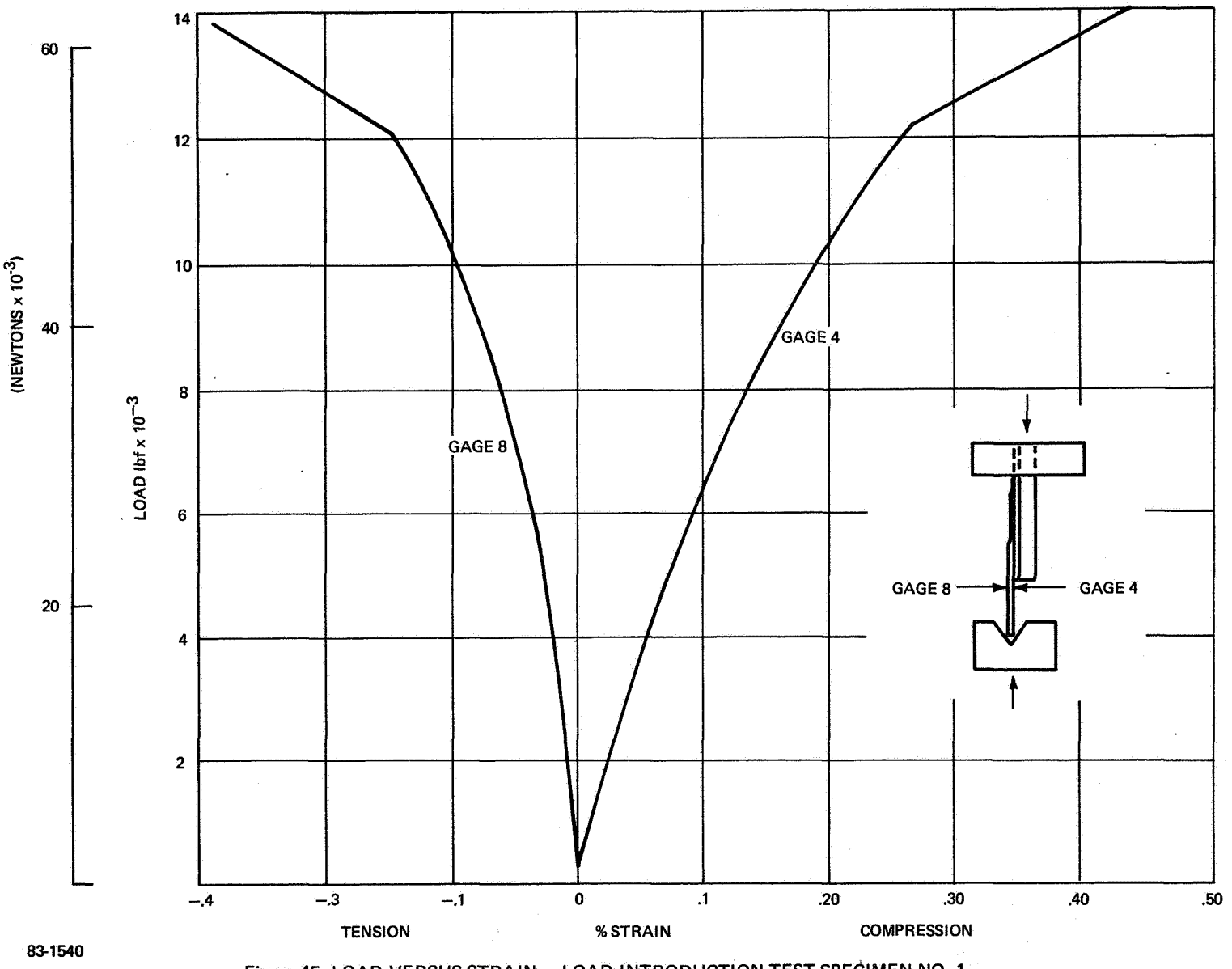

Figure 45 LOAD VERSUS STRAIN – LOAD INTRODUCTION TEST SPECIMEN NO. 1

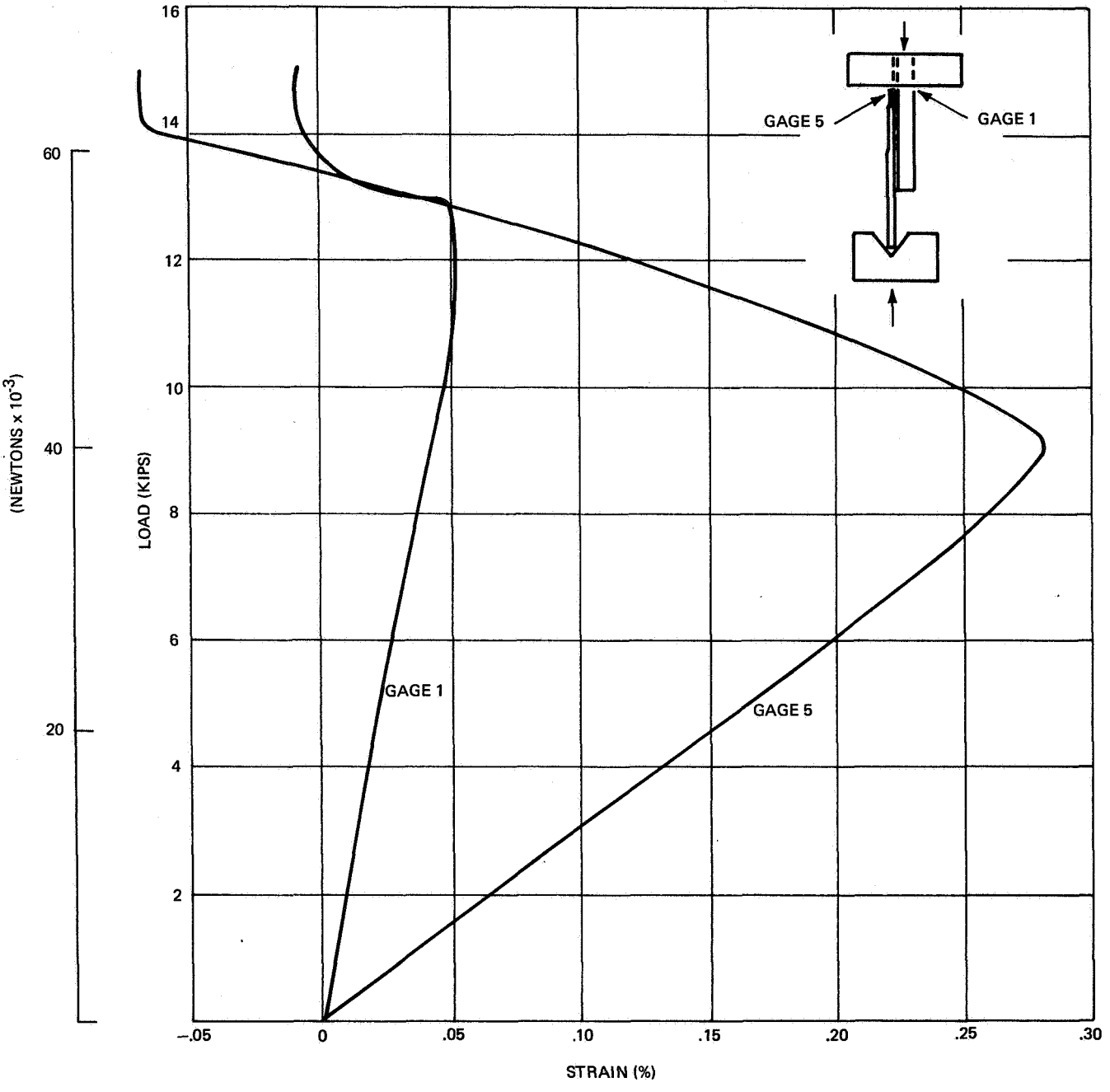

Figure 46 LOAD VERSUS STRAIN – LOAD INTRODUCTION TEST SPECIMEN NO. 1

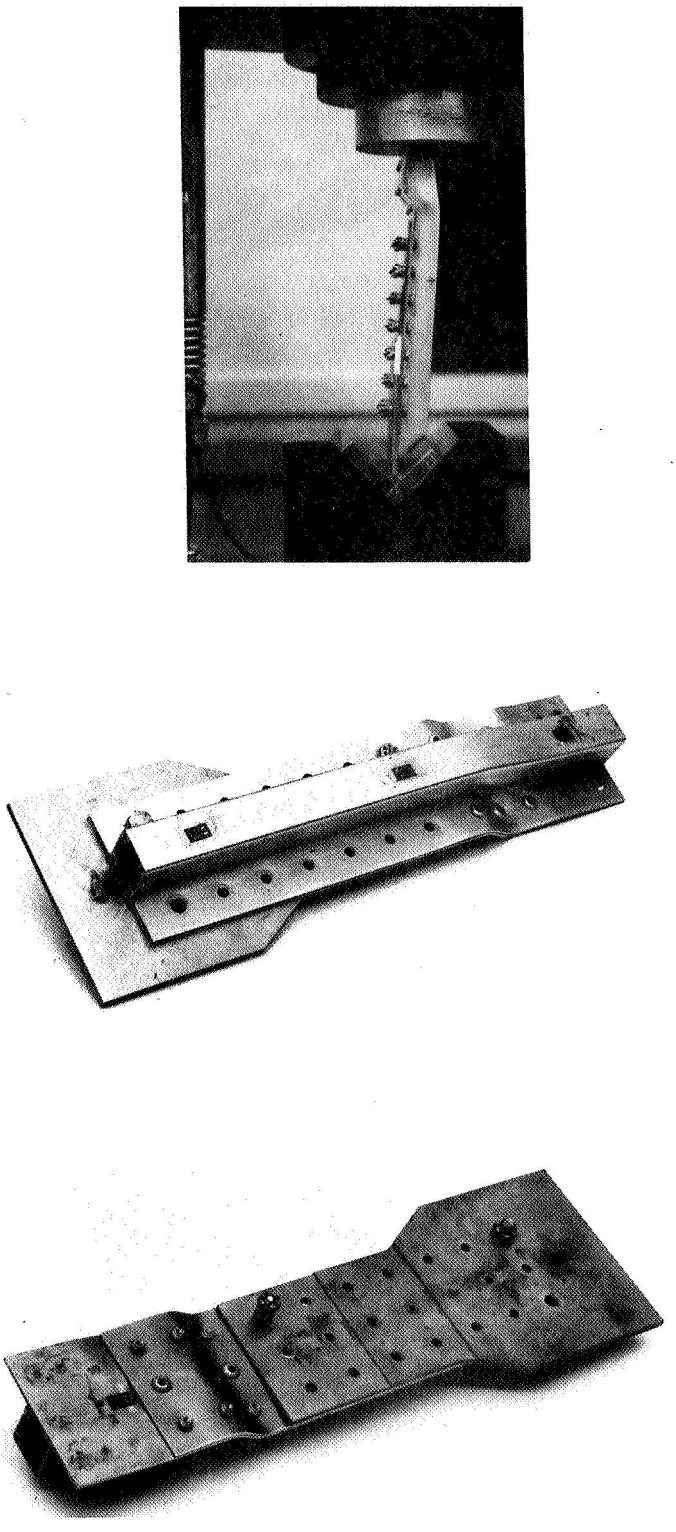

Figure 47 LOAD INTRODUCTION TEST SPECIMEN NO. 2 – POST TEST

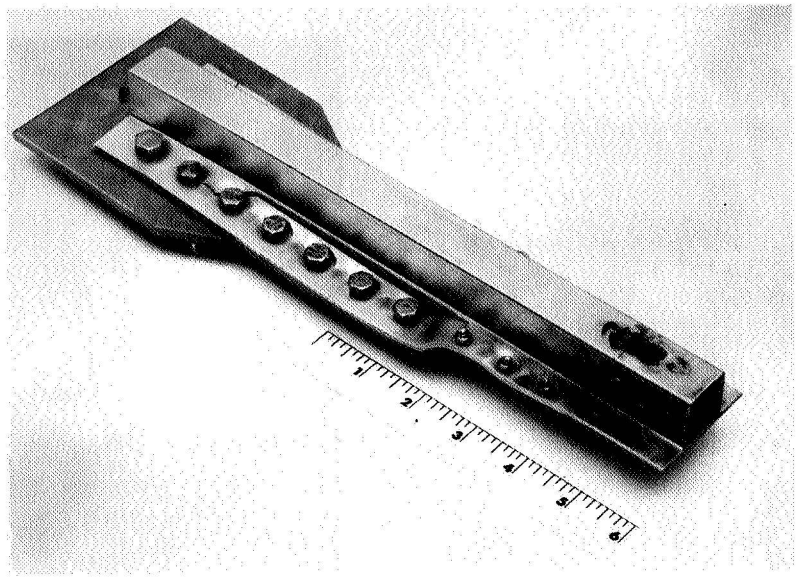

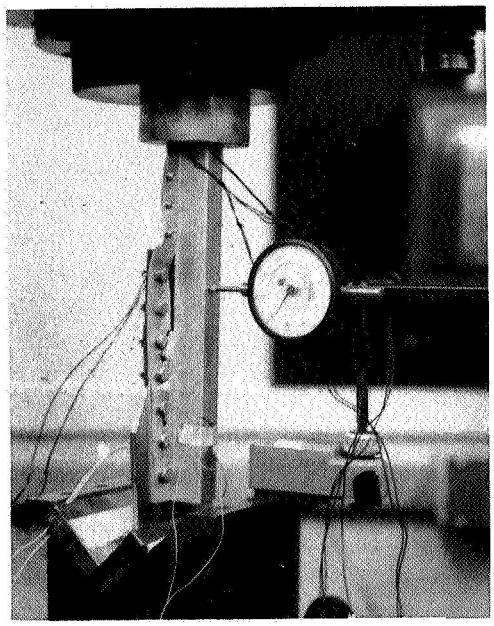

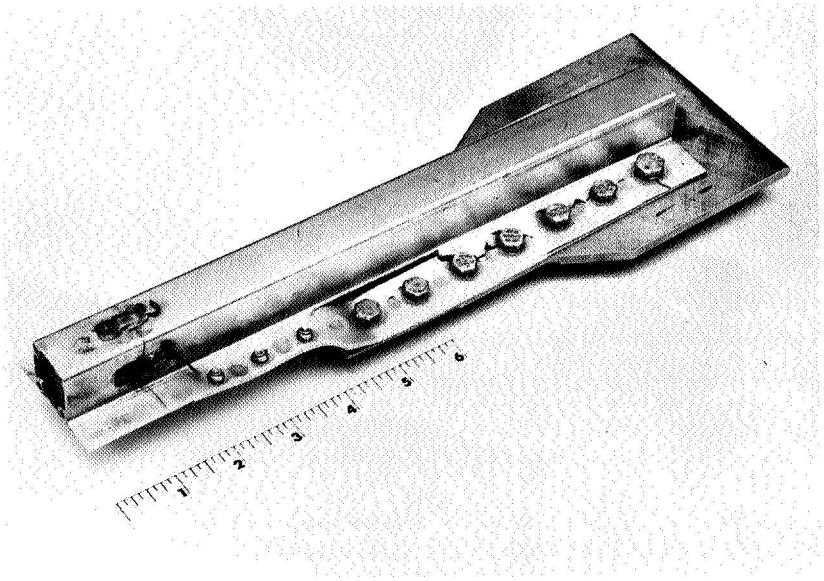

Figure 48 LOAD INTRODUCTION SPECIMEN NO. 3

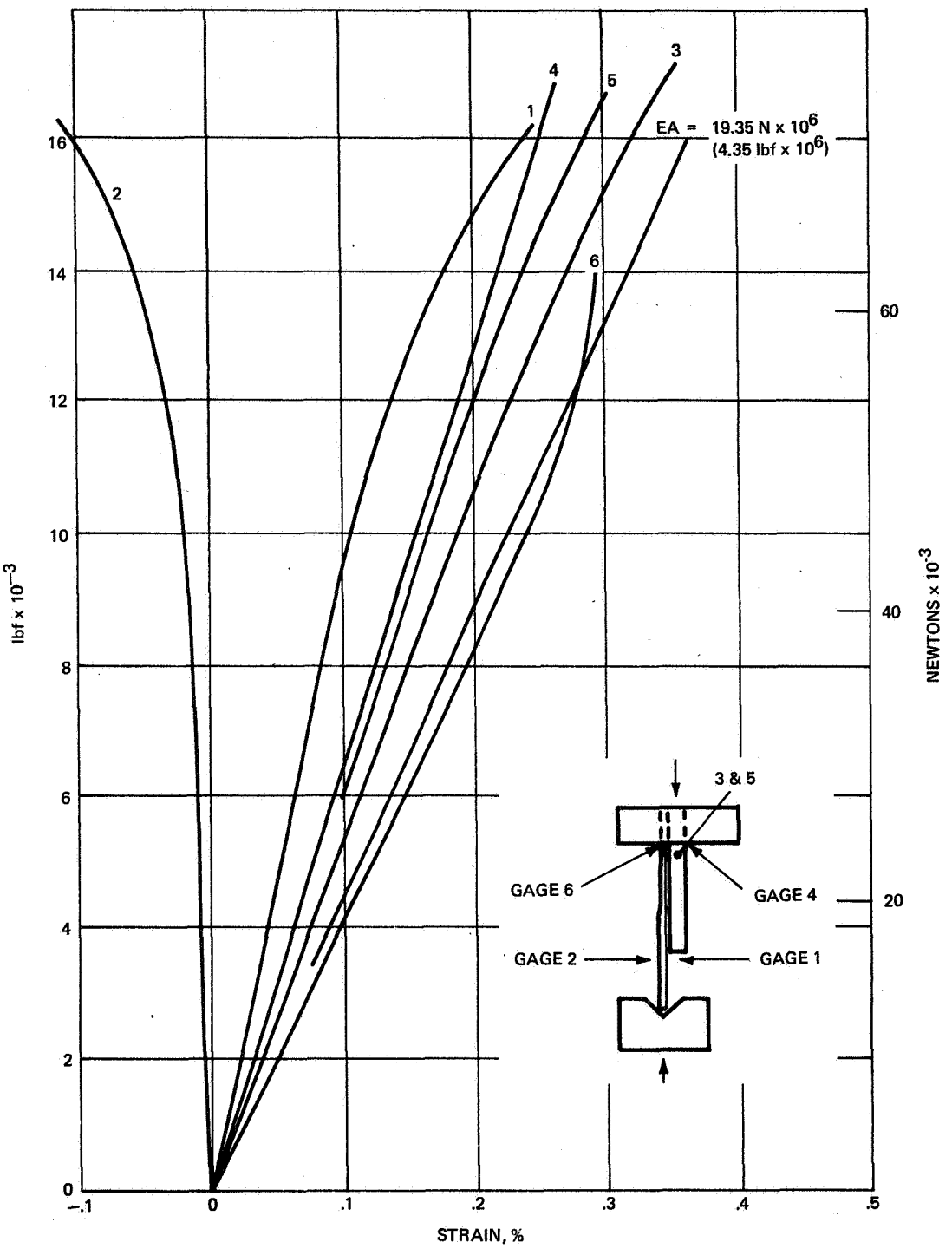

Figure 49 LOAD VERSUS STRAIN – LOAD INTRODUCTION TEST SPECIMEN NO. 3

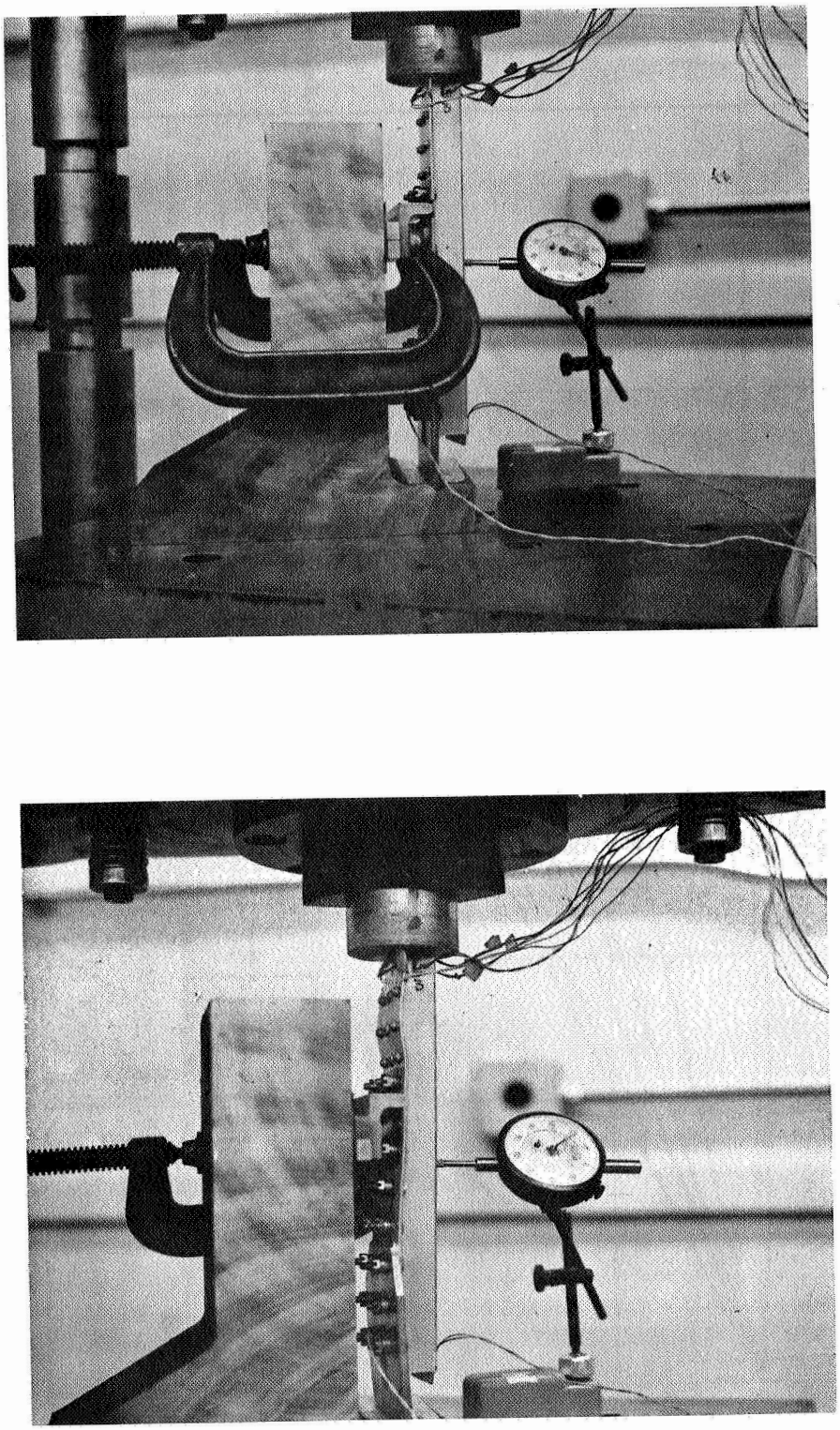

Figure 50 LOAD INTRODUCTION SPECIMEN NO. 4

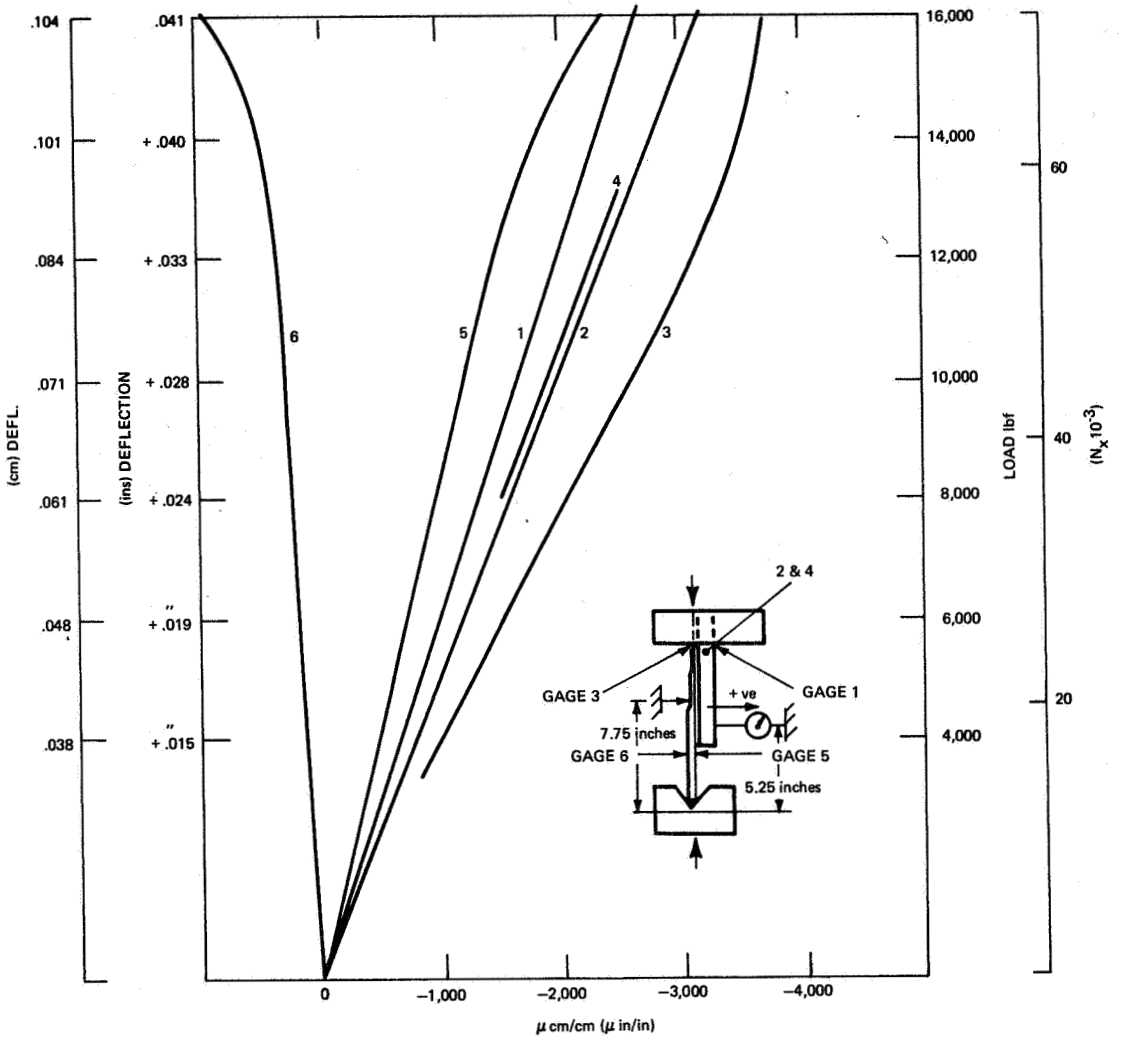

Figure 51 LOAD VERSUS STRAIN – LOAD INTRODUCTION SPECIMEN NO. 4

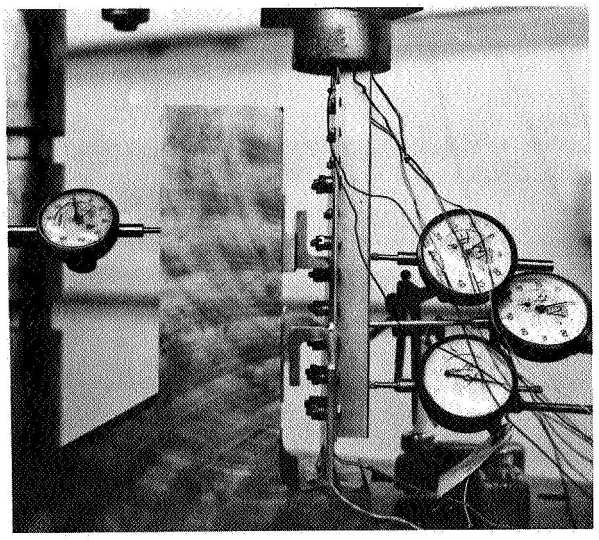

NO LOAD

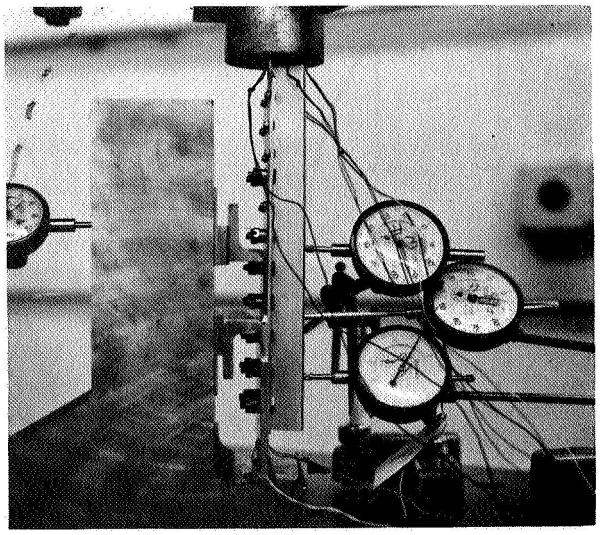

71,000 NEWTONS (16,00 lbs)

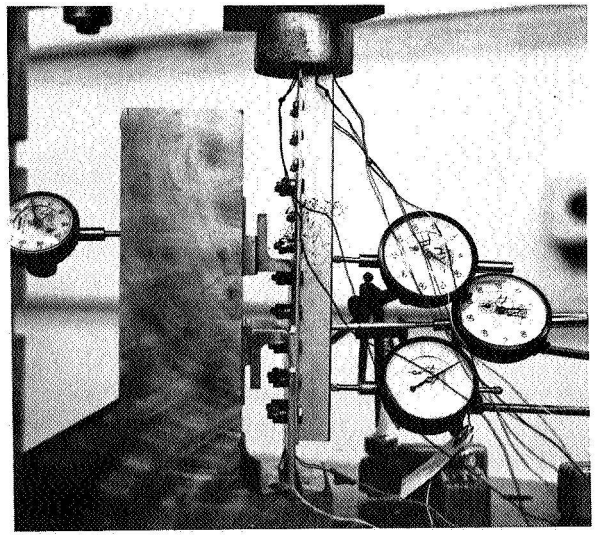

53,300 NEWTONS (12,000 lbs)

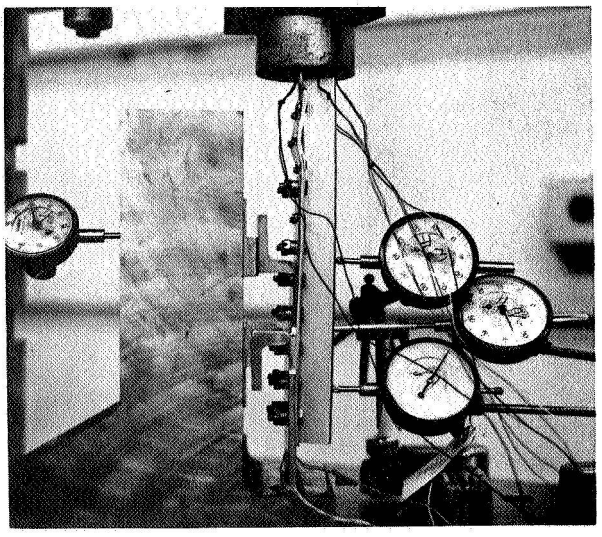

82,300 NEWTONS (18,500 lbs)

Figure 52 LOAD INTRODUCTION SPECIMAN NO. 5

83-1539

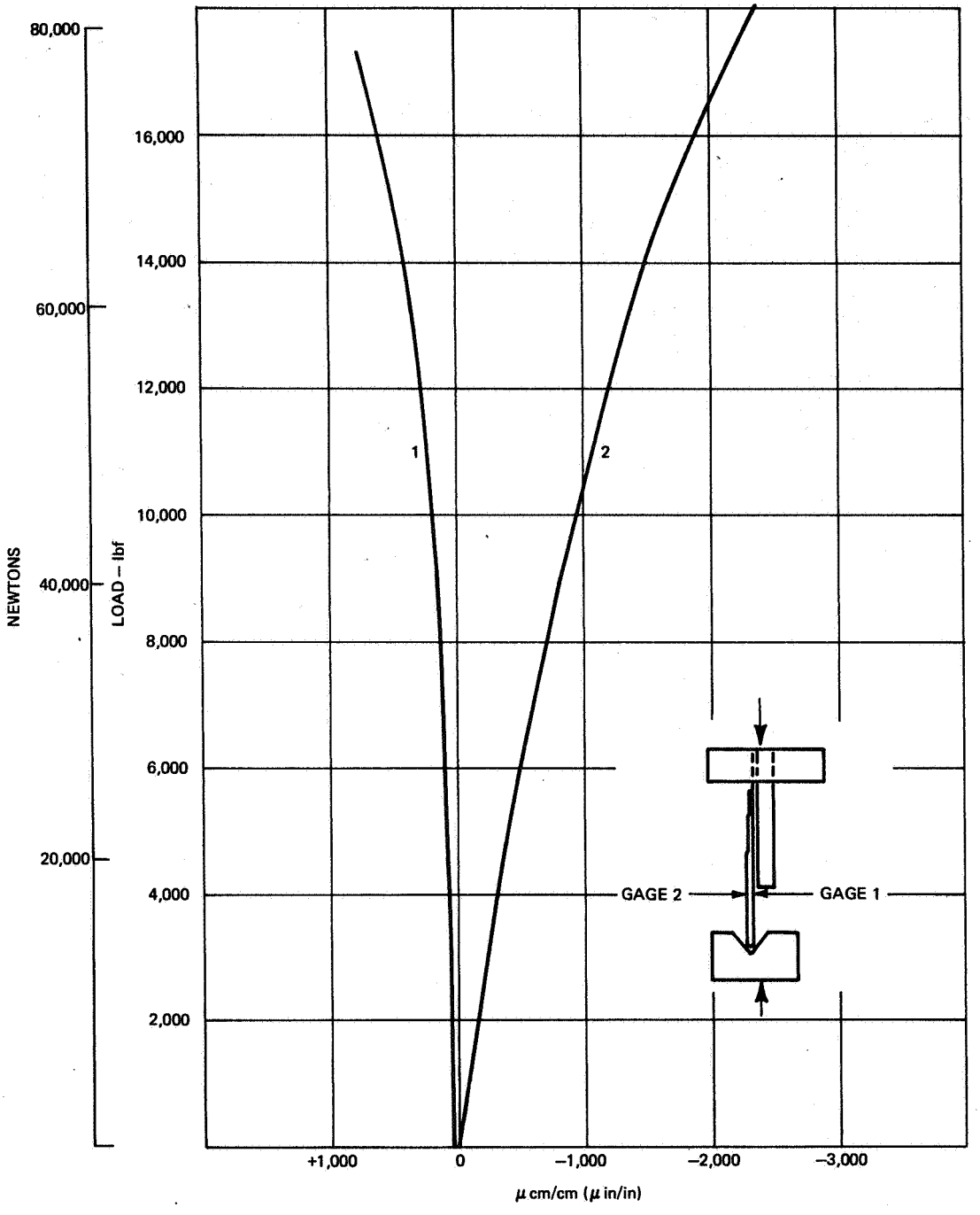

83-1543

Figure 53 LOAD VERSUS STRAIN – LOAD INTRODUCTION TEST SPECIMEN NO. 5

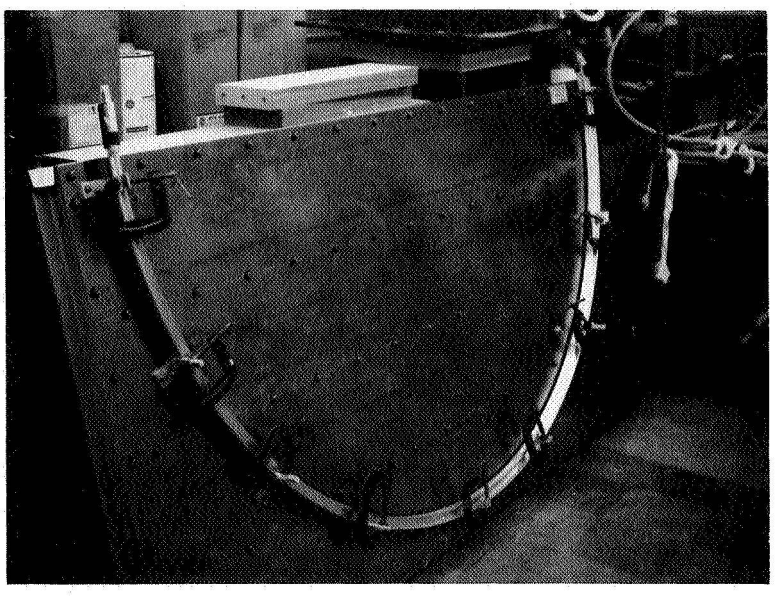

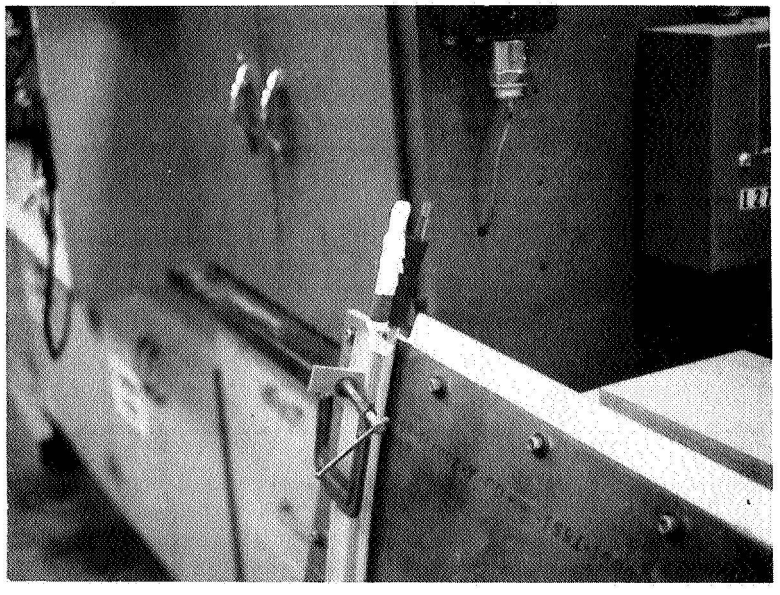

Figure 54 INFILTRATION OF THE BORON REINFORCED RINGS

Figure 55 SEALING OF SLITS IN THE HOLLOW STRINGERS

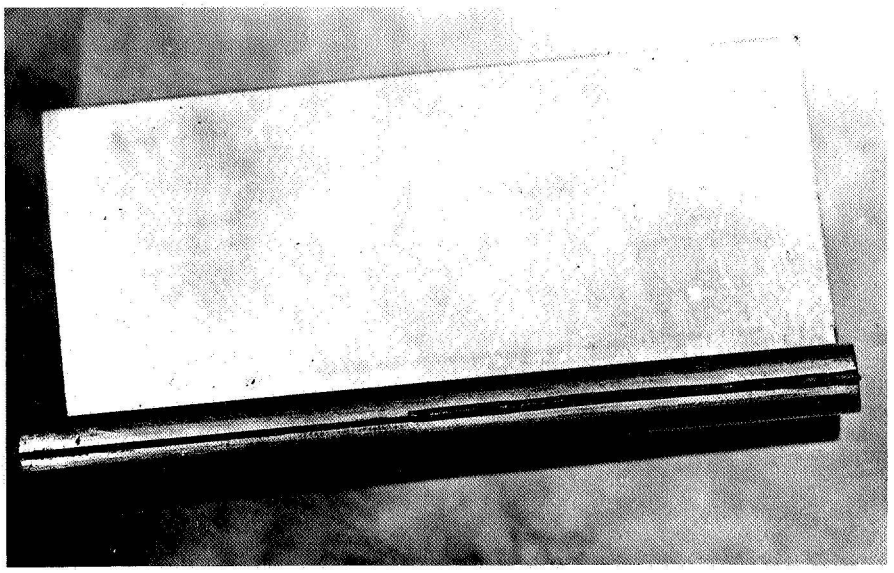

PL 5555-2 EPOXY FILLER: TRI - ELEMENT

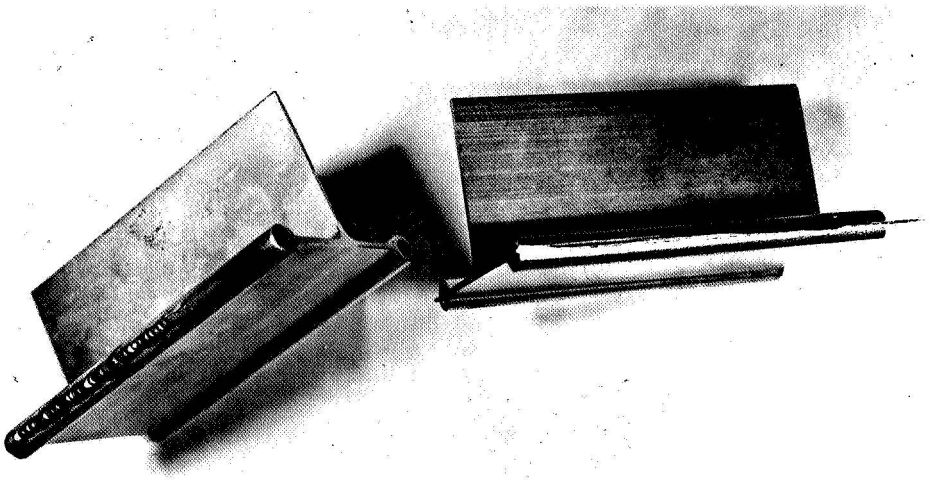

PL 5555-1 FLASH WELD: TRI-ELEMENT

Figure 56 METHODS EVALUATED FOR SEALING OF THE SLITS: EPOXY FILLER AND WELDING

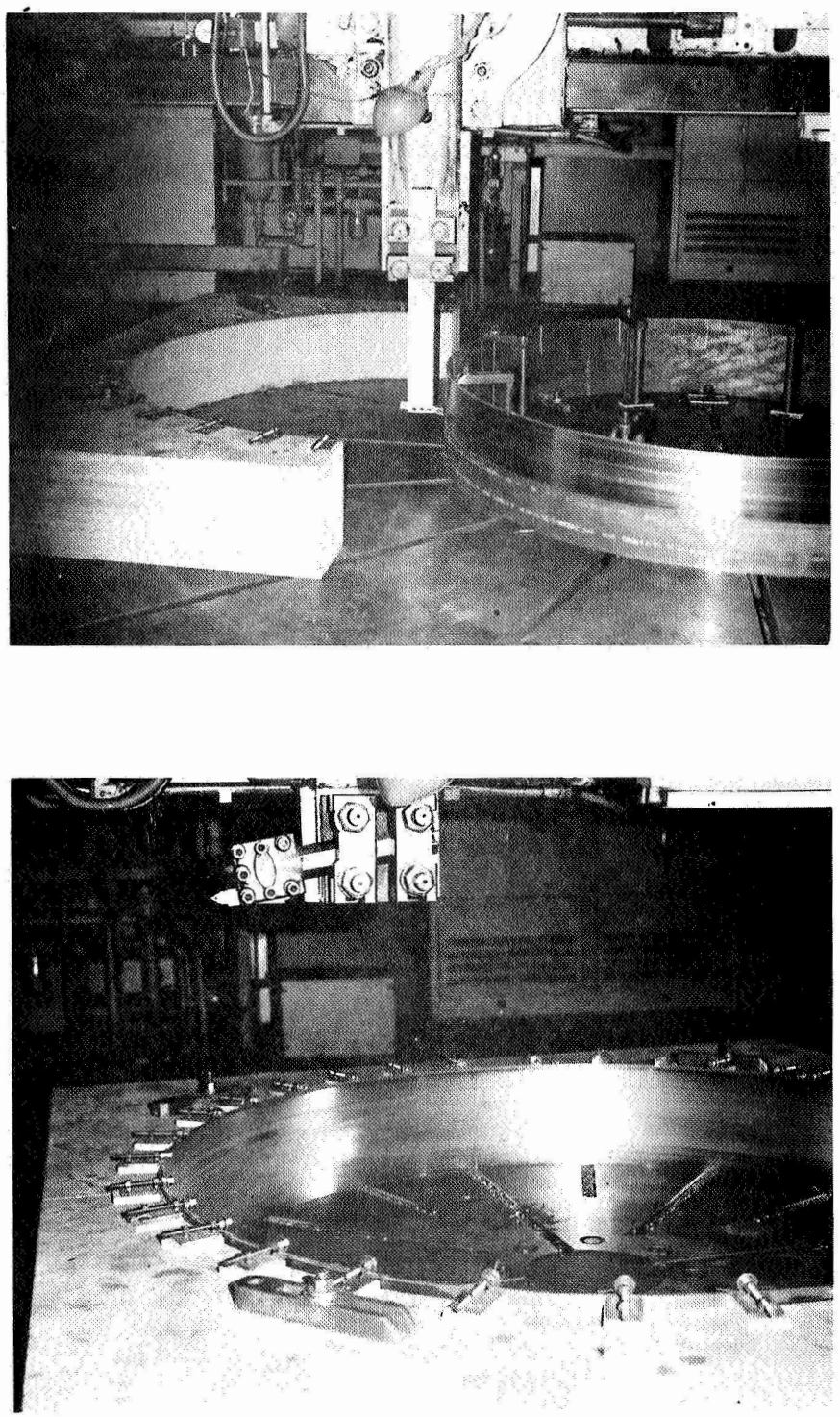

Figure 57 MACHINING FOR STEEL STEPPED LOAD INTRODUCTION RING

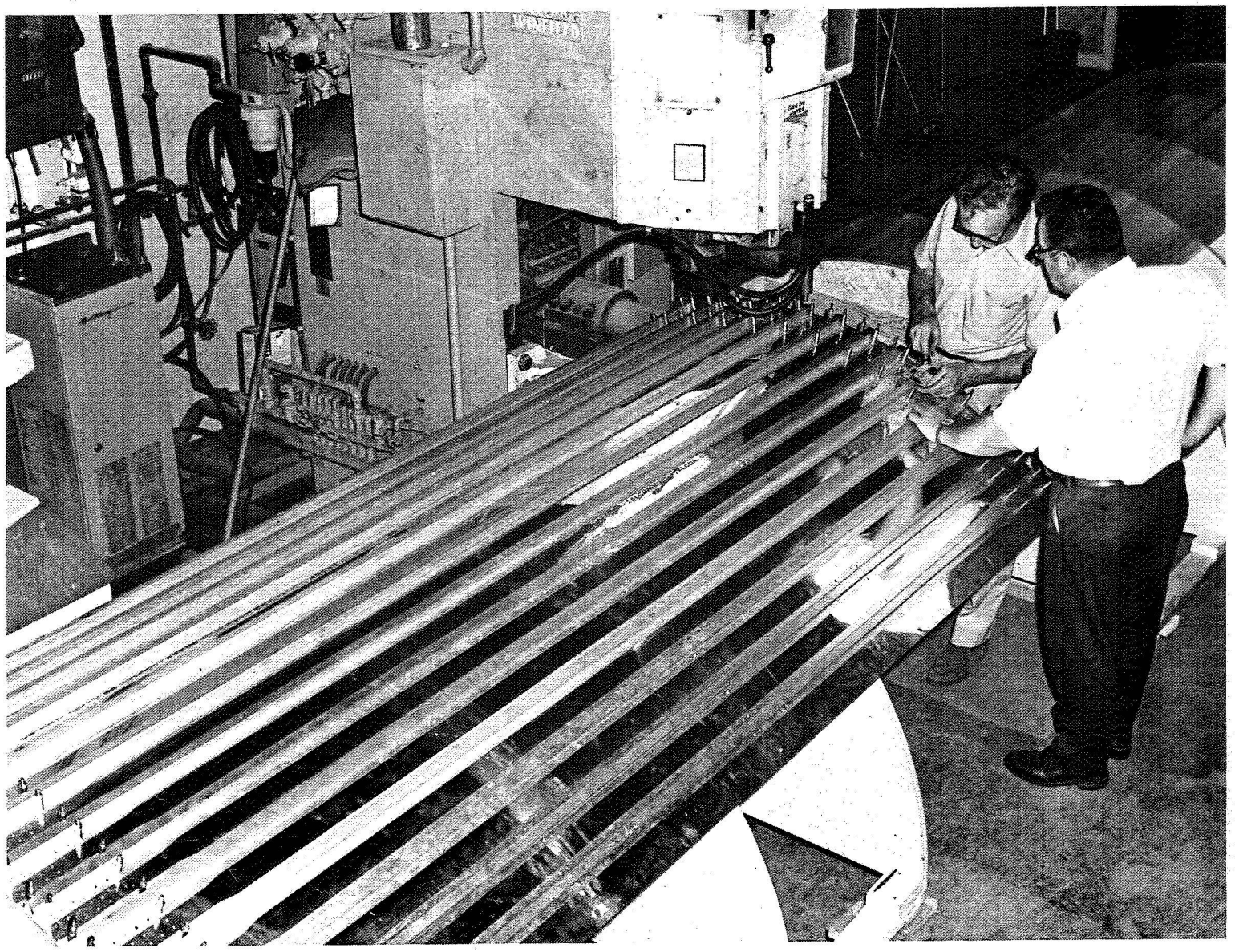

Figure 58 SPOT WELDING FIXTURE

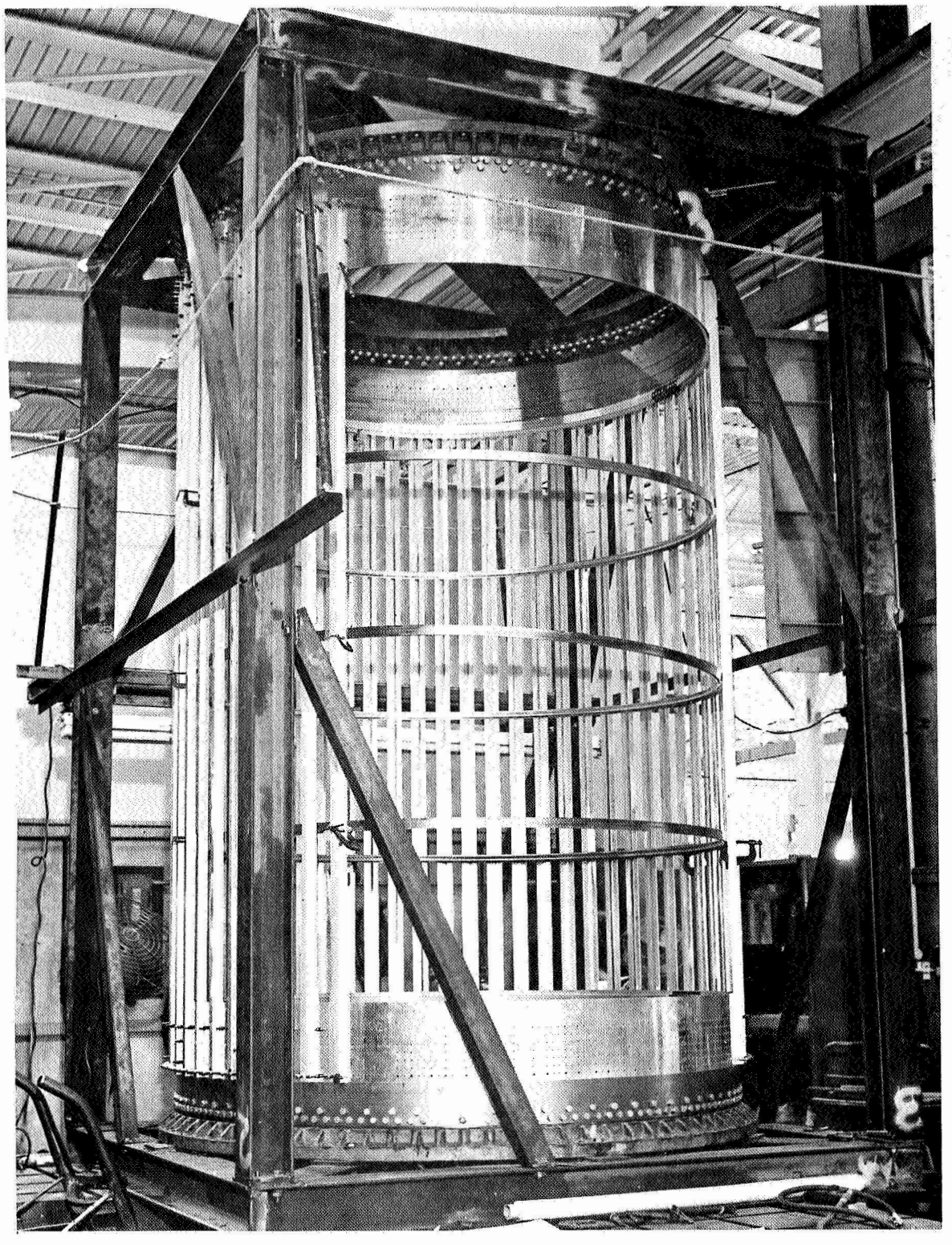

Figure 59 TRIAL ASSEMBLY OF RINGS AND STRINGERS

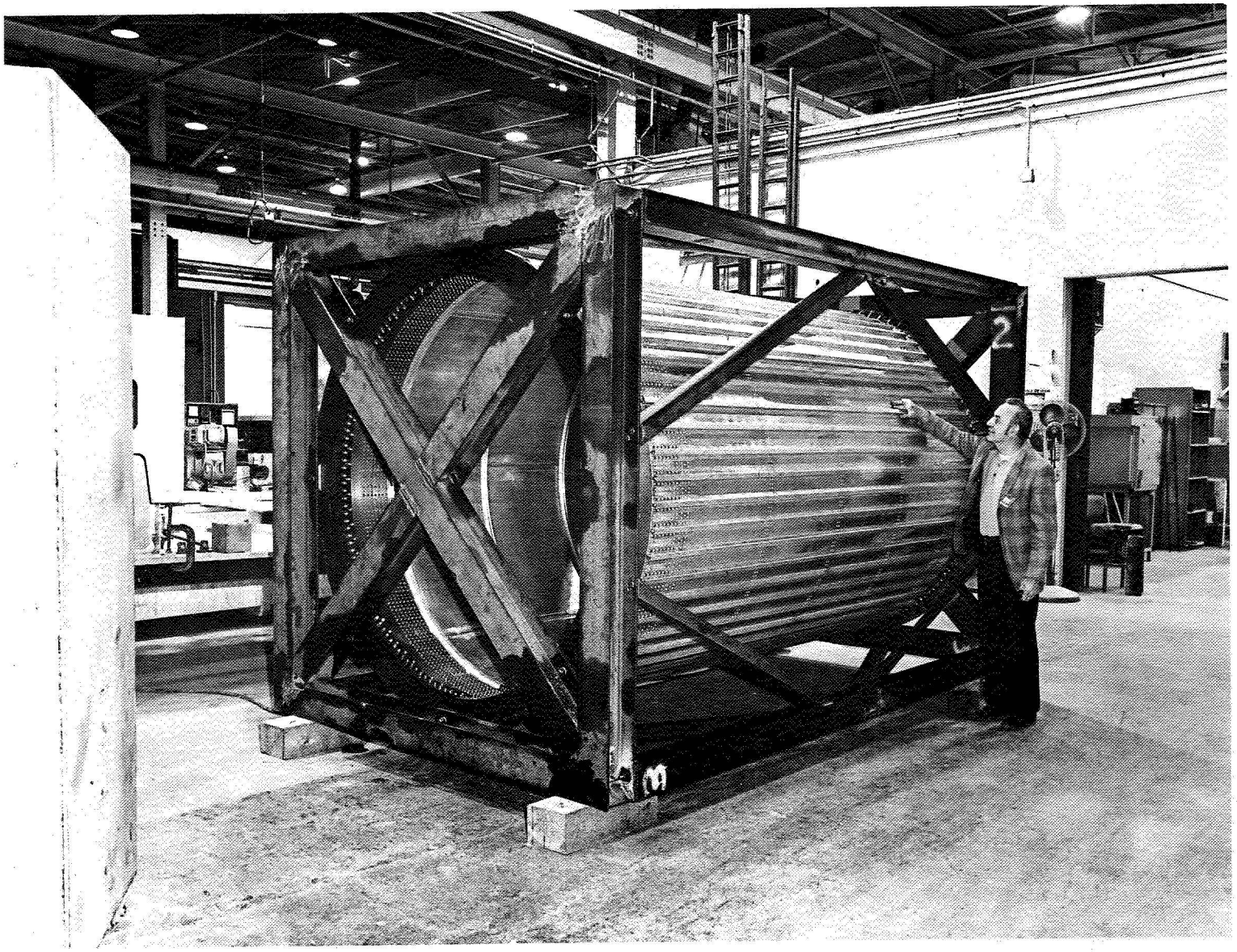

Figure 60 COMPLETED TEST SHELL

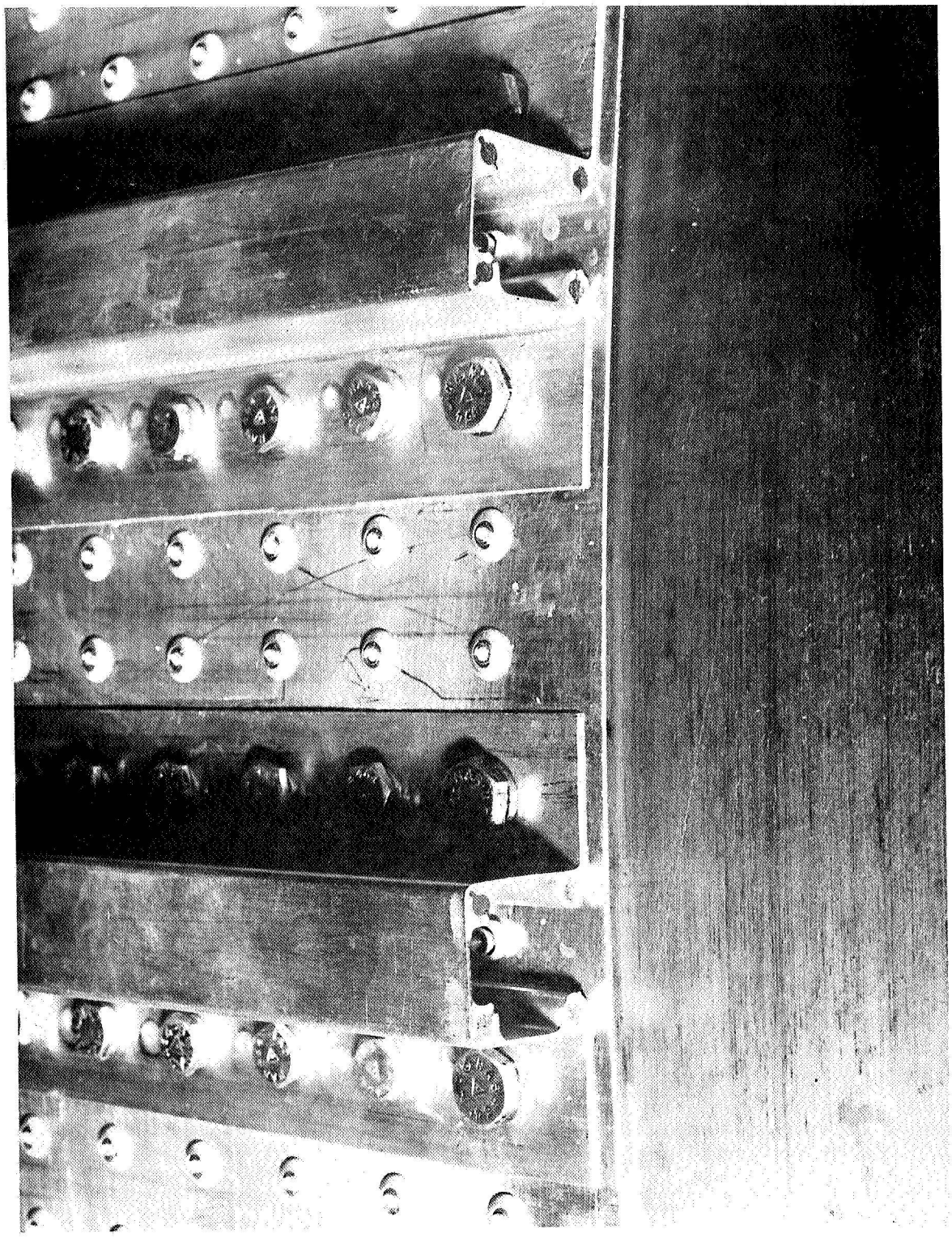

Figure 61 VIEW ON END OF REINFORCED STRINGERS

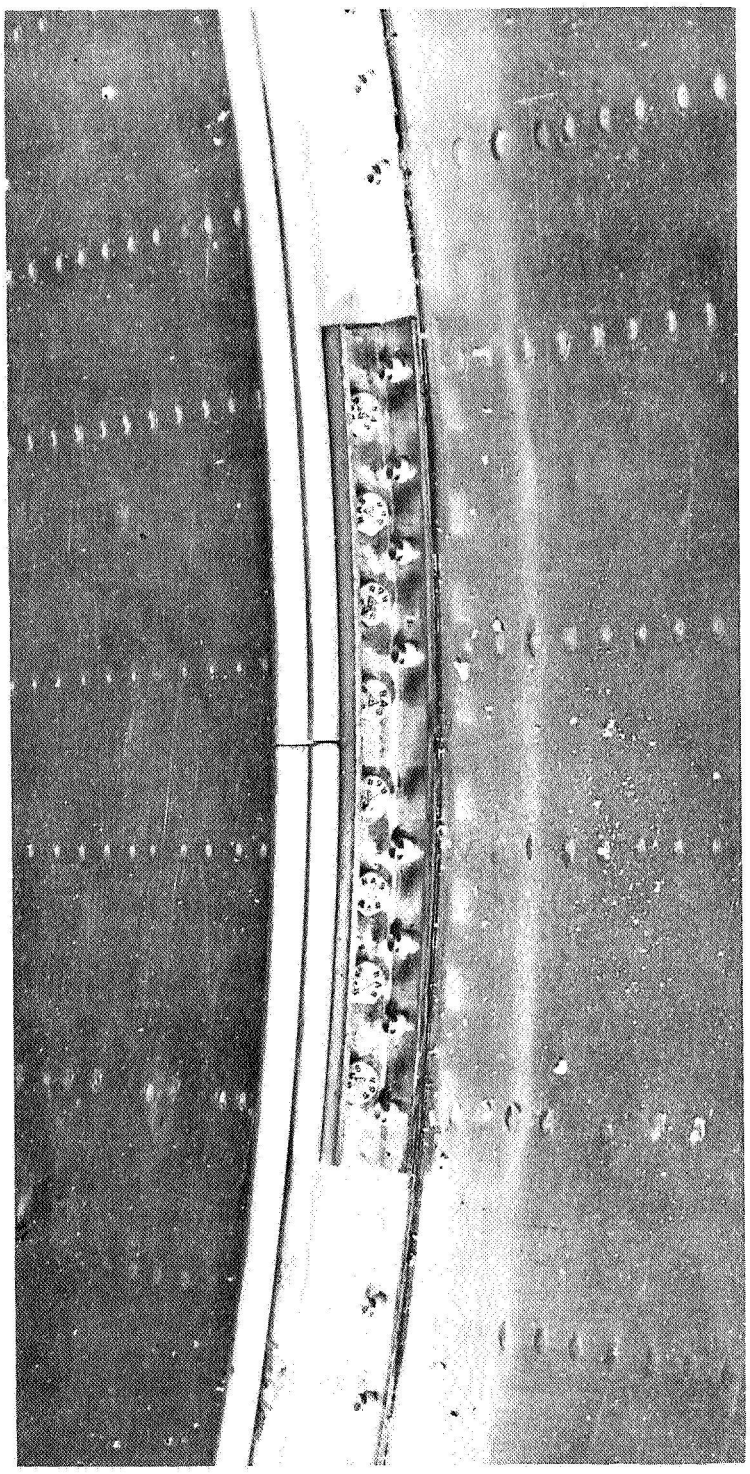

Figure 62 SPLICE JOINT IN REINFORCED RINGS

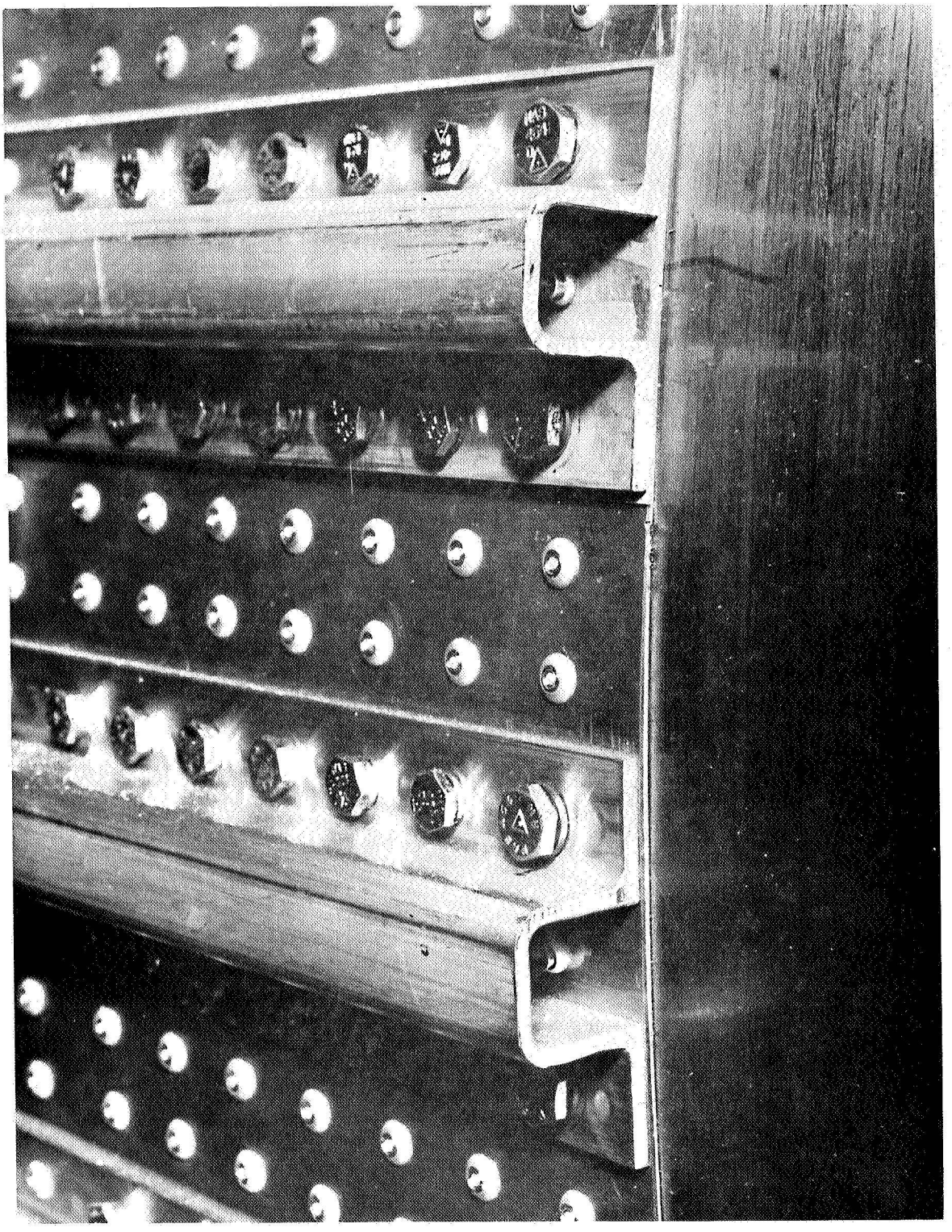

Figure 63 VIEW ON END OF UN-REINFORCED STRINGERS

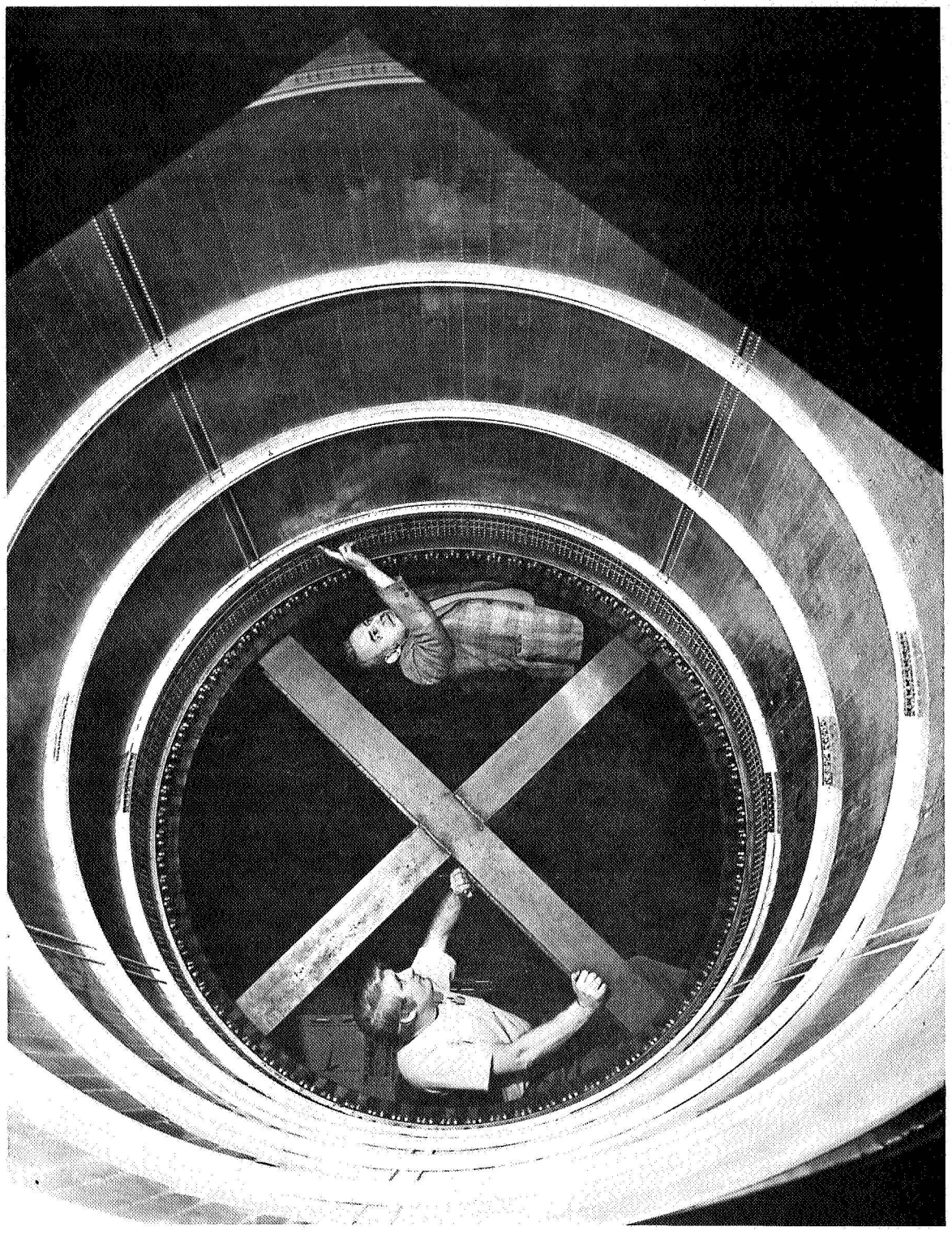

Figure 64 INTERIOR VIEW OF SHELL

Figure 65 INTERIOR VIEW OF SHELL

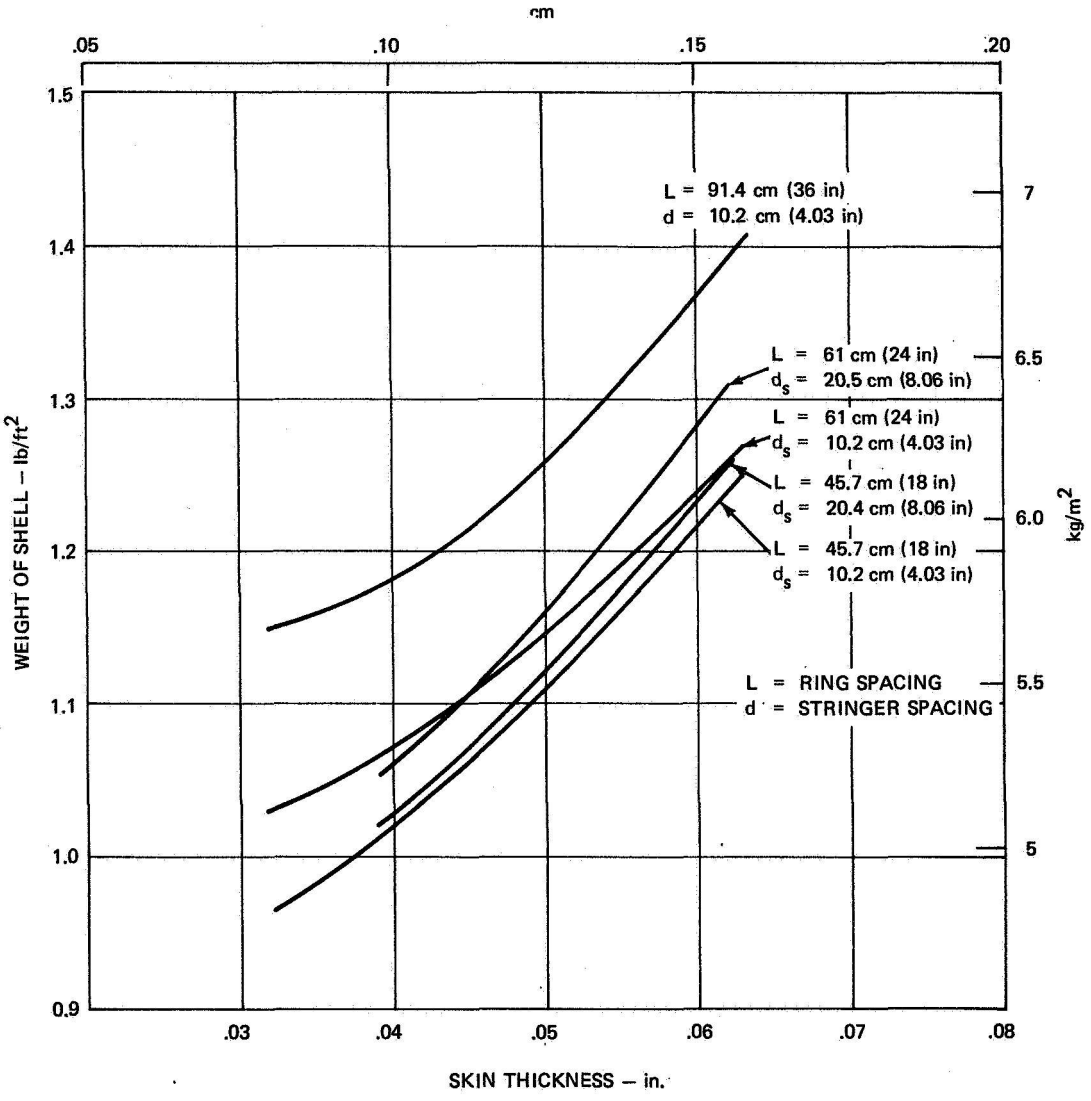

Figure 66 SHELL WEIGHT VERSUS SKIN THICKNESS [3.65 m (144 in) SHELL]

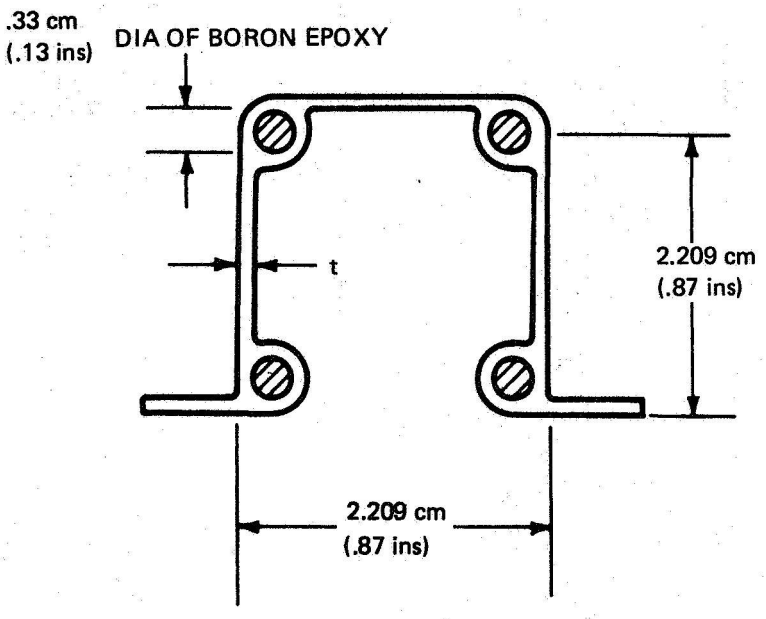

Figure 67 BORON REINFORCED STRINGER FOR 3.65 M (144") DIA SHELL

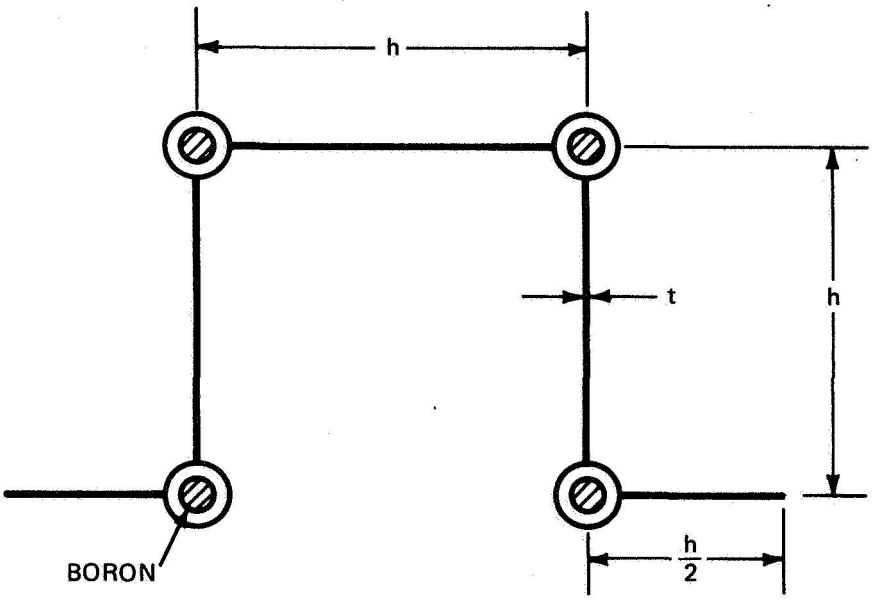

83-1531

Figure A1 THEORETICAL STRINGER SHAPE